Methanobactin: Metal binding proterties, physiological functions and biosynthesis

by

Bipin Sharma Baral

A dissertation submitted to the graduate faculty

in partial fulfillment of the requirements for the degree of

DOCTOR OF PHILOSOPHY

Major: Biochemistry

Program of Study Committee:
Alan DiSpirito, Major Professor
Amy Andreotti
Thomas Bobik
Mark Hargrove
Gregory Phillips

The student author and the program of study committee are solely responsible for the content of this dissertation. The Graduate College will ensure this dissertation is globally accessible and will not permit alterations after a degree is conferred.

Iowa State University

Ames, Iowa

2017

TABLE OF CONTENTS

ACKNOWLEDGEMENTS

First of all I would like to thank my major professor Dr Alan A DiSpirito. Without your support and mentoring this work would not have been possible. I would also like to thank my program of study committee members: Dr. Amy Andreotti, Dr. Thomas Bobik, Dr. Mark Hargrove, and Dr.Gregory Phillips for their guidance and advice.

I would also like to thank faculty, staff and graduate students in Roy J. Carver Department of Biochemistry, Molecular Biology and Biophysics for help in my research needs as well as making BBMB fun place to come to work. Friends in Ames for being there to share joy and sorrows. Finally, I would like to thank my family for their unwavering support for my education.

ABSTRACT

Methanobactins (mbs) are low molecular mass (< 1300 Da) modified peptides secreted by many methanotrophs or methane oxidizing bacteria to sequester copper from the environment. To date, methanobactin has been structurally characterized from six methanotrophs and can be divided into two groups. Group I methanobactins are represented by methanobactins from *Methylosinus trichosporium* OB3b and *Methylosinus sp*. LW4. This group is characterized by the presence of two oxazolone rings with adjacent thioamide groups. Two nitrogens from the oxazolone rings and two sulfurs from the thioamide groups come together to form a copper coordination site in distorted tertrahedral geometry. This group of methanobactin also has two cysteines in the mature protein that form a stable disulfide bond. The second group is composed of methanobactins from four different *Methylocystis* species. This group of methanobactins has a hairpin like structure following copper binding with sulfate group attached to serine or threonine and is structurally more dynamic than group I methanobactins. This group is also characterized by the presence of a C-terminal oxazolone ring with an associated thioamide and either an N-terminal imidazolone or pyrazinedione group and an associated thioamide.

The first part of this dissertation is focused on the study of methanobactin binding to various non-copper metals such as mercury and gold and the role of that binding of non-copper metals has on the physiology of methanotrophs. The second part of this dissertation is focused on understanding the post-translational modifications required for methanobactin. Until recently, the biosynthesis was assumed to be via a non-ribosomal peptide synthase or polyketide synthase. However, during the course of my dissertation, we determined that

methanobactin is indeed produced ribosomally and post-translationally modified. I show in this dissertation that TonB-dependent transporter gene in the methanobactin gene cluster is involved in the uptake of copper-bound methanobactin. In addition, we demonstrate that *mbnN* is involved in the deamination of the N-terminal oxazolone ring, a post-translational modification required in the formation of the N-terminal oxazolone ring in the methanobactin from *Methylosinus trichosporium* OB3b.

The results and methods used in this research would further help determine the role of other genes involved in biosynthesis of methanobactin and bioengineer methanobactin for various human and animal health purposes. In light of recent evidence of methanobactin being effective chelator of excess copper in Wilson's disease in rat models, understanding the biosynthesis of methanobactin has become more important.

CHAPTER 1

GENERAL INTRODUCTION

Methanotrophy

Aerobic methane oxidizing bacteria (AMOB) or methanotrophs are gram-negative bacteria that rely on methane for their carbon and energy demands. They are a ubiquitous microbial group and are found in a variety of environments including oceans, sewage sludge, and marine sediments to swamps and wetlands (1).

Methane is a major greenhouse gas and major component of global carbon cycle. It is twenty-five times more effective than CO_2 in trapping radiation from the Sun (1) and the average concentration of atmospheric methane is gradually increasing. It is known that methanotrophs in soil can utilize significant portion of methane (30 million tons) produced in soil before it escapes to the atmosphere (2). With methane emissions increasing every year and methanotrophic bacteria being one of the major sinks of methane, there is renewed interest for research in the field of methanotrophy. In addition, the ability of methanotrophs to perform unique chemical reactions has also renewed interest in the microbial engineering of methanotrophs for consumption of methane in landfills and environmental bioremediation (3). The price of methane has been continuously decreasing and with the development of new tools in metabolic engineering, methanotrophs could be used to convert this inexpensive carbon source into several products like single cell-protein, polymers, methanol, formaldehyde (4).

In 1970s Whittenbury group, isolated over 100 different methanotrophs and divided them into three different groups: Type I, Type II and Type III (1,5,6). These distributions were based on: i) arrangement of intracytoplasmic membranes, ii) type of carbon assimilation

pathway used and iii) length of carbon of phospholipid fatty acid chains. The basic Whittenbury classification scheme is still relevant in classifying methanotrophs, but the 16sRNA sequence based scheme has reclassified methanotrophs under three groups: Alphaproteobacteria, Gammaproteobacteria and Verrucomicrobia (1,5,6,7).

Methane Oxidation Pathway

The schematic diagram of methane oxidation to CO_2 is shown in Figure 1. The first enzyme in methane oxidation is the methane monooxygenase (MMO), which catalyzes the energy dependent oxidation of methane to methanol (1,7,8). Methanol is then oxidized to formaldehyde by either a Ca or a rare earth dependent pyrroloquinoline quinone (PQQ) containing methanol dehydrogenase (MeDH) (1,7,8,9). A *c*-type cytochrome is the initial electron acceptor of the MeDH (1,7,8). Formaldehyde is then either fixed into cell carbon via the ribulose monophosphate pathway (RUMP) or Serine cycle or oxidized to formate by either a membrane bound quinone-linked formaldehyde dehydrogenase (FalDH) or a cytoplasmic NAD^+-linked formaldehyde dehydrogenase. Formate is then oxidized to CO_2 by NAD^+(P) formate dehydrogenase (FDH) (1,7,8).

Methane Monooxygenases

Two different methane monooxygenases have been shown to oxidize methane, a membrane-associated or particulate methane monooxygenase (pMMO) and a soluble cytoplasmic methane monooxygenase (sMMO) (1,10,11). All but one genus of methanotrophs (i.e. *Methylocella*) express the pMMO and a small set express both forms. The kinetics of methane oxidation by the sMMO and pMMO differ. For sMMO expressing cells, the rate of methane turnover is faster (730 nmols. $min^{-1}mg^{-1}$ versus 80 nmols.min^{-1}mg

$^{-1}$) but pMMO expressing cells have higher affinity for methane (8 μM versus 90 μM) (1,12). For those methanotrophs that express both forms, sMMO is only expressed in low copper to biomass ratio i.e. less than 0.6 μmol Cu per gram of cell protein, whereas pMMO is predominately expressed in higher copper to biomass ratios (1), and this regulation has been called the "copper switch" (1,10)

Soluble Methane Monooxygenase

Soluble methane monooxygenase is a classic monooxygenase, which splits dioxygen and inserts one oxygen atom across C-H bond in methane and uses another to generate water. This enzyme is composed of a 245-kDa hydroxylase (MMOH), a 15.8-kDa reductase (MMOR) and a 38-kDa regulatory protein (MMOB). Hydroxylase exists as a dimer ($\alpha_2\beta_2\gamma_2$) and houses the μ-oxo-bridged diiron active site (13,14). Crystal structures and spectroscopic studies have established the catalytic mechanism and the roles of regulatory proteins in the catalysis. The catalytic site of the hydroxylase component consists of a μ-oxo bridged di-iron center. This center is a strong oxidant. The role of the reductase is to oxidize NADH and reduce the hydroxylase ($MMOH_{ox}$ to $MMOH_{red}$). The regulatory protein (MMOB) binds to the α-subunit of MMOH. This binding is proposed to cause conformation changes in the MMOH active site to facilitate the entry of substrates (oxygen, methane and protons) for the catalysis and the release of product (methanol) (15,16). Genetic and biochemical studies on the MMOs have focused on *Methylosinus trichosporium* OB3b and *Methylococcus capsulatus* Bath (17-23). The sMMO operon is found as a single copy in the genome of methanotrophs (Figure 2). *MmoX* encodes alpha subunit of hydroxylase, *mmoY* encodes for beta subunit and *mmoZ* encodes for gamma subunit. The *mmoB* encodes regulatory protein

while mmoC encodes the reductase. The open reading frame *orfY* encodes for protein MMOD, which is not involved in the catalytic function of sMMO enzyme complex, but is believed to have regulatory function (17,19). *M. capsulatus* Bath genome has σ^{70} and σ^{N} dependent motifs upstream of *mmoX* and are predicted to be transcriptional start sites (22). In *M. trichosporium* OB3b, σ^{54} dependent motif is upstream of *mmoX* and is predicted to be transcriptional start site (17,19). Besides this cluster, the common feature in both the genomes is the presence of *mmoR* and *mmoG* gene. The *mmoR* shows identity to putative σ^{N} dependent transcriptional activator while *mmoG* shows identity to GROEL chaperone family (22). Marker exchange mutagenesis of both genes impaired the sMMO transcription (23). The locations of these genes vary in these two organisms. The *mmoR* and *mmoG* are located downstream (3') of last gene of *mmoXYZBDC*, together with two other genes *mmoQ* and *mmoS* in *M. capsulatus* Bath. The *mmoQ* and *mmoS* show identity to two-component sensor-regulator (22). In *M. trichosporium* OB3b, *mmoR* and *mmoG* are located 5' upstream of *mmoX* of the cluster (17,21,23).

Particulate Methane Monooxygenase

The membrane-associated or particulate methane monooxygenase is an integral membrane protein consisting of three subunits: 27 kDa PmoA (β), 45 kDa PmoB (α) and 25 kDa PmoC (γ) subunits forming a trimer. Each protomer consisting of αβγ subunits is 100kDa (24-26). All groups working in the field agree that pMMO is a metalloprotein, but the number and type of metals as well as proposed active sites differ. Isolation and

purification of highly active protein has been difficult and reports on metal stoichiometry and the active site of the protein differ among the various groups as illustrated in Table 1 (24, 25, 26, 28, and 29).

According to Rosenzweig *et al.* the active site is a dicopper center located in N-terminal periplasmic cupredoxin like domains coordinated by three histidines and a N-terminal amino group from the polypeptide. Recombinant expression of this soluble region of the pmoB in *E. coli* and mutagenesis of histidines in this region proposed that only PMOB was catalytically important (26). However, the activity of the recombinant enzyme represented less than 0.0001% of the physiological rate. This proposed catalytic site is absent in the pMMOs from Verrucomicrobial methanotrophs, suggesting either the proposed active site is wrong or the pMMO from Verrucomicrobial strains have a different active site. Recent studies on a different member in class of monooxygenases, the hydrocarbon monooxygenases (HMO), showed site directed mutagenesis of the three histidines comprising this proposed active site had little effect on activity (27).

Two other metal centers were also determined in the pMMO from *M. capsulatus* Bath, a mononuclear copper center and a diiron-like center that coordinates the major metal (zinc) in the crystallization buffer. The mononuclear copper site is found in soluble region of PmoB where copper is co-ordinated by δ-nitrogen of His 48 and His 72. However, the mononuclear copper center is not present in most pMMOs and is not believed to be directly involved in methane oxidation. The diiron-like center is located in the membrane-spanning region. The residues Asp 156, His 160, and His 173 coordinate it in PmoC subunit and Glu195 coordinates in PmoA (26). The di-iron site is labile and loss of the iron is associated with a loss of methane oxidation activity (28). DiSpirito group has proposed this carboxylate-

bridged metal center is a diiron center and the active site of the enzyme (28). The residues involved in this active site coordination are conserved in all pMMOs and recent mutagenesis study on hydrocarbon monooxygenases, which belong to family of pMMO, ammonia monooxygenases and HMO, showed that the amino acids coordinating this iron center were indispensable for the activity (27).

An alternative model for active site of methane oxidation is provided by Chan's group, which proposed the presence of 15 coppers per protomer. These coppers are divided into trinuclear copper clusters known as catalytic cluster (C-cluster) and electron transfer cluster (E-cluster). C-cluster is proposed to mediate the alkane hydroxylation and dioxygen reduction chemistry while E-cluster is proposed to provide the reducing equivalents to reduce the C-cluster copper ions during the enzyme turnover (29).

As with genetic studies on the sMMO, genetic studies on pMMO have focused on *M. capsulatus* Bath and *M. trichosporium* OB3b. Based on these studies, the three genes encoding the three polypeptides are determined as: *pmoABC* (Figure 2). These genes are clustered in *pmoCAB* order in *M. capsulatus* Bath's chromosome. The *pmoCAB* is transcribed from a single transcriptional start site located 300bp upstream of *pmoC*, initiating at a putative σ^{70} promoter (17, 18, 19, 20). Most methanotrophs appear to have two identical copies of pMMO genes and some have additional third copy of *pmoC* (18).

Regulation of the Methane Monooxygenases

The regulation of methane monooxygenases is believed to be regulated by a "copper switch" (10). Different models have been proposed in regulation of methane monooxygenases by copper. According to one model, three hypothetical proteins are

involved in the regulation; they are copper binding regulator (CBR), activator (A) and repressor (R). Under high copper condition, copper binding regulator binds with copper causing its structural change, which can now bind repressor and activator. With repressor bound by the copper-binding regulator, it cannot repress the expression of pMMO transcripts while activator also cannot activate the expression of sMMO. Under low copper growth condition, copper does not bind to the CBR, hence CBR cannot bind repressor or activator. Under these conditions the repressor is free to bind and inhibit the transcription of pMMO while activator molecule can activate the transcription of sMMO (17).

A different model was proposed based on the discovery of two open reading frames (orfs) upstream of sMMO gene cluster and evidence of requirement of these genes for expression of sMMO in mutant studies. Based on this model, MmoR and σ^N are required for the activation of sMMO while MmoG, which is a homologue of GROEL chaperone family, helps in proper folding of MmoR. In the presence of high copper, this activation is disrupted and cells cannot form an active sMMO (21,23).

In addition to the two MMOs, a small post-translationally modified copper-binding peptide called methanobactin (mb) (described below) and its biosynthetic operon is also regulated by copper. RT-qPCR for structural gene methanobactin (*mbnA*) gene and the genes in the methanobactin operon are inversely regulated by copper, i.e. show increased expression with decrease in copper concentration (19,30). The result prompted the hypothesis that methanobactin is the elusive copper-binding regulator involved in the expression of the two MMOs. For this study, a deletion mutation in the structural gene for the methanobactin from *M. trichosporium* OB3b (mb-OB3b), *mbnA*, was generated by researchers in Drs. Murrell's and Semrau's laboratories. RT-qPCR was used to determine expression of *pmoA*

gene (encoding β-subunit of the pMMO) and *mmoX* (encoding α-subunit of hydroxylase of the sMMO) were compared between *ΔmbnA* mutant and wild type *M. trichosporium* OB3b, under increasing copper biomass ratios. *MmoX* expression decreased by over four orders of magnitude while *pmoA* expression increased by 78-fold with the increase in copper-biomass ratio, in the wild type strain. In the *mbnA* mutant, the expression pattern was similar to wildtype. *MmoX* expression decreased by 3 orders of magnitude, while *pmoA* expression increased by 10-fold. These data demonstrate that MbnA is not essential for "copper switch" but it amplifies the expression of both MMO enzymes (19).

Analyses of a mutant of *M. trichosporium* OB3b in which the genes encoding for polypeptides of sMMO (*mmoXYBZDC*) had been deleted by marker-exchange mutagenesis (ΔSMDM), suggested that some element of the *mmo* operon is responsible for the copper switch. Expression of *mbnA* was orders of magnitude lower in the SMDM mutant than in wild type at low copper-biomass ratios. In the SMDM mutant, *pmoA* expression was greatest in the absence of any added copper and *pmoA* expression dropped approximately 40-fold when the copper biomass ratio was increased to 1.8 μmol.Cu g protein^{-1}. By comparison, in wild-type *M. trichosporium* OB3b, *pmoA* expression increased approximately 35-fold as the copper: biomass ratio changed from 0.67 to 1.77 μmol copper.g protein^{-1} (19).

This suggests that one of the genes in the *mmo* operon plays a role in 'copper switch' of methane monooxygenases regulation. All the genes of the *mmo* operon except gene encoding MmoD already have clearly assigned functions. MmoD encodes a protein of unknown function and is not essential for sMMO activity. The primary structure of MmoD was predicted to bind DNA suggesting that it may be involved in the regulation of gene expression. Based on these results a model was proposed involving methanobactin, copper

and MmoD of sMMO gene cluster. According to this model, at low copper conditions, MmoD from sMMO operon enhances expression of methanobactin, which further enhances sMMO operon transcription. At the same time MmoD depresses expression of pMMO. In high copper conditions, MmoD binds with copper; copper bound MmoD cannot enhance expression of methanobactin. The expression of mmo operon decreases which in turn decreases methanobactin production. Copper bound MmoD also cannot depress expression of pMMO (19).

This model assumes MmoD is constitutively expressed unlike the rest of the *mmo* operon, which is not expressed at high copper to biomass ratios. This model also ignores the role of regulatory proteins like *mmoG*, *mmoR* and putative regulatory proteins *mbnI* and *mbnR*. Recent expression experiments showed that expression of *mmoG*, *mmoR*, *mbnI* and *mbnR* were down regulated within 15 minutes of copper addition while the rest of *mb* and *mmo* operon expression took longer (30). Based on these observations, the regulation of "copper switch" seems to be much more complex and more studies will be required to understand this.

Copper Pathways in Methanotrophs

In addition to the two MMOs, copper has also been shown to control expression of two formaldehyde dehydrogenases, hemerythrin, several outer membrane proteins involved in Cu assimilation, regulation and transport (1,30-34). The copper concentration also affects membrane development in *Methylococcus capsulatus* (Bath), *M. trichosporium* OB3b and in *Methylomicrobium album* BG8 (31,35). Ultrastructure examination of cells grown in increasing copper medium showed the increase in abundance and highly organized

intracellular membranes (31,35). Details have emerged in the past few years on the pathways of copper import, storage and pathways in methanotrophs. In many prokaryotes and eukaryotes, excess copper is regulated by efflux protein P-type ATPase. A homologue of this protein is present in *Methylosinus trichosporium* OB3b (36). As a likely candidate for copper uptake, MopE is an outer membrane protein and an N-terminal truncated form of the protein is found in the extracelluar fraction in *Methylocapsulatus Bath*. An X-ray crystal structure of the extracellular MopE showed the copper bound in a distorted tetrahedral site formed by oxygen from H_2O, imidazoles from two histidines, His 132 and His 203, and nitrogen from kynurenine (an oxidation product of tryptophan 130). MopE has a high copper affinity (K_d $<10^{-20}$ M) and was found associated with copper (0.6 copper ion per MopE protein) (34,37,38). CorA is homologous to MopE expressed by *Methylomicrobium album* BG8 (32,39).

Unlike eukaryotes, prokaryotes generally lack cytosolic copper storage proteins like metallothioneins (MTs) (40-43). However, novel copper storage proteins have recently been identified in *Methylosinus trichosporium* OB3b and *Bacillus subtilis*. These copper storage proteins, Csp1, Csp2 and Csp3, are tertramers of four helix bundle of monomers that can bind copper Cu (I) in the core by cysteines facing the core. Each monomers in Csp1 and Csp2 can bind up to 13 Cu (I) and they have signal peptides targeting twin argininie translocase (Tat) export system. They are predicted to store copper in cytosol for the pMMO and export it to the pMMO located in membrane. They can bind Cu(I) with an affinity of 1 x 10^{17} M^{-1}. Csp3 on the other hand lacks the signal peptide and can hold more copper Cu(I) (up to total of 80) due to the presence of additional cysteines and subunits. The affinity of Csp3

for Cu(I) is comparable to Csp1 and Csp2 and is predicted to stay in cytosol, sequestering excess copper. Currently the physiological pathways of Csps remain elusive (36,43).

Methanobactin

Methanobactins are small post translationally modified peptides (molecular weight of less than 1300 Da). Crystal or NMR-structures for six different methanobactins have been determined. All have a C-terminal oxazolone ring with an associated thioamide as part of the copper binding site. All methanobactins also have an N-terminal heterocyclic ring that varies with species. In two *Methylosinus* species the N-terminal heterocycle is an oxazolone group. In *Methylocystis strain* SB2, the N-terminal chromophore is an imidazolone, while in other *Methylocystis* species like *Methylocystis strain* M, *Methylocystis hirsute* CSC1 and *Methylocystis rosea*, the chromophore is pyrazinedione. The methanobactins from *Methylocystis strain* SB2 and *Methylosinus trichosporium* OB3b represent the structural diversity of characterized methanobactins (Figure 3) (44-49,51). The core structural properties of six known methanobactins are summarized in Figure 4 (31). Methanobactin isolated so far can be divided into two groups. The first group represented by methanobactins from *Methylosinus trichosporium* OB3b and *Methylosinus sp*. LW4, has two oxazolone rings with adjacent thioamide groups (31,51). Two nitrogens form the heterocylces and two sulfurs from the thioamide groups come together to bind copper in a distorted tertrahedral geometry. This group of methanobactins also has two cysteines that form a stable disulfide bond (44-49, 51).

The second group comprises of methanobactins from four different *Methylocystis* species. This group of methanobactins have hairpin like structure with sulfate group attached

to serine or threonine and is structurally more dynamic (47,49). Although the metal coordination sites of Group I and II methanobactins are similar, the structures of the molecule directly effects the biochemical properties. For example: reduction of disulfide bond of methanobactin from *Methylosinus trichosporium* OB3b decreases affinity as does the removal of the sulfonate group in *Methylocystis hirsute* CSC1 (49). However, the shortened forms of methanobactins (loss of C-terminus amino acid(s)) does not effect the three dimensional structure or affinity for copper compared to the respective full-length methanobactins (46,49).

Role of Methanobactin in Copper Uptake and MMO Activity

The initial proposed of role of methanobactin in copper uptake was substantiated by presence of methanobactin in supernatant of culture grown in copper limited medium (48). This role was further corroborated by ability of methanobactin in switchover of MMO expression from sMMO to pMMO (46,49,52). Additionally there is also direct evidence of uptake of copper containing methanobactin into cytoplasm of *Methylosinus trichosporium* OB3B cells (50).

Copper Binding by Methanobactin

Methanobactins can bind both Cu^{2+} and Cu^{+} with high affinity (44,46,47,49,51,53,54). Following the binding of Cu^{2+} methanobactin rapidly (< 3 ms) reduces Cu^{2+} to Cu^{+}, therefore the exact oxidation state of copper for high binding constant after addition of Cu^{2+} to the apo-mb is complicated (46,47,49,53,54). Binding affinities have been determined by various methods with addition of copper as Cu^{2+} and Cu^{+} to the apo-mb.

Cu (I) affinity can be determined by competition experiment with strong copper chelator like bathocuprione disulphonate (BCS). Isothermal titration calorimetry and displacement isothermal titration calorimetry have also been utilized to determine the binding constant. All these studies have shown the affinity in the order of $> 10^{20} M^{-1}$ (46,47,49,53,54). The pH also affects the affinity of copper and affinity decreases at lower pH (46,55). Copper binding is also dependent on the mb to copper ratios, at low copper to mb-OB3b ratios, mb binds copper as oligomer/tetramer, at higher ratios, mb binds as dimer and ratio above 0.5, mb binds as a monomer (53,56). In mb from *Methylosinus trichosporium* OB3b (mb-OB3b) copper is initially bound by the oxazolone ring A and associated thioamide followed by oxazolone B and its associated thioamide (53,56). In mb from *Methylocystis* sp. SB2 (mb-SB2), initial binding is by imidazolone ring followed by oxazolone ring (53,56). In addition to copper, methanobactin from *M. trichosporium* OB3b and *Methylocystis strain* SB2 have been shown to bind most transition and near transition metals (56,57). Thermodynamic, and spectral (absorption spectra, electron paramagnetic, fluorescence and CD-spectra) properties for each metal bound by methanobactin are unique, which makes it easy to monitor metal binding and metal competition in the presence of more than one metal (53,54,56,57). Copper loaded methanobactins show a range of reduction potential as determined by cyclic voltammetry. High E_m values suggest the preference of methanobactin for Cu(I). Binding constant values calculated from these E_m values show lower affinity for Cu (II (46,49).

The release mechanism for copper from copper-bound methanobactin is still elusive. No known metallochaperones in methanotrophs have comparable Cu affinities to methanobactin so regular ligand exchange is highly improbable. In some siderophores, Fe(III) reduction is one mechanism for release of iron, in other cases, enzymatic degradation

of siderophore is the only known mechanism (58,59). For methanobactin, oxidation of bound copper by physiological oxidants can decrease the copper affinity but this affinity is still high (49). One plausible mechanism would be enzymatic degradation to access the metal.

Biosynthesis of Methanobactin

The heterocylic ring with an associated thioamide in methanobactin is a unique structural motif and the molecule was initially believed to be synthesized non-ribosomal synthesis (involving either non-ribosomal peptide synthesis NRPS or polyketide synthase PKS) (44). However, mutations of the two identified NRPS and one PKS in *Methylococcus capsulatus* Bath did not disrupt the production of methanobactin (unpublished results). This result suggested that methanobactin might be produced ribosomally. The acid hydrolysis of OB3b-mb by Krentz *et al.* suggested the oxazolone groups might be modified from a precursor peptide (47). The hydrolysis and decarboxylation of the methanobactin from *M. trichosporium* OB3b generated L*X*GSCYPX*SCM where L* is oxo-leucine and X* is modified glycine (thioamide containing glycine). Bioinformatics analyses using this sequence on known methanotrophs genome did not result in any hits. However, further bioinformatics analyses replacing glycine to cysteine resulted in a 30-residue sequence, MTVKIAQKKVLPVIGRAAA**LCGSCYPCSCM**, where bold capital letters represent the precursor methanobactin sequence (47). The cysteine after leucine and the cysteine after proline are likely to be modified to form the two oxazolone rings. A close example of such posttranslational modification is found in Microcin B17 (MccB17) produced by *Escherichia coli* (60). Bioinformatics analyses have determined methanobactin like precursor peptide sequences in many methanotrophs and non-methanotrophs as shown in the Figure 4

(31,47,61). The common characteristic among these sequences is the leader peptide sequence, that is cleaved before export. The leader polypeptide might be the recognition determinant for the post-translational modifying enzymes as in MccB17 (60). However, the key enzymes involved in ring formation in MccB17 are not present in methanotrophic genomes (31,61). The core peptide goes through modifications to form the heterocyclic rings. All the sequences of core peptide have cysteines, which are modified with an adjacent amino acid into heterocylic rings with the associated thioamide (31,61). To test if precursor peptide in *Methylosinus trichosporium* OB3b is indeed methanobactin precursor peptide, this gene (*mbnA*) was mutated by marker-exchange mutagenesis and the production of methanobactin was not detected in these mutants (19). Further genome analysis determined that this precursor gene was part of a gene cluster. The two genes adjacent to *mbnA* (*mbnB*, *mbnC*) are unannotated but conserved in all known methanobactin gene clusters. A conserved putative export transporter, a multidrug and toxic compound extrusion (MATE; *mbnM)* family and uptake transporter Ton-B dependent receptors (*mbnT*) are also found in all *mbn* gene clusters. Some of the genes are only found in some operons representing diversity in structure of methanobactin. A gene encoding diheme enzyme which is a homologue of diheme cytochrome *c* peroxidase (*mbnH*) is present in some but not all *mbn* gene clusters (19,61). A gene encoding N-terminal transaminase (*mbnN*) is found in operons from *Methylosinus trichosporium* OB3b, and *Methylosinus* sp. LW4 and the N-terminal amino acids in both methanobactins are deaminated (31,51,61). Similarly, threonine sulfonation is also only present in the methanobactins from the *Methylocystis* strains and *mbnS is* believed to be responsible for sulfonation (31). There are additional genes in the mbn gene clusters whose exact function in biosynthetic modification of methanobactin is unknown. With recent

promising results of methanobactin in human and animal health, especially in copper related diseases, dissecting the mechanism of biosynthesis of methanobactin has become more important.

Commercial and Therapeutic Use of Methanobactin

Recently, methanobactin from *Methylosinus trichosporium* OB3b was shown to be an effective chelator in Wilson disease (WD) (62,63,64). Copper homeostasis is maintained by biliary excretion of excess copper by a P-type ATPase, ATP7B. WD individuals have, a mutation in the gene ATP7B causes excessive deposition of copper in liver leading to hepatitis (62-64). Our collaborators tested the effectiveness of methanobactin, in $LPP^{-/-}$ rat models, which mimics severe WD phenotype (64). The *in vitro* and *in vivo* results show that methanobactin can decrease the level of copper deposited in hepatocytic mitochondria and rescue the $LPP^{-/-}$ rats from acute liver failure. Methanobactin was found to be superior in terms of efficacy and absence of major side effects than present pharmacotherapies for WD (64).

Gold nanoparticles are used in biosensors and many other biological applications. There are many chemical methods to make gold nanoparticles, which require toxic chemicals and external reductants. It was shown that methanobactin from *M. trichosporium* OB3b could bind and reduce Au (III) to Au^0 and form gold nanoparticles at high Au(III) to methanobactin ratios. The size of the nanoparticles was large (greater than 25nm) and non-uniform. However, recent studies using the methanobactin from *Methylocystis* strain SB2, (mb-SB2) produced gold nanoparticles with an average size of 2 nm and the particles were stable for up to 7 days in solution without clustering.

Dissertation Organization

As mentioned above methanobactin can bind to many non-cuprous metals with high affinity. Studying the binding of methanobactin to different metals present *in situ* environment of methanotrophs is important to better understand the methanotrophic community and role of methanobactin in bioavailability of metals. Towards this end, studies to understand the effect(s) of mobilization/immobilization of mercury at the Department of Energy (DOE) facility at Savanna River, South Carolina and its effects on methanotrophic community structure and activity were initiated. As a prerequisite to that study the Chapter 2 examines mercury binding by the methanobactin from *Methylocystis* strain SB2 (mb-SB2). Mb-SB2 was chosen because of the similarity of this form of methanobactin to the methanobactin produced by methanotrophic isolates from Savanna River soil samples (Bipin et al., unpublished results.). The result from this study has been published in Journal of Inorganic Biochemistry (56). The ability to bind mercury raises the question, can methanobactin reduce mercury toxicity to *M. trichosporium* OB3b as well as other methanotrophs? The details of this study is described in Chapter 3 and has been published in Applied Environmental Microbiology (65).

The finding that methanobactins can bind other metals and that metals such as mercury, and that mercury can displace copper bound mb-SB2, suggest there is a competition between copper and non-cuprous metals for binding methanobactin in mixed metal environment. In addition to metal detoxification described above, this competition might have some physiological significance such as gene expression of the methane monooxygenases. Gold was chosen as the competing metal to copper due to the toxicity of mercury. The binding of $AuCl_4^-$ and Hg^{2+} by both mb-OB3b and mb-SB2 are similar and the

use of $AuCl_4^-$ for this study reduces the complexity associated with mercury toxicity. The results of this study are detailed in the chapter 4 and has been published in Applied Environmental Microbiology (66).

In chapter 5 we show that the TonB-dependent transporter gene (*mbnT*) in the methanobactin gene cluster in *M. trichosporium* OB3b is responsible for the uptake of copper bound methanobactin. This work has been published in Applied and Environmental Microbiology (67). In chapter 6 we show the aminotransferase gene (*mbnN*) is responsible for deamination of the N-terminal leucine in mb-OB3b. In addition, this post-translational modification appear to be necessary for the formation of the N-terminal oxazolone group. These results were published in Applied Environmental Microbiology (68).

References

1) **Semrau JD, DiSpirito AA and Yoon S.** 2010 Methanotrophs and copper. *FEMS Microbiology Reviews*, **34**: 496–531. doi: 10.1111/j.1574-6976.2010.00212.x

2) **Singh BK, Bardgett RD, Smith P and Reay DS.** 2010. Microorganisms and climate change: terrestrial feedbacks and mitigation options. *Nature Reviews Microbiology*, **8**: 779-790.

3) **Jiang H, Chen, Y Jiang, P, Zhang C, Smith TJ, Murrell JC, Xing XH**. 2010 Methanotrophs: Multifunctional bacteri with promising applications in environmental bioengineering. Biochem. Env. **49(3)**: 277-288.

4) **Kalyuzhnaya MG, Puri AW, Lidstrom M.** 2015. Metabolic engineering in methanotrophic bacteria. Metabolic Engineering. **29**: 142-152.

5**) Sohngen NL**. 1906. ¨ Uber bakterien, welche methan als ¨ kohlenstoffnahrung und energiequelle gebrauchen. Centr Bakt Parasitenkd Infectionsk **15**: 513–517.

6) **Whittenbury R, Phillips KC & Wilkinson JG**. 1970. Enrichment, isolation and some properties of methane-utilizing bacteria. J Gen Microbiol **61**: 205–218.

7) **Hanson RS & Hanson TE**. 1996. Methanotrophic bacteria. Microbiol Rev 60: 439–471.

8) **DiSpirito AA, Kunz RC, Choi DW, Zahn JA**. 2004. Electron flow during methane oxidation in methanotrophs., p 141-169. *In* Zannoni D (ed), Respiration in Archaea and Bacteria Kluwer Scientific, The Netherlands.

9) **Gu W, Farhan UHM, DiSpirito AA, Semrau JD**. 2016. Uptake and effect of rare earth elements on gene expression in *Methylosinus trichosporium* OB3b. FEMS Microbiol Lett **363**: fnw2129.

10) **Stanley SH, Prior SD, Leak DJ, and Dalton H**. 1983. Copper stress underlies the fundamental change in intracellular location of methane monooxygenase in methane oxidizing organisms: studies in batch and continuous cultures. Biotechnology Letters **5(7)**: 487-492.

11**) Chistoserdova L and Lidstrom ME**. 2013. Aerobic Methylotrophic Prokaryotes. The Prokaryotes 267–285.

12) **Lee S-W, Keeney DR, Lim D-H, DiSpirito AA, Semrau JD**. 2006. Mixed pollutant degradation by *Methylosinus trichosporium* OB3b expressing either soluble or particulate methane monooxygenase: can the tortoise beat the hare? Appl. Environ. Microbiol. **72**: 7503-7509.

13) **Lipscomb JD**. 1994. Biochemistry of the Soluble Methane Monooxygenase. Annu. Rev. Microbiol. **48**: 371-399. doi: 10.1146/annurev.mi.48.100194.002103.

14) **Fox BG, Froland WA, Dege JE and Lipscomb JD**. 1989. Methane monooxygenase from *Methylosinus trichosporium* OB3b: purification and properties of a three component system with high specific activity from a type II methanotroph. J Biol Chem. **264(17)**: 10023-33.

15) **Lee SJ, McCormick MS, Lippard SJ and Cho U-S**. 2013. Control of substrate access to the active site in methane monooxygenase. Nature **494**:380-384.

16) **Tinberg CE and Lippard SJ.** 2011. Dioxygen activation in soluble methane monooxygenase. Accounts of chemical research **44**:280-288.

17) **Murrell JC, McDonald IR and Gilbert B**. 2000. Regulation of expression of methane monooxygenases by copper ions. Trends Microbiol. **8**:221 – 225.

18) **Gilbert B, McDonald IR, Finch R, Stafford GP, Nielsen AK and Murrell JC**. 2000. Molecular analysis of the pmo (particulate methane monooxygenase) operons from two type II methanotrophs. Appl. Environ. Microbiol. **66**:966-975.

19) **Semrau JD, Jagadevan S, DiSpirito AA, Khalifa A, Scanlan J, Bergman BH, Freemeier BC, Baral BS, Bandow NL, Vorobev A, Haft DH, Vuilleumier S, Murrell JC**. 2013. Methanobactin and MmoD work in concert to act as the 'copper-switch' in methanotrophs. Environ Microbiol. **15(11)**:3077-3086.

20) **Nielsen AK, Gerdes K and Murrell JC**. 1997. Copper-dependent reciprocal transcriptional regulation of methane monooxygenase genes in *Methylococcus capsulatus* and *Methylosinus trichosporium*. Mol Microbiol. **25(2)**: 399-409.

21) **Stafford G, Sclanlan J, McDonald IR and Murrell JC**. 2003. ropN, mmoR and mmoG, genes involved in regulating the expression of soluble monooxygenase in *Methylosinus trichosporium* OB3b. Microbiology **149**: 1771-1784.

22) **Csáki R, Levente B, Klem J, Murrell JC and Kovács KL**. 2003. Genes involved in the copper-dependent regulation of soluble methane monooxygenase of *Methylococcus capsulatus* (Bath): cloning, sequencing and mutational analysis. Microbiology **149**:1785-1795.

23) **Scanlan J, Dumont, MG and Murrell JC**. 2009. Involvement of MmoR and MmoG in the transcriptional activation of soluble methane monooxygenase genes in *Methylosinus trichosporium* OB3b. FEMS Microbiology Letters **301**: 181–187. doi: 10.1111/j.1574-6968.2009.01816.x.

24) **Zahn JA and DiSpirito AA**. 1996. Membrane-associated methane monooxygenase from *Methylococcus capsulatus* (Bath). J Bacteriol **178**: 1018-1029.

25) **Choi DW, Kunz RC, Boyd ES, Semrau JD, Antholine WE, Han JI, Zahn JA, Boyd JM, de la Mora A.M and DiSpirito AA.** 2003. The Membrane-Associated Methane Monooxygenase (pMMO) and pMMO-NADH: Quinone Oxidoreductase complex from *Methylococcus capsulatus* Bath. J. Bacteriol. **185 (19):**5755-5764.

26) **Lieberman RL and Rozenzweig AC.** 2005. Crystal structure of a membrane-bound metalloenzyme that catalyses the biological oxidation of methane. Nature **434(7030):**177-82.

27) **Liew E.F, Tong D, Coleman NV, and Holmes AJ.** 2014. Mutagenesis of the hydrocarbon monooxygenase indicates a metal center in subunit-C, and not subunit-B, is essential for copper-containing membrane monooxygenase activity. Microbiology. **160:**1267-1277.

28) **Martinho M, Choi DW, DiSpirito AA, Antholine WE, Semrau JD, Mu□nck W**. 2007. Mössbauer studies of the membrane-associated methane monooxygenase from *Methylococcus capsulatus* Bath: evidence for a diiron center. J. Am. Chem. Soc. **129**:15783–15785.

29) **Chan SI, Chen KH, Yu SS, Chen CL and Kuo SS**. 2004. Toward delineating the structure and function of the particulate methane monooxygenase from methanotrophic bacteria. Biochemistry **43(15)**: 4421-30.

30) **Kenney GE, Sadek M, Rosenzweig AC**. 2016. Copper-responsive gene expression in the methanotroph *Methylosinus trichosporium* OB3b. Metallomics **8**: 931-940.

31) **DiSpirito AA, Semrau JD, Murrell JC, Gallagher WH, Dennison C, Vuilleumier S**. 2016. Methanobactin and the link between copper and bacterial methane oxidation. Microbiol Mol Bio Rev. **80(2)**: 387-409.

32) **Berson O and Lidstrom ME**. 1997. Cloning and characterization of CorA, a gene encoding a copper-repressible polypeptide in the type I methanotroph, Methylomicrobium album BG8. FEMS Microbiol. Lett. **148**:169-174.

33) **Fjellbirkeland A, Kleivdal H, Joergensen C, Threstrup H and Jensen HB**. 1997 Outer membrane proteins of *Methylococcus capsulatus* (Bath). Arch. Microbiol. **168**:128-135.

34) **Fjellbirkeland A, Kruger PG, Bemanian V, Hogh BT, Murrell JC, and Jensen HB.** 2001. The C-terminal part of the surface-associated protein MopE of the methanotroph *Methylococcus capsulatus* (Bath) is secreted into the growth medium. Arch. Microbiol. **176**:197-203.

35) **Brantner CA, Buchholz LA, McSwain CL, Newcomb LL, Remsen CC, and Collins MLP**. Intracytoplasmic membrane formation in *Methylomicrobium album* BG8 in the growth medium. Can. J. Microbiol. **43**:672-676.

36) **Vita N, Landolfi G, Basle, A Platsaki S, Lee J, Waldron KJ, Dennison C**. 2016. Bacterial cytosolic proteins with a high capacity for Cu(I) that protect against copper toxicity. Sci Rep. **6**: 39065.doi. 10. 1058/Srep39065.

37) **Ve T, Mathisen K, Helland R et al**. 2012 The *Methylococcus capsulatus* (Bath) secreted protein, MopE, binds both reduced and oxidized copper. PLoS ONE **7(8)**: e43146. doi: 10.1371/journal.pone.0043146.18

38) **Helland R, Fjellbirkeland A, Karlsen OA, Ve T, Lillehaug JR, et al**. 2008. An oxidized tryptophan facilitates copper binding in *Methylococcus capsulatus* Bath secreted protein MopE. J Biol Chem. **283**: 13897–13904.doi: 10.1074/jbc.m800340200.

39) **Johnson KA, Ve T, Larsen Ø, Pedersen RB, Lillehaug JR, et al**. (2014) CorA Is a Copper Repressible Surface-Associated Copper (I)-Binding Protein Produced in *Methylomicrobium album* BG8. PLoS ONE **9(2)**: e87750. doi: 10.1371.

40**) Robinson NJ.** 2008. A bacterial copper metallothionine. Nature Chem Biol **4:**582-583.

41) **Suzuki KT, Someya A, Komada Y, Ogra Y.** 2002. Roles of metallothionine in copper homeostasis: responses to Cu-deficient diets in mice. J Inorgan Biochem **88:**173-182.

42) **Ogra Y, Aoyama M, Suzuki KT.** 2006. Protective role of metallothionein against copper depletion. Arch Biochem Biophys **451:**112-118.

43) **Vita N, Platsaki S, Basle A, Allen SJ, Paterson NG, Crombie AT, Murrell JC, Waldron KJ, Dennison C.** 2015. A four-helix bundle stores copper for methane oxidation. Nature **525 (7567)**: 140-143.

44) **Kim HJ, Graham DW, DiSpirito AA, Alterman MA, Galeva N, Lavire CK, Asunskis D and Sherwood PMA**. 2004. Methanobactin, a copper-acquisition compound from methane-oxidizing bacteria. Science **305(5690)**: 1612-1615.

45) **Behling LA, Hartsel SC, Lewis DE, DiSpirito AA, Choi DW, Masterson LR, Veglia G, Gallagher WH**. 2008. NMR, mass spectrometry and chemical evidence reveal a different chemical structure for methanobactin that contains oxazolone rings. J Am Chem Soc. **130**: 12604-12605.

46) **El Ghazouani A, Baslé A, Firbank SJ, Knapp CW, Gray J, Graham DW, Dennison C.** 2011. Copper-binding properties and structures of methanobactins from *Methylosinus trichosporium* OB3b. Inorg Chem. **50**:1378–1391.

47) **Krentz BD, Mulheron HJ, Semrau JD, DiSpirito AA, Bandow NL, Haft DH, Vuilleumier S, Murrell JC, McEllistrem MT, Harstel SC and Gallagher WH**. 2010. A comparison of methanobactins from *Methylosinus trichosporium* OB3b and *Methylocystis strain* SB2 predicts methanobactin are synthesized from diverse peptide precursors modified to create a common core for binding and reducing copper ions. Biochemistry **49**:10117-10130.

48) **Bandow NL, Gallagher WH, Behling L, Choi DW, Semrau JD, Hartsel SC, Gilles VS, DiSpirito AA**. 2011. Isolation of methanobactin from the spent media of methane-oxidizing bacteria. Meth Enzymol **495**: 259-269.

49) **El Ghazouani A, Basle A, Gray J, Graham DW, Firbank SJ, Dennison C**. 2012. Variations in methanobactin structure influence copper utilization by methane-oxidizing Bacteria. Proc Natl Acad Sci USA. **109(22)**: 8400-8404.

50) **Kenney GE, Rosenzweig AC**. 2011. Chemistry and Biology of the copper chelator Methanobactin. ACS Chem. Biol. **7**: 260-268.

51**) Kenney GE, Goering AW, Ross MO, DeHart CJ, Thomas PM, Hoffman BM, Kelleher NL, Rosenzweig AC**. 2016. Characterization of methanobactin from *Methylosinus sp*. LW4. J Am Chem Soc. **138(35):**11124-7.

52) **Fru EC, Gray ND, McCann C, Baptista JdC, Christgen B, Talbot HM, El Ghazouani A, Dennison C, Graham DW**. 2011. Effects of copper mineralogy and methanobactin on cell growth and sMMO activity in *Methylosinus trichosporium* OB3b. Biosciences **8**:2887 - 2894.

53) **Choi DW, Zea CJ, Do YS, Semrau JD, Antholine WE, Hargrove MS, Pohl NL, Boyd ES, Geesey GG, Hartsel SC, Shafe PH, McEllistrem MT, Kisting CJ, Campbell D, Rao V, De la Mora AM and DiSpirito AA**. 2006. Spectral, Kinetic and Thermodynamic properties of Cu (I) and Cu(II) binding by methanobactin from *Methylosinus trichosporium* OB3b. Biochemistry **45**: 1442-1453.

54) **Bandow N, Gilles VS, Freesmeier B, Semrau JD, Krentz B, Gallagher W, McEllistrem MT, Hartsel SC, Choi DW, Hargrove MS, Heard TM, Chesner LN, Braunreiter KM, Cao BV, Gavitt MM, Hoopes JZ, Johnson JM, Polster EM, Schoenick BD, Umlauf AM and Dispirito AA**. 2012. Spectral and copper binding properties of methanobactin from the facultative methanotrophs *Methylocystis* strain SB2. J Inorg Biochem **110**: 72-82.

55) **Pesch ML, Hoffmann M, Christl I, Kraemer SM and Kretzschmar R**. 2013. Competitive ligand exchange between Cu-humic acid complexes and methanobactin. Geobiology **11(1)**: 44-54.

56) **Baral BS, Bandow NL, Vorobev A, Freemeier BC, Bergman BH, Herdendorf TJ, Fuentes N, Ellias L, Turpin E, Semrau JD and DiSpirito AA**. 2014. Mercury binding by methanobactin from *Methylocystis* strain SB2. J. Inorgan. Biochem. **141**:161-169.

57) **Choi DW, Do YS, Zea CJ, McEllistrem MT, Lee SW, Semrau JD, Pohl NL, Kisting CJ, Scardino LL, Hartsel SC, Boyd ES, Geesey GG, Riedel TP, Shafe PH, Kranski KA, Tritsch JR, Antholine WE, DiSpirito AA**. 2006. Spectral and thermodynamic properties of Ag(I), Au(III), Cd(II), Co(II), Fe(III), Hg(II), Mn(II), Ni(II), Pb(II), U(IV), and Zn(II) binding by methanobactin from *Methylosinus trichosporium* OB3b. J. *Inorg. Biochem*. **100**:2150–2161.

58) **Schalk I**. 2008. Metal trafficking via siderophores in gram-negative bacteria: Specificities and characteristics of the pyoverdine pathway. J Inorgan. Biochem. **102**: 1159-1169.

59**) Cooper SR, McArdle JV, Raymond KN**. 1978. Siderophore electrochemistry: Relation to intracellular iron release mechanism. Proc Natl Acad Sci USA **75**: 3551-3554.

60) **Li YM, Milne JC, Madison LL, Kolter R, Walsh, CT**. 1996. From peptide precursors to oxazole and thiazole-containing peptide antibiotics: microcin B17 synthase. Science **15(274)**: 1188-93.

61) **Kenney GE and Rosenzweig AC**. 2013. Genome mining for methanobactins. BMC Biology **11**:17.

62) **Summer KH, Litchmanneger J, Bandow NL, Choi DW, DiSpirito AA, and Michalke B.** 2011. The biogenic methanobactin is an effective chelator for copper in a rat model for Wilson disease. J. Trace Elements in Medicine and Biology **26(1)**: 36-41.

63) **Zischka H, Lichtmannegger J, Schmitt S, Jagemann N, Schulz S, Wartini D, Jennen L, Rust C, Larochette N, Galluzzi L, Chajes V, Bandow N, Gilles VS, DiSpirito AA, Esposito I, Goettlicher M, Summer KH, Kroemer G.** 2011. Liver mitochondrial membrane crosslinking and destruction in a rat model of Wilson disease. J Clin Invest **121:**1508-1518.

64) **Lichmannegger J, Leitinger C, Winner R, Schmitt S, Schulz S, Kabiri Y, Eberhagen C, Rieder T, Janik D, Neff F, Aichler M, DiSpirito AA, Bandow NL, Baral BS, Flatler A, Kremmer E, Denk G, Hohenester S, Eckardt-Schupp F, Dencher N, Adamski J, Merle U, Gotthardt DN, Kroemer G, Weiss KH, Zischka H.** 2016. Methanobactin: a new effective treatment strategy against acute liver failure in a Wilson disease rat model. J Clin Inves **126:**2721-2735.

65) **Vorobev A, Jagadevan S, Baral BS, DiSpirito AA, Freemeier BC, Begman BH, Bandow NL, Semrau JD**. 2013. Detoxification of mercury by methanobactin from *Methylosinus trichosporium* OB3b. Appl Environ Microbiol **79(19)**: 5918-5926.

66) **Kalidass B, Ul-Haque MF, Baral BS, DiSpirito AA, Semrau JD**. 2015. Competition between metals for binding to methanobactin enables expression of soluble methane monooxygenase in the presence of copper. Appl Environ Microbiol **81(3)**: 1024-1031

67) **Gu W, Ul Haque MF, Baral BS, Turpin EA, Bandow NL, Kremmer E, Flatley A, Zischka H, DiSpirito AA, Semrau JD**. 2016. A TonB-dependent transporter is responsible

for methanobactin uptake by *Methylosinus trichosporium* OB3b. Appl Environ Microbiol **82(6)**: 1917-1923.

68) **Gu W, Baral BS, DiSpirito AA, Semrau JD**. 2016. An aminotransferase is responsible for the deamination of the N-terminal leucine and required for formation of oxazolone ring A in methanobactin of *Methylosinus trichosporium* OB3b. Appl Environ Microbiol **83(1)** : 2 e03039-16

Table 1: Summary of proposals of copper, iron and active site of particulate methane monooxygenase (pMMO) in methanotrophs.

Group	Copper	Iron	Catalytic center	Techniques used
DiSpirito	2	2	Dioxybridged Fe-Fe center	EPR and Mossbauer
Dalton	2	2	Not determined	EPR
Chan	15-20	None	trinuclear Cu	EPR
Rosenzweig	2	None	Dinuclear Cu	Crystallography and XANES spectroscopy

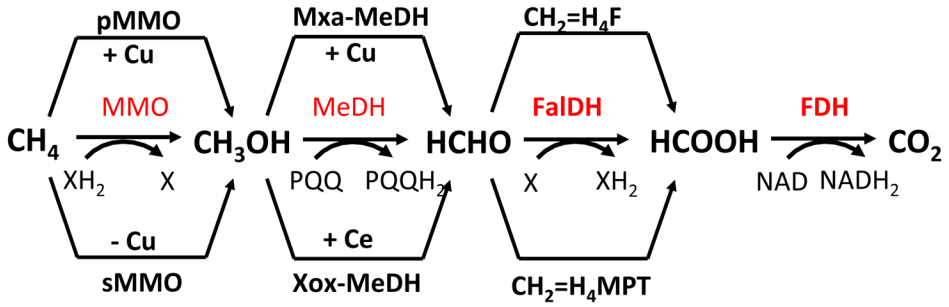

Figure 1: Schematic diagram of methane oxidation to carbon dioxide in a methanotroph *Methylococcus capsulatus* Bath. Abbreviations: sMMO, soluble MMO; pMMO, membrane associated MMO; Mxa-MeDH, Ca-dependent MeDH; XoX-MeDH, rare earth dependent MeDH; CH_3=H_4F, methylene tetrahydropholate; CH_3H_4MPT, methylene tetrahydromethopterin

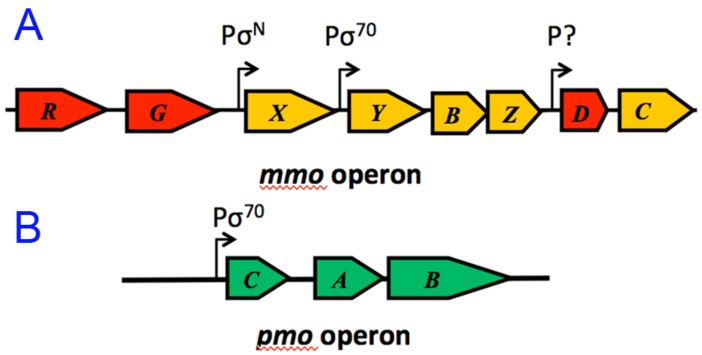

Figure 2: Schematic diagram of gene cluster of the soluble (A) and membrane-associated (B) methane monooxygenase in *Methylosinus trichosporium* OB3b. Red represents proposed regulatory genes, yellow represents structural genes of the sMMO and green represents structural genes of the pMMO (From Semrau et al., 2013).

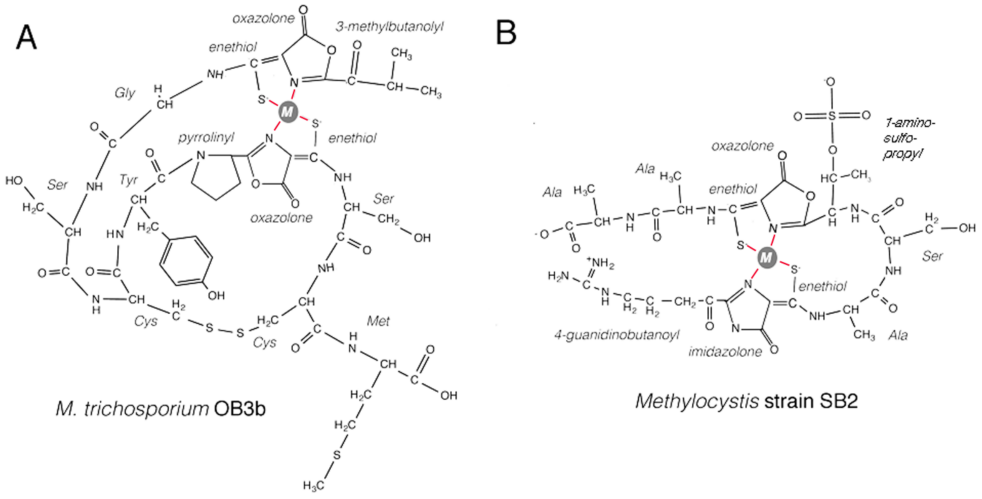

Figure 3: Chemical structures of methanobactin from *M. trichosporium* OB3b (A) and *Methylocystis strain SB2* (B). Abbreviation: M, metal that is coordinated by both rings and enethiol groups of methanobactin (From Baral et al.,2014).

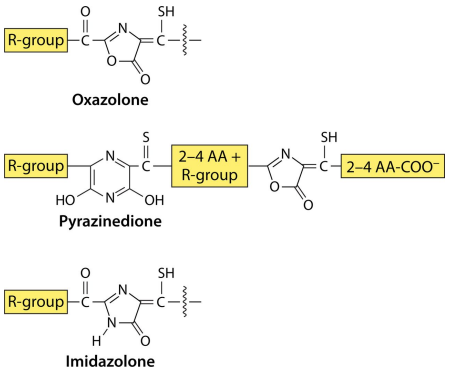

Figure 4: Core structures of methanobactin. (From DiSpirito et al., 2016)

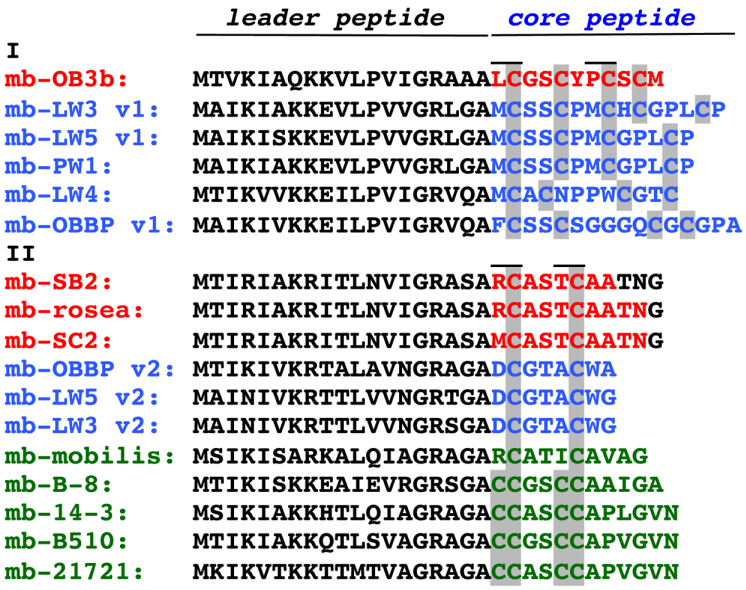

Figure 5: Putative methanobactin gene precursor peptide in methanotrophs and non-methanotrophs. (From DiSpirito et al., 2016)

CHAPTER 2

MERCURY BINDING BY METHANOBACTIN FROM *METHYLOCYSTIS* STRAIN SB2

Bipin S. Baral, Nathan L. Bandow, Alexy Vorobev, Brittani C. Freemeier, Brandt H. Bergman, Timothy J. Herdendorf, Nathalie Fuentes, Luke Ellias, Erick Turpin, Jeremy D. Semrau and Alan A. DiSpirito

Modified from the paper published in Journal of Inorganic Biochemistry

Abstract

Methanobactin (mb) is a post-translationally modified copper-binding compound, or chalkophore, secreted by many methane-oxidizing bacteria or methanotrophs in response to copper limitation. In addition to copper, methanobactin from *Methylosinus trichosporium* OB3b (mb-OB3b) has been shown to bind a variety of metals including Hg^{2+}. In this report, Hg binding by the structurally unique methanobactin from *Methylocystis* strain SB2 (mb-SB2) was examined and compared to mb-OB3b. Mb-SB2 is shown to bind the common forms of Hg found in aqueous environments, Hg^{2+}, $Hg(CN)_2$ and CH_3Hg^+. The spectral and thermodynamic properties of binding for each form of mercury differed. UV-visible absorption spectra suggested Hg^{2+} binds to both the oxazolone and imidazolone rings of mb-SB2, whereas CH_3Hg^+ appeared to only bind to the oxazolone ring. $Hg(CN)_2$ showed spectral properties between Hg^{2+} and CH_3Hg^+. Isothermal titration calorimetry (ITC) showed both $Hg(CN)_2$ and CH_3Hg^+ fit into two-site binding models. For $Hg(CN)_2$ the first site was exothermic and the second endothermic. Both binding sites in CH_3Hg^+ were exothermic, but at equilibrium the reaction never moved back to the baseline, suggesting a slow residual reaction. ITC results for Hg^{2+} were more complex and suggested a 3- or 4-site model. The

spectral, kinetic and thermodynamic changes following Hg binding by mb-SB2 also differed from the changes associated with mb-OB3b. Like mb-OB3b, copper did not displace Hg bound to mb-SB2. In contrast to mb-OB3b Hg^{2+} could displace Cu from Cu-containing mb-SB2 and preferentially bound Hg^{2+} over Cu^{2+}at metal to mb-SB2 molar ratios above 1.0.

Introduction

Methanobactin (mb) is a small, <1,200 Da, post-translationally modified, copper binding compound, or chalkophore, produced by many methane-oxidizing bacteria (methanotrophs) and potentially several non-methanotrophic bacteria as well based on bioinformatic analyses (1,2,3,4,17)**.** The molecule has been structurally characterized in 5 different methanotrophs (3, 5, 6,7,8), and this class of metal-binding peptides is characterized by the presence of one oxazolone ring and a second five or six membered ring, which is either an oxazolone, imidazolone or a pyrazinedione ring (Fig. 1) (3,5,6). Both rings are associated with an enethiol group, which together form the metal coordination site. Depending on the metal, the coordination site consists of one of the rings and its associated enethiol or both rings and associated enethiols [Table S1; 9]. The two rings are separated by 2 to 5 amino acids. Methanobactin from *M. trichosporium* OB3b (mb-OB3b) and from Methylocystis strain SB2 (mb-SB2) have different rings, amino acid composition, and molecular size. Despite these differences, the copper binding properties of the different form were similar, suggesting the pair of rings and associated enethiols confer the unique metal binding properties associated with this class of metal binding peptides (1,6,7,10,11,12,13,14). In addition to copper, mb from *M. trichosporium* OB3b (mb-OB3b) has also been shown to bind many transition and post-transition metals (Table S1) (9,19). In general, the binding

constants for most of the tested metals are well below those observed for copper, and copper will displace most other metals bound to mb-OB3b (9). However, some metals, such as Au^{3+} and Hg^{2+} appear to have binding properties similar to Cu^{2+}, and Cu^{2+} cannot displace these metals (9). A recent study by Vorobev et al. (19) demonstrated that mb-OB3b reduced Hg toxicity to *M. trichosporium* OB3b as well as to other methanotrophs even in the presence of Cu^{2+}. That study also showed that when exposed to equimolar concentrations of Hg^{2+} and Cu^{2+}, mb-OB3b will bind approximately 1 Hg for every 10 Cu. Here we extend current analyses of mercury binding by chalkophores by examining the mechanism of mercury binding by mb from *Methylocystis* species SB2 (Fig. 1) (mb-SB2). With the exception of the core methanobactin features stated above, the structure of methanobactin from *Methylocystis* strain SB2 differs from mb-OB3b (Fig.1). In mb-SB2 the redox active and metal binding amino acids found in mb-OB3b are replaced with Ala or are missing. The disulfide bond providing structural stability in mb-OB3b is also missing in mb-SB2. Thus, a comparison of the properties between these two forms of methanobactins provides a means to determine the role of the protein backbone in the mercury binding properties of the methanobactin.

Materials and Methods

Growth and isolation of mb-SB2

Methylocystis strain SB2 was cultured for mb-SB2 production in NMS medium (20) in sequential batch reactors. To maintain high (50 μM) concentrations of mb-SB2 in the spent medium, the copper concentrations in the reactor were varied, with two turnovers of NMS medium containing 0.2 μM Cu followed by one turnover of NMS media containing 1.0 μM $CuSO_4$. This sequence was generally repeated 2 to 4 times. Varying copper

concentrations in the culture media maintained high culture density and high concentrations of mb-SB2 in the spent medium.

Mb-SB2 was isolated from the spent medium as previously described (16). Purity of mb- SB2 samples was determined as previously described (3,8,10,11,16). Sample purity was > 97%, with breakdown fragments of mb-SB2 comprising most of the trace contaminants. Mb-SB2 samples used in this study contained less than 0.02 Cu per mb-SB2 as determined by atomic absorption spectroscopy described below. Following purification the samples were stored in the dark.

Acid hydrolysis of mb-SB2

Acid hydrolysis of the oxazolone ring in mb-SB2 was carried out in reaction mixtures containing 50μM mb-SB2 in 85μM acetic acid. The reaction mixtures were incubated at 25º C for 7-9 h and monitored by UV-visible spectroscopy to determine the time required for the complete hydrolysis of the oxazolone ring. In contrast to the procedure reported by Krentz et al. (3), the final pH of the solution was 6.8 and therefore did not require neutralization. The hydrolyzed solutions were kept on ice and used within 12 h of preparation.

Spectroscopy

UV-visible absorption, fluorescence, and circular dichroism spectroscopy were performed as previously described (10, 16). Briefly, either 50μM (for UV-visible absorption and fluorescence) or 500 μM (for UV-visible CD) mb-SB2 solutions were prepared in > 18MΩ▪cm H_2O and titrated with 10 mM metal stock solutions of metals also prepared in >

18MΩ▪cm H_2O.Titrations involved sequential 0.05 or 0.1 molar additions of metal to mb-SB2 pre-loaded into a cuvette and rapidly mixed by hand for 10 – 20 s. Spectra were taken immediately after mixing.

Metal determination

Copper and mercury were determined on an Agilent 55AA atomic absorption spectrometer (Agilent Technologies Inc., Santa Clara, CA) coupled with a vapor diffusion VGA system and run in either the flame or cold vapor mode for copper or mercury, respectively. All measurements were taken in triplicate. Mercury volatilization was determined as described by Takeuchi et al. (21) and modified as previously described by Vorobev, et al. (19)

Mb-SB2 mediated solubility of Hg^0

The solubility of Hg^0/Hg^{2+} in the aqueous phase was determined by incubating Hg^0 in > 18MΩ▪cm H_2O at room temperature (25ºC). Reaction solutions contained 25 µl Hg^0 in 25 ml of > 18MΩ▪cm H2O with or without the addition of either 50 µM mb-SB2 or 50 µM bovine serum albumin (BSA). Reaction mixtures were incubated at room temperature with continuous stirring. Periodically, the stirring was stopped for 30 sec and 1ml was removed from the top and diluted with 14 ml of 5% HCl, 5 % HNO_3 and 90% H_2O (v/v). Hg in the aqueous phase was determined by metal analysis as described above. Similar experiments were performed under anaerobic conditions in an atmosphere of 96% argon and 4% hydrogen inside an anaerobic chamber (Coy Laboratories, Michigan, United States). The presence of O_2 inside the chamber was monitored via a Coy oxygen/hydrogen meter and by

anaerobic indicator strips (Oxoid Ltd, Hants, UK). All solutions were checked for oxygen contamination before and after each experiment using Oxoid anaerobic indicator strips. Mercury concentrations in the aqueous phase were determined by atomic absorption spectroscopy in vapor diffusion mode as described above. Reaction mixtures containing mb-SB2 were also examined by UV-visible absorption spectroscopy. For spectral analysis of samples incubated under anaerobic conditions, the reaction mixtures were loaded into septa-sealable cuvettes, sealed in the Coy chamber and the spectra taken outside the chamber.

Kinetics of mercury and copper binding to mb-SB2

The rates for mercury and copper binding to mb-SB2 were determined by measuring absorption changes at 338 nm and 387 nm, using a four-syringe Biologic SFM/4000/S stopped flow reactor coupled to a MOS-500 spectrophotometer (Bio-Logic Science Instrument SA, Claix, France). Metal stock solutions of $CuCl_2$, $HgCl_2$, or $Hg(CN)_2$ were prepared in > 18MΩ▪cm H_2O. The stock solutions for mb-SB2 were prepared by dissolving freeze-dried mb- SB2 in > 18MΩ▪cm H_2O. The stock solutions of $CuCl_2$, $HgCl_2$ and mb-SB2 were chilled on ice, then filtered through a 0.22 μm filter before loading into sample syringes. The final concentration of the stock mb-SB2 after filtration was determined by UV-visible absorption spectroscopy as previously described (15). The path length for the cuvette used in the Biologic SFM/4000/S stopped flow reactor was 1.5 mm. The dead time of the system was 1.4 ms. The system was cooled and maintained at 4 °C. The reaction mixture contained 400 μM of mb-SB2 and either 40, 100, 200, 240, 280, 320, 360, 400, 600, 700, or 800 μM of $CuCl_2$, $HgCl_2$, or $Hg(CN)_2$. Rates obtained for each concentration were an average of a minimum of five traces. Traces following metal addition were divided by traces

with no metal additions before the traces were fit. The rates were determined by fitting the traces to the exponential function in Biokine operational software (Bio-Logic Science Instrument SA). Binding rates were calculated in mol metal bound per sec per mol mb-SB2 and reported as s^{-1}.

Copper and mercury mixed-metal binding experiments

Binding of mercury and copper in mixed metal conditions by mb-SB2 was determined in solutions containing $CuCl_2$, $HgCl_2$, $Hg(CN)_2$ or CH_3HgCl and mb-SB2 in molar ratios of copper to mercury to methanobactin of 0.25:0.25:1, 0.5:0.5:1, 1:1:1, 1.5:1.5:1, and 2:2:1. The solutions were incubated with stirring (200 rpm) at room temperature for 5 min. Following this incubation period, the samples were loaded on to pre-equilibrated Sep-Pak cartridges (Millipore Corporation, Billerica, MA USA) as previously described to separate methanobactin from unbound metal (15). Sep-Pak cartridges contain hydrophobic reverse-phase C-18 resin. Sep-Pak cartridges were washed with 6 ml of $> 18M\Omega\cdot cm$ H_2O three times, then eluted with 6 ml of 60 % acetonitrile : 40% H_2O (v/v). Copper and mercury were determined as described above in the reaction mixture, in the wash solution as well as in the sample eluent. Similarly, copper and mercury were measured in control solutions containing: i) mercury and copper only; ii) mercury and mb-SB2 only, and; iii) copper and mb-SB2 only.

Displacement of mb-SB2-bound metals

AgCl, $FeCl_3$, $CdCl_2$, $CoCl_2$, $NiCl_2$, $ZnSO_4$, $PbNO_2$, or $CuCl_2$ was added to mb-SB2 in a molar ratio of 1.1 metal per mb-SB2 and the UV-visible absorption spectrum between 200

and 500 nm determined. A second metal, either $HgCl_2$, $Hg(CN)_2$ or CH_3HgCl was added at an equimolar concentration and the UV-visible absorption spectra measured again. The UV-visible absorption spectra for each metal bound to mb-SB2 is unique (results not shown) and was used to determine displacement. The potential displacement of Cu(II) by $HgCl_2$, $Hg(CN)_2$ or CH_3HgCl was also assayed by metal analysis as described above for mixed-metal binding experiments.

Isothermal titration calorimetry (ITC)

Isothermal titration calorimetry (ITC) measurements were performed at 25 °C using a GE Microcal ITC200 microcalorimeter (GE Health Sciences, Piscataway, NJ, USA) to determine the affinity of mb-SB2 for different forms of mercury. Titrant solutions were 0.35, 1.0 or 4 mM CH_3HgCl, $HgCl_2$ and $Hg(CN)_2$ were prepared in > 18MΩ▪cm H_2O. A 100 mM CH_3HgCl stock solution was prepared first in CH_3OH and then diluted to 4 mM with > 18MΩ▪cm H_2O to achieve a final methanol concentration of 4% (v/v). Mercury compounds were then injected at volumes ranging from 1 – 2 µl into a cell containing 100 µM mb-SB2 stirred at 1000 rpm. Injections were added at 180 s intervals, with the length of each injection pre-determined by instrument software based on the volume of injection. The instrument was cleaned between experiments using > 18MΩ▪cm H_2O, and the sample cell also washed according to manufacturer recommendations when sample build-up was observed. Following each titration, the sample cell was also washed with 1 – 3 cell volumes of 100 µM mb-SB2 to remove any residual metal. The data were analyzed using nonlinear least-squares curve fitting in Origin 7.0 software (GE Health Sciences). Due to fitting limitations of the software, some of the data were fit by hand. Other more unusual titration curves had sections

that could not be fit and were listed as unable to fit (UTF). Origin 7.0 software requires the titration curve to return to zero in order to be fitted and in the case of CH_3HgCl binding to mb-SB2, the entire data curve was shifted along the y-axis by 2000 calories per mole to allow the curve to be fit by the software. Following this shift, the changes in enthalpy (ΔH) values were corrected by the magnitude of the shift before calculating the change in Gibbs free energy (ΔG). The stoichiometry for the binding of each form of mercury is indicated in Table 1 as calculated by the binding algorithm used by the Origin software.

Results

UV-visible absorption spectroscopy

The addition of $HgCl_2$, $Hg(CN)_2$, or CH_3HgCl to mb-SB2 showed absorption changes in the 240 to 300 nm range characteristic of metal-ligand charge transfer transitions in compounds containing thiol groups (Fig. 2) (22-26). The shape and absorption maxima in this spectral range have also been shown to differ for different metals bound to the same protein (22,23), which was also observed in the spectra in this region for the three different forms of mercury (Figs. 2A, 2C and 2E).

Based on the UV-visible absorption spectra changes following $HgCl_2$ additions between 0.1 and 0.7 Hg^{2+} per mb-SB2 (Figs. 2A and 2B), Hg^{2+} appeared to bind to both the oxazolone (338 nm) and imidazolone (387 nm) rings of mb-SB2 as evidenced by a decreased absorbance at 338 and 387 nm associated with the oxazolone and imidazolone rings, respectively. This was accompanied by a red shift of the 387 nm maxima to 402 nm with an additional increased absorbance at higher Hg^{2+} to mb-SB2 molar ratios. CH_3Hg^+, however, appeared to only bind to the oxazolone ring as little or no absorbance change at 387 nm was

observed (Figs. 2E and 2F) and required higher ratios of CH_3Hg+ per mb-SB2 to saturate the sample (~ 2.0 CH_3Hg+ per mb-SB2). The UV-visible absorption spectral change following $Hg(CN)_2$ additions had properties in between $HgCl_2$ and CH_3HgCl and was saturated at 0.5 $Hg(CN)_2$ per mb-SB2 (Figs. 2C and 2D). It should be noted here that $Hg(CN)_2$ is soluble in H_2O, but the dissociation constant is low and can form complexes such as $Hg(CN)_4^{-2}$ (27, 28). The UV-visible absorption spectra as well as the kinetic, metal displacement, fluorescence spectra and thermodynamic data, described below, all suggest mb-SB2 binds $Hg(CN)_2$ or one of the Hg-CN complexes and not the dissociated Hg^{2+}.

Previous studies on mb from *Methylosinus trichosporium* OB3b (mb-OB3b) demonstrated that CH_3Hg^+ bound to both oxazolone A and oxazolone B (19). In mb-OB3b, the two oxazolone rings are separated by five amino acids, while in mb-SB2 the two rings are separated by only two amino acids suggesting the imidazolone ring does not coordinate CH_3Hg^+ due to steric inhibition of the bulky methyl group. To test this hypothesis, the oxazolone group of mb-SB2 was selectively hydrolyzed, which may eliminate this apparent steric inhibition (Figs. S1A and S1B). Based on the UV-visible absorption spectra of the acid-hydrolyzed sample, the imidazolone group of acid-hydrolyzed samples of mb-SB2 failed to bind CH_3Hg^+ suggesting the imidazolone group does not bind this organic form of Hg (Figs. S1A and S1B). Fluorescence spectra (Figs. S2C and S2D), however, demonstrated acid-hydrolyzed sample does bind approximately one CH_3Hg^+ per mb-SB2. The decreased absorption in the 240-300 nm range of suggests CH_3Hg^+ binds to the enethiol groups in the absence of the oxazolone ring (Fig. S1A).

Steric inhibition by methyl group may still be responsible for the inability of the imidazolone ring to coordinate CH_3Hg^+, but this inhibition could not be verified by elimination of the oxazolone ring.

Under aerobic conditions, mb-SB2 appeared to increase the solubility of metallic Hg^0 as determined by its increased concentration in the aqueous phase and by the changes in the UV-visible absorption spectra of mb-SB2 in the reactions mixtures containing Hg (Figs. S3A and S3C). However, the UV-visible absorption spectral changes following incubation in the presence of Hg^0 were identical to Hg^{2+} suggesting Hg^0 was first oxidized to Hg^{2+} and then bound by mb- SB2 (Fig. 2 and S3A). A similar result could be obtained by the addition of a non-reactive protein, bovine serum albumin again suggesting the adventitious binding of Hg^{2+} to bovine serum albumin following the chemical oxidation of Hg^0 (Fig. S3C). To verify this observation, these experiments were repeated under anoxic conditions. Under such conditions, no Hg was detected in the aqueous phase, nor were spectral changes observed in mb-SB2 confirming mb-SB2 bound Hg^{2+} following the chemical oxidation of Hg^0 (results not shown). Volatile Hg^0 was never observed, suggesting no reduction of Hg^{2+} to Hg^0. Reduction of Hg^{2+} was expected, since both mb-OB3b and mb-SB2 have been shown to reduce Cu^{2+} to Cu^+ and mb-OB3b to reduce Au^{3+} to Au^0 (9-11). If reduction does occur, Hg remained associated with mb-SB2.

Fluorescence spectroscopy

With one exception, the fluorescence spectra following excitation at 341 nm and mercury addition to mb-SB2 differed from the spectra following copper addition (11). As observed following copper addition, all three forms of mercury resulted in an increased

emission at 427 – 441 nm (Figs. 3A, 3C and 3E). In the case of Cu^{2+}, the increase in emission stopped at a copper to mb-SB2 molar ratios of 0.4 Cu per mb-SB2 (11). With mercury, the increase in emission continued at Hg to mb-SB2 molar ratios between 2.0 and 6.0 depending on excitation wavelength and form of mercury added. In all cases, the increased emissions continued well beyond the saturation points observed for UV-visible absorption spectra, UV-visible CD spectra or ITC titrations (described below).

The increased emissions cannot be explained solely by internal quenching between the imidazolone and oxazolone rings, since a similar trend was observed following hydrolysis of the oxazolone ring (Fig. S2). In fact, as observed following Cu^{2+} addition (11) , the intensity of the emission spectra following Hg additions increased approximately two fold following acid- hydrolysis of the oxazolone ring. As previously observed (11), the emission spectra at 417 nm following excitation at 341 nm and following hydrolysis of the ring suggest the fluorescence properties of mb-SB2 is associated with the imidazolone ring (Fig. S2). The increased emission may be due to the binding of Hg to other functional groups in the molecule or to Hg^{2+} reduction to Hg^{+} or Hg^{0} followed by aggregate formation (29).

Following excitation at 394 nm and the addition of $HgCl_2$, $Hg(CN)_2$ or CH_3HgCl, the emission at 610 nm decreased and the emission at 441 nm increased (Fig. 3B, 3D, and 3F). The emission intensity at 441 nm following $HgCl_2$ addition was particularly unusual. The emission at 441 nm initially increased in a broad peak between 0 and 1.0 Hg per mb-SB2. This emission was followed by a decrease between 1.0 – 2.0 Hg per mb-SB2, and then by a splitting of the peak at higher Hg to mb-SB2 molar ratios (Fig. 3B). As observed following excitation at 341 nm, the intensity of the emission spectra following Hg additions increased approximately two fold following acid hydrolysis of the oxazolone ring (Figs. S2A and S2C).

UV-visible circular dichroism spectroscopy

As observed in mb-OB3b and other small molecules the UV-CD of mb-SB2 in the absence of any added metal was of an unordered polypeptide with strong negative shoulders at 202 nm and 223 nm and a positive band at 300 nm (Fig. 4A). The addition of Cu^{2+} resulted in a shift of the 202 to 215 nm and increased positive intensity at 264 nm between 0.1 and 0.5 Cu^{2+} per mb-SB2 followed by a decreased at higher Cu^{2+} to mb-SB2 molar ratios (Fig. 4 B and E). The UV-CD spectra following addition of $Hg2^{+}$ differed from the spectra following Cu^{2+} addition. Specifically, there was little to no change in the 202 nm range but a major increase in absorption at 242 nm at Hg^{2+} to mb-SB2 between 0.1 and 0.75 Hg^{2+} per mb-SB2. At higher Hg^{2+} to mb-SB2 molar ratios this absorption decreased (Figs. 4B and 4E verses Figs. 4C and 4F). The CD bands at 264 or at 242 nm following Cu^{2+} addition or Hg^{2+} addition, respectively, can be assigned to the metal-enethiol charge transfer transitions (23-25).

In contrast to the UV-CD spectra, the visible-CD spectra were complex following metal addition. The major properties of the CD spectra from mb-SB2 did not coincide with the absorption maxima suggesting potential charge transfer evens between the oxazolone and imidazolone rings (Fig. 4A) (30,31). Surprisingly, the intensity of the visible CD bands from mb-SB2 were approximately 100-fold high than that observed with mb-OB3b, which is probably a reflection of either the shorter distance between the oxazolone and imidazolone rings and/or to the absence of the disulfide bond in mb-SB2.

To assign the CD signals to each ring, the oxazolone ring was selectively hydrolyzed. Unfortunately, hydrolysis of the oxazolone ring in mb-SB2 resulted in the loss of all visible-CD properties in the absence of added metals (Fig. 4A and S4). The visible absorbance

maximum associated with the imidazolone ring (387 nm) was not affected by this treatment suggesting the CD bands in this region results from the dipolar interaction between the rings. New CD bands in the visible-CD occurred following the binding of Cu^{2+} (Fig. 4B) or Hg^{2+} (Fig. 4C) and allows assignment of the CD maxima at 300 and 380 nm to the imidazolone ring and at 343 nm to the oxazolone ring.

The addition of Cu^{2+} (Fig. 4B) or Hg^{2+} (Fig. 4C) resulted in an increased molar ellipticity as well as the development of coupled oscillators or an exciton couple, suggesting dimer formation (32-34). Consistent with dimer formation, the maximal changes in the CD spectra were observed at a molar ratio of 0.5 to 0.7 metal per mb-SB2. At higher ratios, such changes were reduced, suggesting dimer dissociation (Fig. 4E and 4F). Comparison of the CD spectra following addition of $CuCl_2$ (Fig. 4B), $HgCl_2$ (Fig. 4C) and CH_3HgCl (Fig. 4D) suggested the following: (1) the rotation following Cu^{2+} and Hg^{2+} binding are in opposite directions, and, (2) the conformational changes following CH_3HgCl additions were comparatively minor (Fig. 4D).

Previous studies on mb-OB3b demonstrated the metals that are coordinated by both rings utilize a two-step mechanism. The first step involves metal binding to one ring followed by a conformational change and then coordination to the second ring (9). On the other hand, metals that bind to only one of the rings show comparatively minor conformational changes as determined by the CD spectra following metal additions. The CD spectra following CH_3Hg^+ binding by mb-SB2 showed a similar trend, again suggesting the imidazolone group is not involved in CH_3Hg^+ coordination to mb-SB2.

Isothermal titration calorimetry (ITC)

Of the forms of mercury examined, only $Hg(CN)_2$ fit directly as two-site model (Table 1; Fig. 5D). The $Hg(CN)_2$ titration also differed from the other mercury titrations in that the second binding site was endothermic. Both results were unexpected, since mb-SB2 does not bind CN^- as measured by ITC, nor were any changes observed in the UV-visible absorption or fluorescence spectra following CN^- addition, suggesting little to no coordination of CN^- to mb-SB2, the results thus suggest mb-SB2 binds $Hg(CN)_2$ or one of the Hg-CN complexes and not the dissociated Hg^{2+}. CH_3HgCl also fit a two-site model (Fig. 5C), however, the CH_3HgCl titrations never moved back to zero as it approached equilibrium, i.e. at equilibrium each titration remained exothermic. The heat of dilution due to the mixing of the organic and aqueous phases was accounted for before attempting to fit the data, as was the addition of CH_3HgCl in 4% methanol solution to H_2O. However, a consistent thermodynamic change remained after reaching a molar ratio of 2:1 CH_3HgCl to mb-SB2 (Fig 5C). The residual heat may be a consequence of the high affinity thiol groups for CH_3Hg^+ (37). Mb-SB2 has two enethiol groups and 2 CH_3Hg^+ per mb- SB2 was required before the residual thermodynamic stabilized, whereas the equilibrium for both HgCl2 and $Hg(CN)_2$ was reached at 0.5 (Fig. 5A, 5B, and 5C). However, association to the thiol groups does not account for the consistent change in heat content as the ratio of CH_3Hg^+ per mb-SB2 increased above 2.0. The consistent thermodynamic change per injection may result from a CH_3Hg^+ ligand exchange with the already bound CH_3Hg-S-R (38). This potential ligand exchange would also account for the decreased thermodynamic change at higher CH_3Hg^+. As described in Materials and Methods, the entire data curve was shifted along the y-axis by 2000 calories per mole in order to fit the CH_3HgCl titration into a two-site model.

Following this shift, the enthalpy (ΔH) values were corrected by the magnitude of the shift before calculating the Gibbs free energy (ΔG). Data from $HgCl_2$ were more complex and suggested a three or four- site binding model. This complexity made fitting of the data to particular segments of the $HgCl_2$ curve impossible. Segments of the titration curves that could not be fit are listed as unable to fit (UTF) (Table 1).

Kinetics of Cu^{2+} and Hg^{2+} binding

The time course for the binding of Cu^{2+}, Hg^{2+} and $Hg(CN)_2$ to the oxazolone and imidazolone rings in mb-SB2 were measured as the decrease in absorbance at 341 and 389 nm, respectively, following stopped-flow mixing of mb-SB2 with $Cu^{2+,}$ Hg^{2+}, or $Hg(CN)_2$. The reaction was monitored at 4°C, since at 25°C less than 10% of the total absorbance change remained following stopped-flow mixing of the reaction sample (1.4 ms). However, even at4°C, initial Cu^{2+} binding rates could only be determined to the oxazolone ring. Binding rates to the oxazolone ring increased with increasing copper at low Cu^{2+} to mb-SB2 ratios with a maximum value of 496 ± 10 s^{-1} at 0.25 Cu^{2+} per mb-SB2 (Fig. S5, Table S2). Between 0.25 to 1.0 $Cu^{2+,}$ the rate decreased to 143 ± 3 s^{-1} at 1.0 Cu^{2+} per mb-SB2. Above 1.0 Cu^{2+} per mb-SB2 the rate increased to > 2000 s^{-1}. The observation that different trends were observed at different copper to mb ratios is common to both mb-OB3b and mb-SB2 (10,11). Previous studies have shown different spectral and thermodynamic properties of mb-OB3b and mb-SB2 at Cu^{2+} to mb ratios below 0.25 metal to mb ratio, at Cu^{2+} to mb ratios between 0.25 – 0.5, at Cu^{2+} to mb ratio between 0.5 to 1.0 and at Cu^{2+} to mb ratios above 1.0 (3,9-12). The results in figure S5 are consist with a model proposing that mb binds as a tetramer at low metal to mb ratios, as a dimer at metal to mb ratios between 0.25 and 0.5 mb

and as a monomer above 1.0 metal per mb. The decreasing rates between 0.25 and 1.0 Cu^{2+} per mb-SB2 may reflect the transitions from a tetramer to a dimer then to a monomer. Between 40 and 100% of the reaction was complete at 4 °C following stopped-flow mixing of Hg^{2+} to mb-SB2 (1.4 ms). Only minor (< 12% of the total absorbance change) secondary binding rates could be measured to the oxazolone and imidazolone rings (Table S3). $Hg(CN)_2$ binding rates by mb-SB2 could not be determined since 100% of the reaction was complete before mixing of the reaction mixture was complete (data not shown).

Metal binding in the presence of both Cu^{2+} and Hg^{2+}

To determine if mb-SB2 bound Hg^{2+}, $Hg(CN)_2$ (or one of its dissociated forms) or CH_3Hg^+ in the presence of $Cu^{2+,}$ mb-SB2 was incubated in the presence of both metals at different mercury to copper to mb-SB2 molar ratios. Preliminary analysis via UV-visible absorption spectroscopy indicated mb-SB2 does not bind $Hg(CN)_2$ or CH_3Hg^+ in the presence of Cu^{2+}. However, UV-visible absorption as well as copper and mercury analysis of the metals bound to mb-SB2 in the presence of both Cu^{2+} and Hg^{2+} demonstrated the binding of both metals (Fig. 6). At sub-stochiometric concentrations of Cu^{2+} and Hg^{2+} mb-SB2 showed a slight preference for Cu^{2+}. However, at Cu^{2+} and Hg^{2+} to mb-SB2 at or above saturation, mb-SB2 preferentially bound Hg^{2+} over Cu^{2+} (Fig. 6).

Metal displacement

Based on the results from the mixed metal experiments, the capacity of mercury compounds to displace metals bound to mb-SB2 was examined. Hg^{2+}, $Hg(CN)_2$ and CH_3Hg^+ was found to displace Fe^{3+}, Co^{2+}, Ni^{2+}, Zn^{2+}, and Pb^{2+}. Hg^{2+} was also found to displace Cd^{2+},

Ag^{+} and Cu^{2+} from mb-SB2 (Table S4). The displacement of Cu from mb-SB2 was surprising considering the high binding constant for Cu^{2+} (11). To determine the displacement rate the decrease in absorbance at 324 nm was measured at 4˚C (Fig. S6). The displacement showed an initial fast rate, $118 \pm 0.2\ s^{-1}$, representing <25% of the total reaction followed by a slow rate of $1.6 \pm 0.1\ s^{-1}$.

Discussion

Methanobactin appears to be the extracellular component of a copper acquisition system used by many methanotrophs (1,2,19) Consistent with its role in copper acquisition, the Cu binding constants for both mb-OB3b and mb-SB2 are > $1021\ M^{-1}$ (10,11). In addition to Cu, mb- OB3b has been shown to bind a variety of metals including Hg (18,19). Recent studies have also demonstrated that mb-OB3b will reduce the toxicity of Hg to the host organism as well as to other bacterial species tested even in the presence of Cu (19). In this report we show that mb from Methylocystis strain SB2 also binds the common forms of Hg found in the environment.

Although mb-OB3b and mb-SB2 have some similarities, they also represent the known diversity of methanobactins. For example, mb-OB3b forms a cross-linked cyclic structure and is partially composed of the redox active amino acids, Met, Tyr and Cys. Further, the two oxazolone rings of mb-OB3b are separated by five amino acids. Mb-SB2 is a much simpler molecule, with only two amino acids separating the oxazolone and imidazolone rings, and the reactive amino acids found in mb-OB3b are either missing or replaced with Ala. Thus, a comparison of mercury binding properties by these structurally different forms of methanobactin provides a means to determine the role of the peptide

backbone in the mercury binding. Previous comparisons in Cu^{2+} between mb-OB3b and mb-SB2 showed similar Cu binding properties (10,11) . The results presented here also suggest that the capacity to bind different forms of mercury is a common property of chalkophores. However, in contrast to the copper-binding properties, these two forms of methanobactin show different mercury binding properties. Regardless of the Hg : Cu : mb-OB3b molar ratio, the Hg to Cu molar ratio bound by mb-OB3b never exceeded 0.1 Hg to 1 Cu (23). Mb-SB2 on the other hand showed a Hg to Cu molar ratio between 0.5 to 6 depending on the Hg : Cu: mb-SB2 ratio. Also in contrast to mb-OB3b, Hg^{2+} was shown here to displace Cu from copper containing mb-SB2 and the displacement rate suggested an active process. One unexplained observation in this study was the increased fluorescence emissions of mb-SB2 following mercury binding. Increased emission was observed following Cu^{2+} addition to mb-SB2, however, the increase was comparatively small (11). Increased emissions are often observed following the physical disruption of two closely associated chromophores where exciton transfer occurs (29-42). The only chromophores in mb-SB2 are the imidazolone and oxazolone rings. If internal quenching does occur, elimination of the oxazolone ring should increase emission from the imidazolone ring, which is what was observed here. However, increased emissions from the imidazolone ring continued following mercury addition even in the absence of the oxazolone ring, suggesting an additional mechanism is involved. This second mechanism could not be determined from the data collected.

The results presented here also demonstrate that the binding of mercury compounds by methanobactin is a function of the heterocyclic rings and associated enethiols. The rest of the molecule appears to only provide the structure to coordinate the metal binding rings and

enethiol groups in an appropriate conformation. However, the structural differences between mb-SB2 and mb-OB3b appear to influence the mechanism of coordination and kinetics of binding. For example, mb-SB2 shows a greater capacity to bind Hg^{2+} in the presence of copper than does mb-OB3b (19). On the other hand, only the oxazolone ring and the two enethiols in mb-SB2 appear capable of binding CH_3Hg^+, whereas both oxazolone rings and enethiols of mb-OB3b are involved in CH_3Hg^+ coordination (19). The inability of the imidazolone ring in mb-SB2 to coordinate CH_3Hg^+ may reflect the overall structural differences between the two methanobactins, but the results presented here suggest the difference is due to the inability of the imidazolone ring to coordinate $CH3Hg^+$. Three types of rings have been identified in the five structurally characterized methanobactins (3,5,6,7,8), oxazolone, imidazolone and pyrazinedione rings, and the results presented here indicate the different rings may confer different properties to the molecule.

Conclusions

The data presented in this report demonstrate that different forms of methanobactin, mb-OB3b and mb-SB2, bind both inorganic and organic forms of mercury and that the binding properties are dependent on the two rings and associated enethiol groups. However, the results also demonstrate that in contrast to mb-OB3b, mb-SB2 will preferentially bind Hg^{2+} over Cu^{2+}. The data also suggest the structurally more rigid and complex mb-OB3b is a more selective Cu^{2+} binding molecule. Mb-SB2, on the other hand, behaves more like the copper-binding protein metallothionine (25), and will preferentially bind other metals such as Hg over Cu. The preferential binding of Hg suggest the enethiol groups in mb-SB2 may serve a more prominent role in metal binding than observed in mb-OB3b.

In addition to the environmental implications in the binding of toxic metals, the capacity to bind toxic metals may also have medical applications. In rat models, mb-OB3b has been shown to be an effective treatment for Wilson disease, a genetic defect in the copper-transporting ATPase7B resulting in copper accumulation and liver failure (43,44). Intravenous application of methanobactin results in the prompt release of copper from the liver into the bile (43). Based on the results presented here, methanobactin, especially mb-SB2, may prove an effective treatment for mercury poisoning.

Cu-mb-OB3b	copper containing methanobactin from *M. trichosporium* OB3b
Cu-mb-SB2	copper containing methanobactin from *Methylocystis* strain SB2
ITC	isothermal titration calorimetry
mb	methanobactin
mb-OB3b	methanobactin from *M. trichosporium* OB3b
mb-SB2	methanobactin from *Methylocystis* strain SB2
UTF	unable to fit

Acknowledgements

We thank Dr. V. Frasca at GE Microcal for assistance in modeling the ITC results. This research was supported by the Office of Science (BER), U.S. Department of Energy (JDS and ADS) and the National Science Foundation (CHE10112271) (ADS). Use of the ITC and stopped-flow systems were made possible through a generous gift from the Roy J. Carver Caritable Trust (Muscatine, Iowa).

References

1. **Semrau JD, DiSpirito AA, Yoon S.** 2010. Methanotrophs and copper. FEMS Microbiol Rev **34:**496-531.

2. **Semrau JD, Jagadevan S, DiSpirito AA, Khalifa A, Scanlan J, Bergman B, Freemeir BC, Baral BS, Bandow NL, Vorobev A, Haft DH, Vuilleumier S, Murrell JC.** 2013. Methanobactin and MmoD work in concert to act as the "copper switch" in methanotrophs. Environ Microbiol **15:**3077 - 3086.

3. **Krentz BD, Mulheron HJ, Semrau JD, DiSpirito AA, Bandow NL, Haft DH, Vuilleumier S, Murrell JC, McEllistrem MT, Hartsel SC, Gallagher WH.** 2010. A comparison of methanobactins from *Methylosinus trichosporium* OB3b and *Methylocystis* strain SB2 predicts methanobactins are synthesized from diverse peptide precursors modified to create a common core for binding and reducing copper ions. Biochemistry **49:**10117-10130.

4. **Kenney GE, Rosenzweig AC.** 2013. Genome mining for methanobactin. BMC Biol **11:**17.

5. **Kim HJ, Graham DW, DiSpirito AA, Alterman MA, Galeva N, Larive CK, Asunskis D, Sherwood PM.** 2004. Methanobactin, a copper-acquisition compound from methane-oxidizing bacteria. Science **305:**1612-1615.

6. **El Ghazouani A, Basle A, Firbank SJ, Knapp CW, Gray J, Graham DW, Dennison C.** 2011. Copper-binding properties and structures of methanobactins from *Methylosinus trichosporium* OB3b. Inorg Chem **50:**1378-1391.

7. **El Ghazouani A, Basle A, Gray J, Graham DW, Firbank SJ, Dennison C.** 2012. Variations in methanobactin structure influences copper utilization by methane-oxidizing bacteria. Proc Natl Acad Sci U S A **109:**8400-8404.

8. **Behling LA, Hartsel SC, Lewis DE, DiSpirito AA, Choi DW, Masterson LR, Veglia G, Gallagher WH.** 2008. NMR, mass spectrometry and chemical evidence reveal a different chemical structure for methanobactin that contains oxazolone rings. J Am Chem Soc **130:**12604-12605.

9. **Choi DW, Do YS, Zea CJ, McEllistrem MT, Lee SW, Semrau JD, Pohl NL, Kisting CJ, Scardino LL, Hartsel SC, Boyd ES, Geesey GG, Riedel TP, Shafe PH, Kranski KA, Tritsch JR, Antholine WE, DiSpirito AA.** 2006. Spectral and thermodynamic properties of Ag(I), Au(III), Cd(II), Co(II), Fe(III), Hg(II), Mn(II), Ni(II), Pb(II), U(IV), and Zn(II) binding by methanobactin from *Methylosinus trichosporium* OB3b. J Inorg Biochem **100:**2150-2161.

10. **Choi DW, Zea CJ, Do YS, Semrau JD, Antholine WE, Hargrove MS, Pohl NL, Boyd ES, Geesey GG, Hartsel SC, Shafe PH, McEllistrem MT, Kisting CJ, Campbell D, Rao V, de la Mora AM, Dispirito AA.** 2006. Spectral, kinetic, and thermodynamic properties of Cu(I) and Cu(II) binding by methanobactin from *Methylosinus trichosporium* OB3b. Biochemistry **45:**1442-1453.

11. **Bandow NL, Gilles VS, Freesmeier B, Semrau JD, Krentz B, Gallaghe W, McEllistrem MT, Hartse SC, Cho DW, Hargrove MS, Heard TM, Chesner LM, Braunreiter KM, Cao BV, Gavitt MM, Hoopes JZ, Johnson JM, Polster EM, Schoenick BD, A.M. U, DiSpirito AA.** 2012. Spectral and copper binding properties of methanobactin from the facultative methanotroph *Methylocystis* strain SB2. J Inorgan Biochem **110:**72 - 82.

12. **Choi DW, Semrau JD, Antholine WE, Hartsel SC, Anderson RC, Carey JN, Dreis AM, Kenseth EM, Renstrom JM, Scardino LL, Van Gorden GS, Volkert AA, Wingad AD, Yanzer PJ, McEllistrem MT, de la Mora AM, DiSpirito AA.** 2008. Oxidase, superoxide dismutase, and hydrogen peroxide reductase activities of methanobactin from types I and II methanotrophs. J Inorg Biochem **102:**1571-1580.

13. **Choi DW, Antholine WE, Do YS, Semrau JD, Kisting CJ, Kunz RC, Campbell D, Rao V, Hartsel SC, DiSpirito AA.** 2005. Effect of methanobactin on the activity and electron paramagnetic resonance spectra of the membrane-associated methane monooxygenase in *Methylococcus capsulatus* Bath. Microbiology **151:**3417-3426.

14. **Zahn JA, DiSpirito AA.** 1996. Membrane-associated methane monooxygenase from *Methylococcus capsulatus* (Bath). J Bacteriol **178:**1018-1029.

15. **Tellez CM, Gaus KP, Graham DW, Arnold RG, Guzman RZ.** 1998. Isolation of copper biochelates from *Methylosinus trichosporium* OB3b and soluble methane monooxygenase mutants. Appl Environ Microbiol **64:**1115-1122.

16. **Bandow NL, Gallagher WH, Behling L, Choi DW, Semrau JD, Hartsel SC, Gilles VS, Dispirito AA.** 2011. Isolation of methanobactin from the spent media of methane-oxidizing bacteria. Meth Enzymol **495:**259-269.

17. **Yoon S, Kraemer SM, DiSpirito AA, Semrau JD**. 2010. An assay for screening microbial cultures for chalkophore production. Environ Microbiol Rep **2(2)**: 295-303.

18. **Yoon S, Dispirito AA, Kraemer SM, Semrau JD.** 2011. A simple assay for screening microorganisms for chalkophore production. Meth Enzymol **495:**247-258.

19. **Vorobev A, Jagadevan S, Baral BS, Dispirito AA, Freemeier BC, Bergman BH, Bandow NL, Semrau JD.** 2013. Detoxification of mercury by methanobactin from *Methylosinus trichosporium* OB3b. Appl Environ Microbiol **79:**5918-5926.

20. **Whittenbury R, Phillips KC, Wilkinson JF.** 1970. Enrichment, isolation and some properties of methane-utilizing bacteria. J Gen Microbiol **61:**205-218.

21. **Takeuchi F, Negishi A, Maeda T, Kamimura K, Surgio T.** 2003. Volatilization and recovery of mercury from mercury wastewater produced in work in the course of laboratory work using *Acidthiobacillus ferrooxidans* SUG2-2 cells. J Biosci Bioeng **95:**239-244.

22. **Vasàk M, Kägi JH, H.A. H.** 1981. Zinc(II), cadmium(II), and mercury(II) thiolate transitions in metallothionein. Biochemistry **20:**2852.

23. **Nielson KB, Winge DR.** 1083. Order of metal binding in metallothionein. J Biol Chem **258:**13063 - 13069.

24. **Kägi JH, Valleee BL.** 1961. Metallothionein: a cadmium and zinc-containing protein from equine renal cortex. II. Physio-chemicals properties. J Biol Chem **263:**2435-2442.

25. **Nielson KB, Atkin CL, Winge DR.** 1985. Distinct metal-binding configurations in metallothionein. J Biol Chem **260:**5342-5350.

26. **Carson GK, Dean PAW, Sillman MJ.** 1981. A multinuclear (^{1}H, ^{13}C, ^{113}Cd) nuclear magneic resonance and magnetic circular dichroism spectroscopic study of thiolate

complexes of dadmium. Inorgan Chim Acta **56:**59-71.
27. **Lattamer WM, Hildebrand JH.** 1940. Reference Book of Inorganic Chemistry. The Macmillan Co. , New York, NY, USA.

28. **Beck MT.** 1987. Critical survey of stability constants of cyano complexes. Pure Appl Chem **59:**1703-1720.

29. **Kaupp M, von Schnering HG.** 1994. Dominance of linear 2-coordination in mercury chemistry: quasirelativistic ab initio pseudopentenial study of $(HgX_2)_2$ (X = F, Cl, Br, I, H). Inorg Chem **33:**2555 - 2564.

30. **Georgakopoulou S, van Grondelle R, van der Zwan G.** 2004. Circular dichroism of carotenoids in bacterial light-harvesting complexes: experiments and modeling. Biophys J **86:**3010-3022.

31. **Georgakopoulou S, van der Zwan G, Olsen JD, Hunter CN, Niederman RA, van Grondelle R.** 2006. Investigation of the effects of different carotenoids on the absorption and CD signals of light harvesting 1 complexes. J Phys Chem B **110:**3354-3361.

32. **Strickland EH, Mercola D.** 1976. Near-ultraviolet tyrosyl circular dichroism of pig insulin monomers, dimers, and hexamers. Dipole-dipole coupling calculations in the monopole approximation. Biochemistry **16:**3875-3884.

33. **Goldman J, Carpenter FH.** 1974. Zinc binding, circular dichroism, and equilibrium sedimentation studies on insulin (bovin) and several of its derivatives. Biochemistry **13:**4566-4574.

34. **Superchi S, Giorgio E, Rosini C.** 2004. Structural determinatins by circular dichroism spectra analysis using coupled oscillator methods: an update of the applications of the DeVoe polarizability model. Chirality **16:**422-451.

35. **Seibt J, Lohr A, Wurthner F, Engel V.** 2007. Circular dichroism and absorption spectroscopy of merocyanine dimer aggregates: molecular properties and exciton transfer dynamics from time-dependent quantum calculations. Phys Chem Chem Phys **9:**6214-6218.

36. **Amirbahman A, Reid AL, Haines TA, Kahl JS, Arnold C.** 2002. Association of methylmercury with dissolved humic acids. Environ Sc Techol **36:**690-695.

37. **Yoon S-J, Diener LM, Bloom PR, Nater EA, Bleam WF.** 2005. X-ray absorption studies of methylmercury-binding sites in humic substances. Geochim Cosmochim Acta **69:**1111-1121.

38. **Rabenstein DL, Reid RS.** 1984. Nuclear magnetic resonance studies of the solution chemistry of metal complexes. 20. Ligand-exchange kinetics of methylmercury(II)-thio complexes. Inorg Chem **23:**1246-1250.

39. **Vandal GM, Fitzgerald WF, Rolfnus KR, Lamborg CH.** 1995. Modeling the elemental mercury cycle in Pallette Lake, Wisconsin, USA. Water Air Soil Pollut **80:**529-538.

40. **Ye J, Sun K, Zhao Y, Yu Y, Lee CK, Cao J**. 2012. Excitonic energy transfer in light-harvesting complexes in purple bacteria. J Chem Phys 136:245104-245104-18).

41. **Stirbet A.** 2013. Excitonic connectivity between photosystem II units: what is it, and how to measure it? Photosynth Res **116:**189 - 214.

42. **Freer AA, Prince SM, Sauer K, Papiz MZ, Hawthornthwaite-Lawless AM, McDermott G, Cogdell RJ, Isaacs NW**. 1996. Pigment-protein interactions and energy transfer in the antenna complex of the photosynthetic bacterium. Structure **4**:449-462.

43. **Summer KH, Lichtmannegger J, Bandow N, Choi DW, DiSpirito AA, Michalke B.** 2011. The biogenic methanobactin is an effective chelator for copper in a rat model for Wilson disease. J Trace Elem Med Biol **25:**36-41.

44. **Zischka H, Lichtmannegger J, Schmitt S, Jagemann N, Schulz S, Wartini D, Jennen L, Rust C, Larochette N, Galluzzi L, Chajes V, Bandow N, Gilles VS, DiSpirito AA, Esposito I, Goettlicher M, Summer KH, Kroemer G.** 2011. Liver mitochondrial membrane crosslinking and destruction in a rat model of Wilson disease. J Clin Invest **121:**1508-1518.

Table 1. Thermodynamic parameters for $HgCl_2$, $Hg(CN)_2$ and CH_3ClHg binding to mb-SB2 at 25 ˚C

Parameter	$HgCl_2$	CH_3HgCl	$Hg(CN)_2$
N_1 (Hg mb-SB2^{-1})	UTF†	0.62	0.19
K_1 (M^{-1})	UTF	1.2×10^8	7.5×10^7
$^{\Delta H}{}_1$ (cal mol-1)	UTF	-11,190*	-11800
ΔS_1 (cal mol^{-1}deg^{-1})	UTF	6.07	-3.55
ΔG_1 (cal mol^{-1})	UTF	-13,000*	-10,742
N_2 (Hg mb-SB2^{-1})	0.37	1.52	0.30
K_2 (M^{-1})	7.5×10^9	1.7×10^6	1.8×10^6
ΔH_2 (cal mol^{-1})	-25,000	-8,300*	9,000
ΔS_2 (cal mol^{-1}deg^{-1})	-38.7	7.4	58.8
ΔG_2 (cal mol^{-1})	-13,462	-10,506*	-8,531
N_3 (Hg mb-SB2^{-1})	0.07	-	-
K_3 (M^{-1})	6.87×10^6	-	-
ΔH_3 (cal mol^{-1})	-5800	-	-
ΔS_3 (cal mol^{-1}deg^{-1})	11.8	-	-
ΔG_3 (cal mol^{-1})	-9318	-	-
$\chi 2$	8.36×10^5	1.48×10^5	2.04×10^5

*calculated values following a 2000 cal mol^{-1} shift.

†UTF, unable to fit

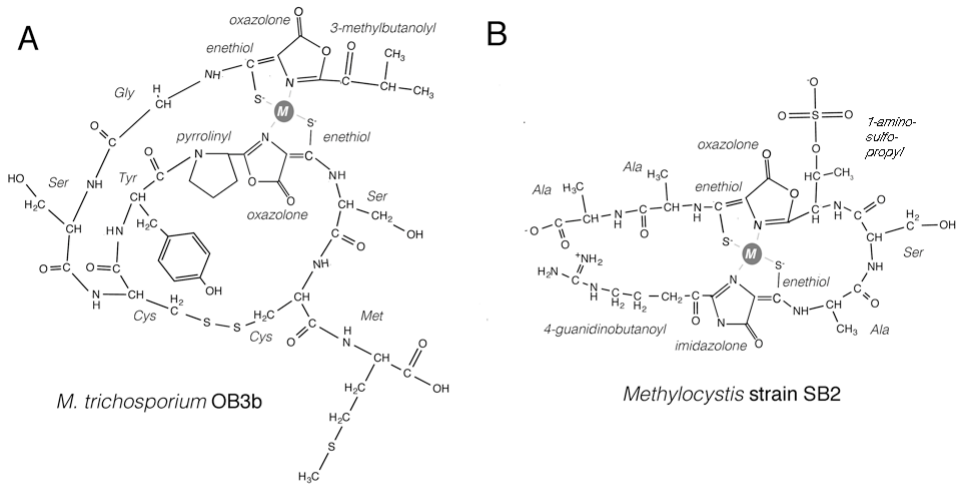

Figure 1. Chemical structures of methanobactin from *M. trichosporium* OB3b (A) and *Methylocystis* strain SB2 (B). Abbreviation: M, metal that is coordinated by both rings and enethiol groups of methanobactin.

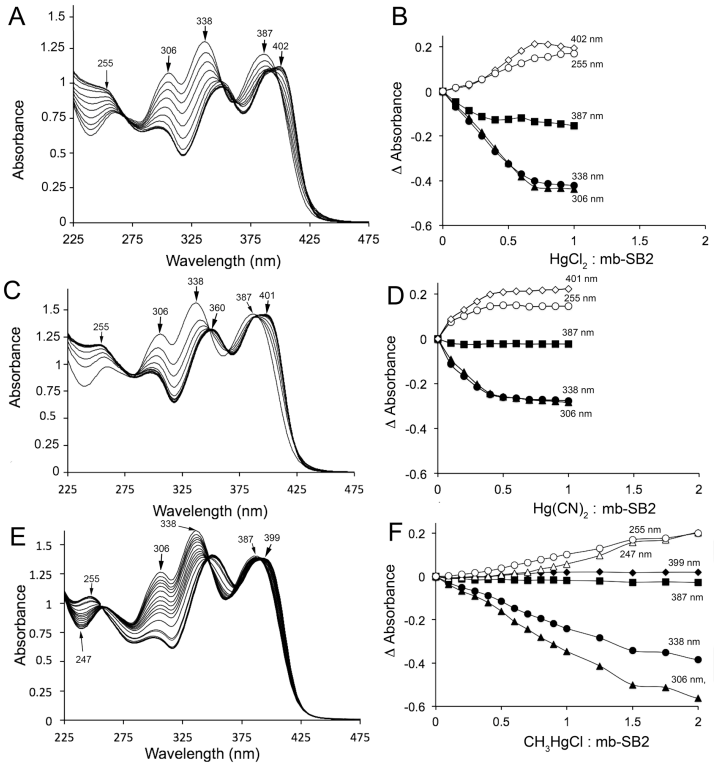

Figure 2. UV-visible absorption spectra of mb-SB2 as isolated and following the addition of: $HgCl_2$ (A, B); $Hg(CN)_2$ (C, D) or CH_3ClHg (E, F). Absorbance changes at 247 ( ), 255 (○)

306 (▲), 338 (●), 387 (■), 399 (♦) and 402/401 nm (◊) following the addition of $HgCl_2$ (B), $Hg(CN)_2$ (D), or CH_3HgCl (F).

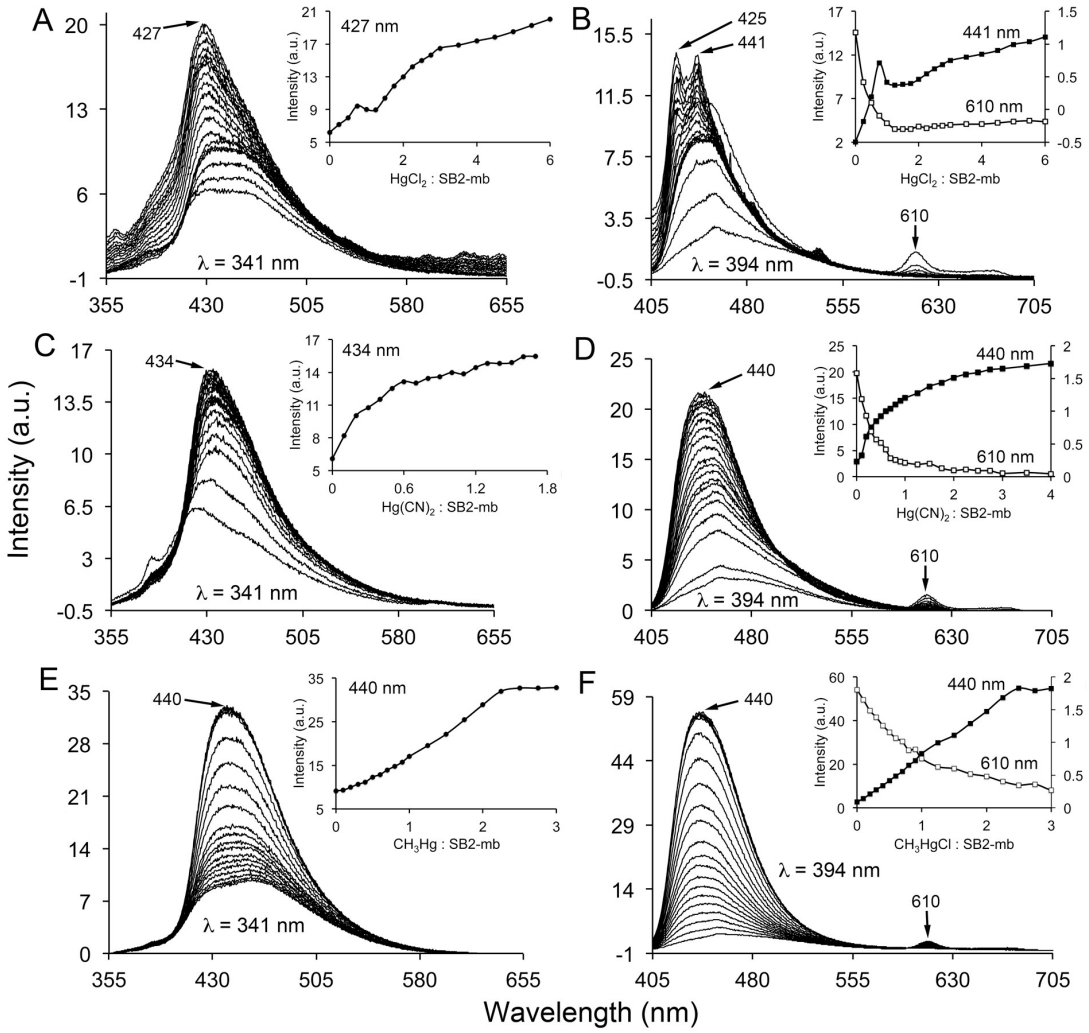

Figure 3. Emission spectra from mb-SB2 following excitation at 341 (A, C and E) or 394 nm (B, D and F) as isolated and following the addition of $HgCl_2$ (A and B), $Hg(CN)_2$ (C and D), or CH_3HgCl (E and F). Inserts emission intensities at 427 (A), 434 (C) or 440 (●) following excitation at 341 nm and at 441 or 440 (■) and 610 (□) following excitation at 394 nm (B, D, and F).

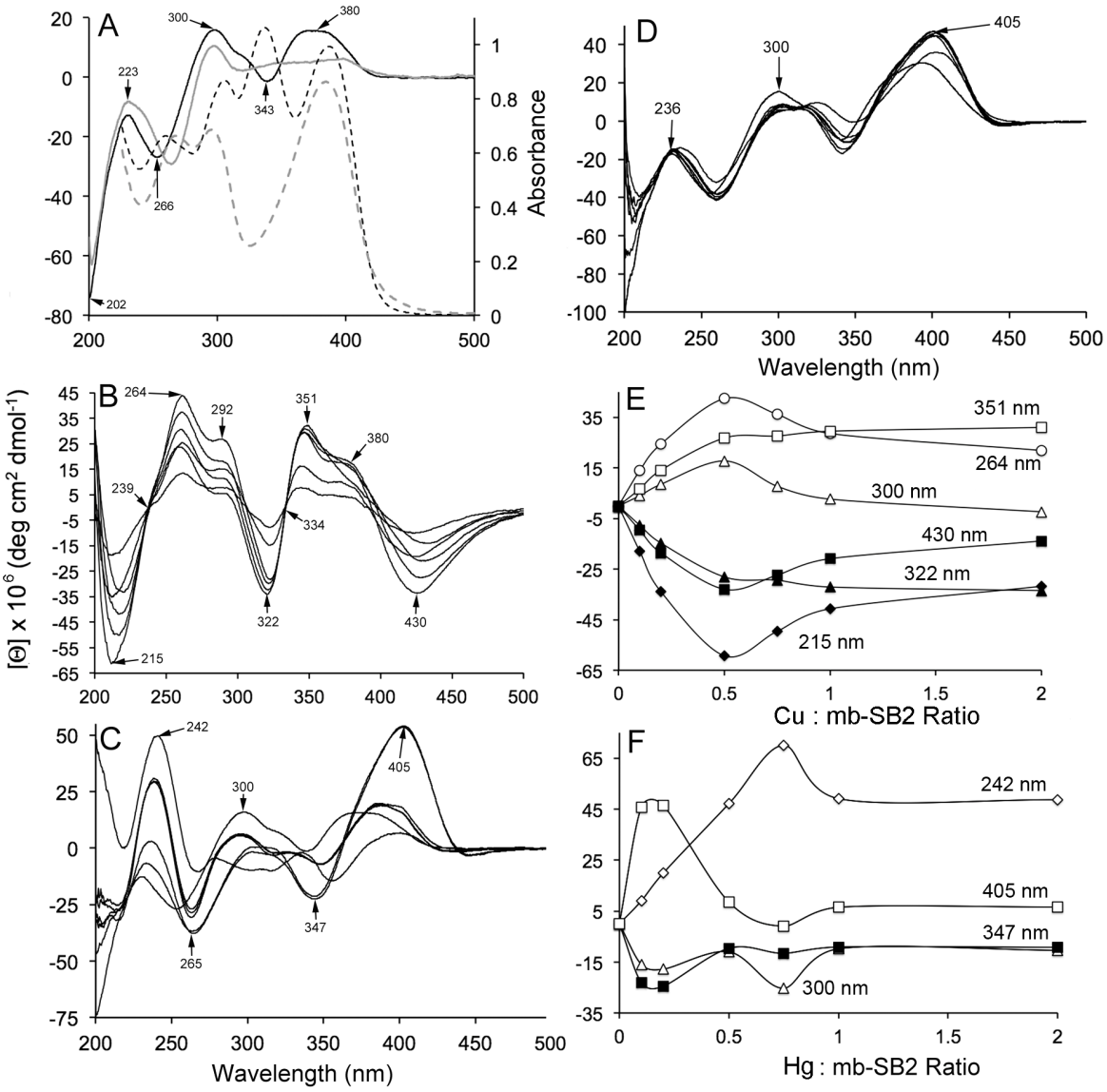

Fig. 4. (A) UV-visible absorption (———) Circular dichroism (—) spectra of mb-SB2 as isolated and following acid hydrolysis of the oxazolone ring (— —) and (—)UV-visible circular dichroism of mb-SB2 as isolated and following the addition of (B) 0.1, 0.2, 0.5 0.75, 1.0 and 2.0 $CuCl_2$; (C) 0.2, 0.5, 0.75, 1.0 and 2.0 $HgCl_2$; and (D) 0.2, 0.5, 0.75, 1.0 and 2.0 CH_3HgCl per mb-SB2. (E) Change in molar ellipticity at 215 (♦), 264 (O), 300 (Δ), 322(▲), 351 (□), and 430 (■) nm following the addition of $CuCl_2$. Change in molar ellipticity at 242 (◊), 300 (Δ), 347 (■) and 405 (□) nm following the addition of $HgCl_2$.

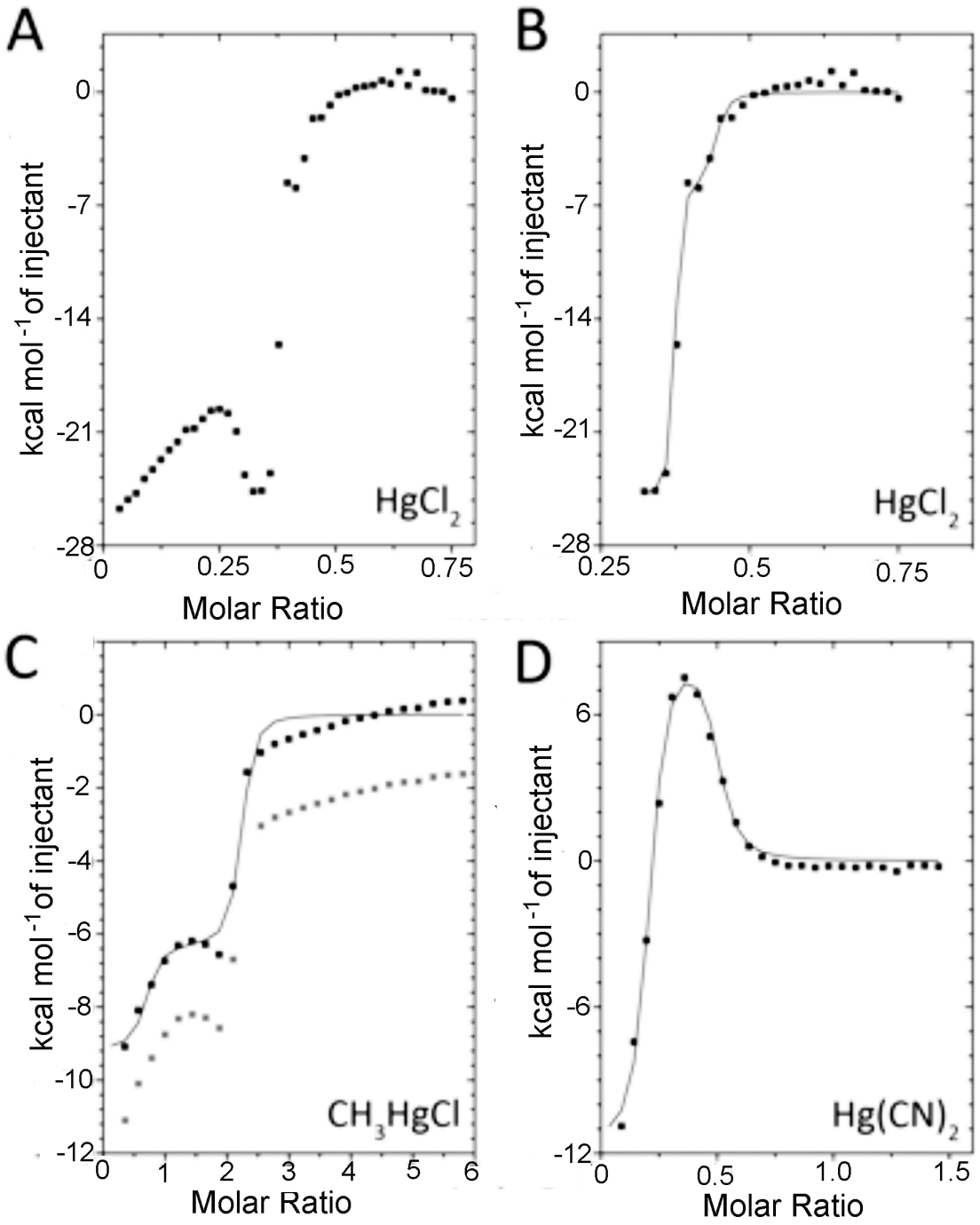

Figure 5 Fig. 5. A. Binding isotherm following the addition of $HgCl_2$ to mb-SB2. B. The binding isotherms for the second and third binding sites of $HgCl_2$ of mb-SB2. C. The binding isotherm following the addition of CH_3HgCl to mb-SB2 (●) and following a 2000 cal per mole adjustment to the binding isotherm (●). D. The binding isotherm following the addition of $Hg(CN)_2$ to mb-SB2. The solid lines in panels B, C and D shows the curve fitting for a two-site binding algorithm.

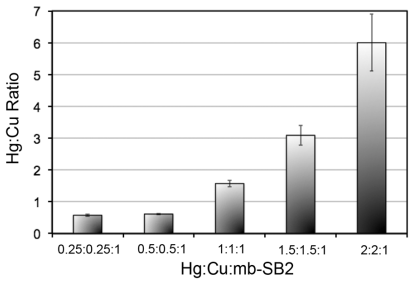

Figure 6 Ratio of Hg to Cu bound to mb-SB2 following incubaction of the mb-SB2 in solutions containing Cu2+, Hg2+ and mb-SB2 in molar ratios of 0.25:0.25:1, 0.5:0.5:1, 1:1:1, 1.5:1.5:1, and 2:2:1, respectively. Error bars represent the pooled standard deviations.

Supplemental Information

Table S1. Metals tested for binding to methanobactin from *M. trichosporium* OB3b. Results from Choi et al. (1,2) and Bandow et al. (unpublished results). Abbreviations: Oxa, oxazolone, K_1, binding constant, nd, not determined.

Metal	Rings of mb-OB3b			Metal	Rings of mb-OB3b		
	Oxa A	Oxa B	K_1 (M^{-1})		Oxa A	Oxa B	K_1 (M^{-1})
Cr^{3+}	-	-	nd	Ag^{+}	+	+	2.6×10^{7}
Cr^{6+}	+	+	nd	Sn^{+2}	+	-	nd
Mn^{+2}	+	-	7.7×10^{5}	Cd	+	-	1.3×10^{6}
Fe^{+2}	+	-	nd	Al^{+}	+	-	nd
Fe^{+3}	+	-	9.7×10^{5}	Pt^{+4}	+	+	nd
Co^{+2}	+	-	1.1×10^{6}	Au^{+3}	+	+	1.0×10^{5}
Ni^{+2}	+	-	4.9×10^{5}	Hg^{+2}	+	+	9.9×10^{6}
Cu^{2+}	+	+	3.3×10^{34}	Nd^{+3}	-	-	nd
Cu^{+}	+	+	nd	Ce^{+3}	+	+	nd
Zn	+	-	4.5×10^{6}	Pr^{+3}	-	-	nd
Mo^{+2}	+	-	nd	U^{6+}	+	+	nd
Pd^{+2}	+	+	6.8×10^{5}				

Table S2. Rates of Cu^{2+} binding to the oxazolone and imidazolone rings of mb-SB2 at different Cu^{2+} to mb-SB2 at 4°C.

Cu^{2+} : mb-SB2 Ratio	**Ring**	**Rate 1 Percent Reaction**	**Rate 1 Rate (s^{-1})**	**Rate 2 Percent Reaction**	**Rate 2 Rate (s^{-1})**
	Oxazolone				
0.1		85	237 ± 5	-	-
0.25		61	496 ±10	15	11 ± 1
0.5		60	378 ± 3	19	13 ± 0.05
0.6		58	301 ± 2	15	17 ± 0.1
0.7		38	237 ± 3	9	32 ± 0.3
0.8		40	177 ± 1	5	18 ± 0.6
0.9		24	183 ± 2	7	20 ± 0.3
1.0		14	143 ± 3	10	19 ± 2
1.25		100	>2000	12	7 ± 0.1
1.5		100	>2000	-	-
1.75		100	>2000	-	-
2.0		100	>2000	-	-
	Imidazolone				
0.1		100	>2000	-	-
0.25		100	>2000	-	-
0.5		100	>2000	-	-
0.6		97.3	>2000	2.7	10 ± 0.2
0.7		100	>2000	-	-
0.8		100	>2000	-	-

Table S2 continued

0.9	100	>2000	-	-
1.0	97.5	>2000	2.5	4 ± 0.03
1.25	100	>2000	-	-
1.5	100	>2000	-	-
1.75	100	>2000	-	-
2.0	100	>2000	-	-

Table S3. Rates of Hg^{2+} binding to the oxazolone and imidazolone rings of mb-SB2 at different Hg^{2+} to mb-SB2 at 4°C.

Hg : mb-SB2 Ratio	**Ring**	**Rate 1 Percent Reaction**	**Rate 1 Rate (s^{-1})**	**Rate 2 Percent Reaction**	**Rate 2 Rate (s^{-1})**	**Rate 3 Percent Reaction**	**Rate 3 Rate (s^{-1})**
	Oxazolone						
0.1		100	>2000	-	-	-	-
0.25		100	>2000	-	-	-	-
0.5		100	>2000	-	-	-	-
0.6		97.4	>2000	2.6	2.4±0.03	-	-
0.7		97.6	>2000	2.4	3.7±0.02	-	-
0.8		100	>2000	-	-	-	-
0.9		100	>2000	-	-	-	-
1.0		100	>2000	-	-	-	-
1.25		97.7	>2000	2.3	2.6±0.07	-	-
1.5		97.7	>2000	2.3	2.3±0.04	-	-

Table S3 continued

1.75	97.7	>2000	2.3	2.3±0.03	-	-
2.0	97.7	>2000	2.3	4.4±0.16	-	-
Imidazolone						
0.1	100	>2000	-	-	-	-
0.25	100	>2000	-	-	-	-
0.5	100	>2000	-	-	-	-
0.6	100	>2000	-	-	-	-
0.7	100	>2000	-	-	-	-
0.8	100	>2000	-	-	-	-
0.9	100	>2000	-	-	-	-
1.0	95.3	>2000	4.7	11.1±1.2	-	-
1.25	88.2	>2000	7.1	2.6±0.07	4.7	2.1±0.009
1.5	88.1	>2000	9.5	2.3±0.04	2.4	2.3±0.006
1.75	85.8	>2000	9.5	2.3±0.03	4.7	2.4±0.006
2.0	88.2	>2000	7.1	4.4±0.16	4.7	2.2±0.004

Table S4. Mercury displacement of metals bound to mb-SB2

Initial Metal Addition	**Displacement Metal**		
	$HgCl_2$	**$Hg(CN)_2$**	**CH_3HgCl**
Fe^{3+}	+	+	+
Ni^{2+}	+	+	+
Zn^{2+}	+	+	+

Table S4 continued

Co^{2+}	+	+	+
Cd^{2+}	+	-	-
Pb^{2+}	+	+	+
Ag^{+}	+	-	-
Cu^{2+}	+	-	-

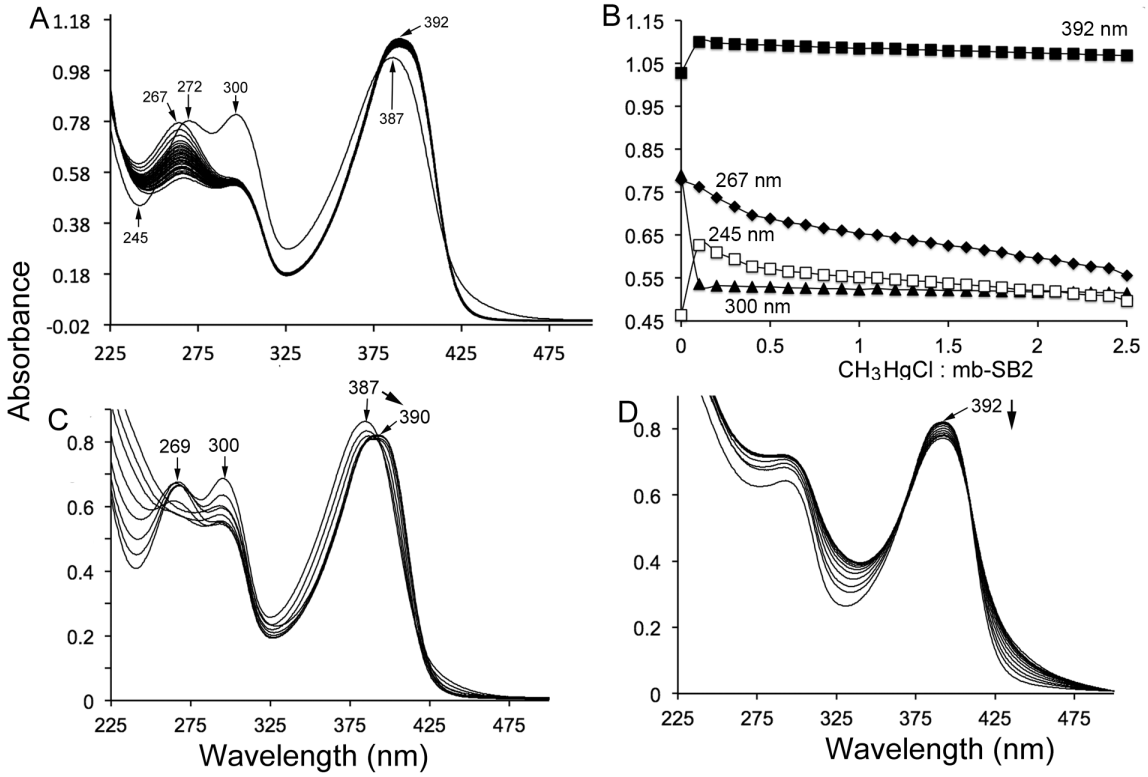

Fig S1. A. UV-visible absorption spectra of mb-SB2 following acid hydrolysis of the oxazolone ring and following the addition CH_3HgCl. B. Absorbance changes at 245 (□), 267 (◆), 300 (▲) and 392 (■) nm following the addition of CH_3HgCl to acid hydrolyzed-mb-SB2. C. UV-visible absorption spectra of acid hydrolyzed mb-SB2 following the addition 0.1, 0.2, 0.3, 0.4, 0.5, 0.6 and 0.7 $HgCl_2$ per AH-mb-SB2. D. UV- visible absorption spectra of acid hydrolyzed mb-SB2 following the addition 0.8, 0.9, 1.0, 1.1, 1.2, 1.3, 1.4, 1.5, 1.6, 1.7 and 1.8 $Hg(CN)_2$ per AH-mb-SB2.

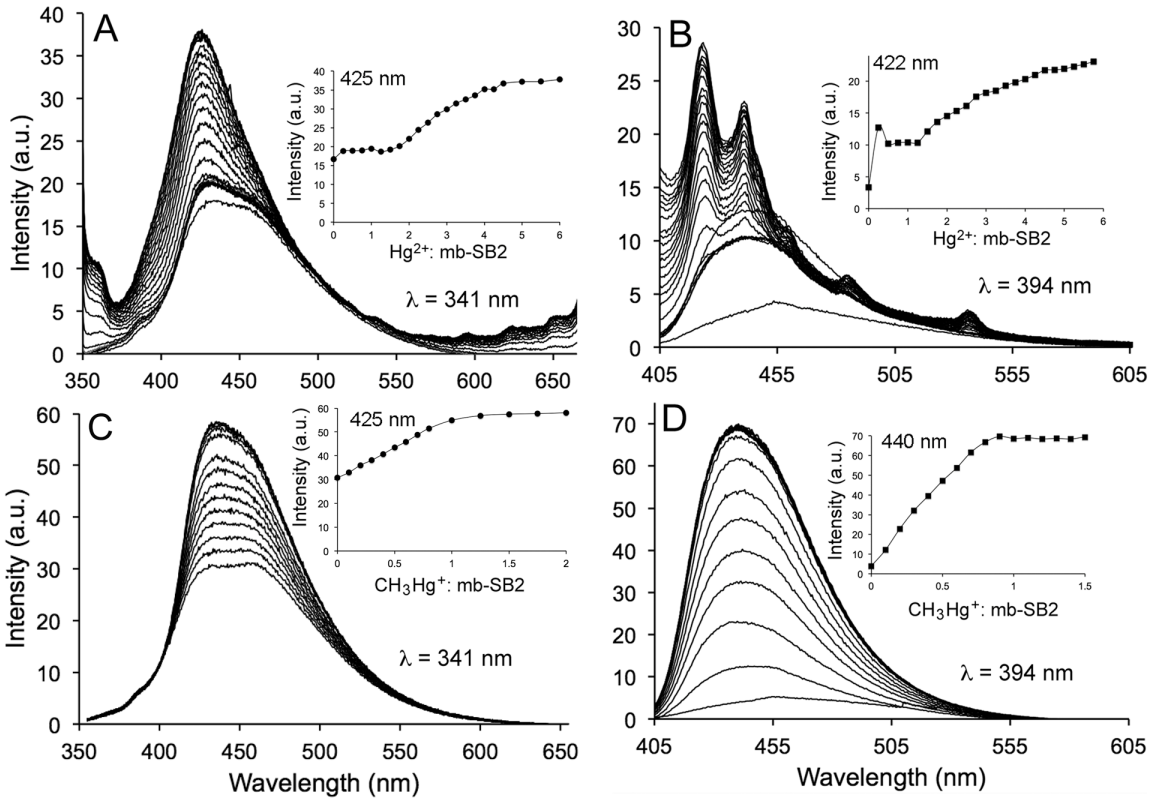

Fig. S2. Emission spectra from acid hydrolysed-mb-SB2 following excitation at 341 (A and C) and at 394 nm (B and D) as isolated and following the addition of $HgCl_2$ (A and B), or CH_3HgCl (C and D) . Inserts emission intensities at 425 nm (A and C) (●) following excitation at 341 nm and at 422 or 440 nm (■) following excitation at 394nm (B and D).

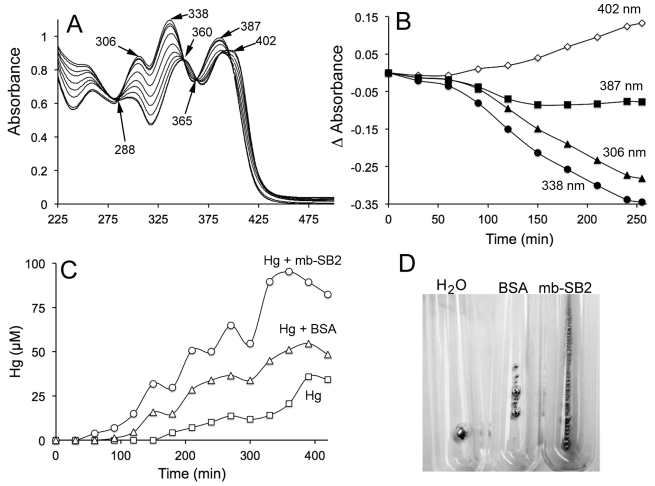

Fig S3. (A). Spectral changes in mb-SB2 when incubated in the presence of Hg(0) in H_2O under aerobic conditions over a 400 minute period. B) Changes in absorbance of Fig. 2A at 306 (▲), 338 (●), 387 (■) and at 402 (◇) nm. C) Solubilization of Hg^0 in H_2O under aerobic conditions (□), in the presence of 50μM BSA (△), and in the presence of 50μM mb-SB2 (○). Spectral reading were taken every 30 min. D) Hg(0) in the aqueous phase after incubation for 400 min in H_2O (H_2O), in 50μM BSA in H_2O (BSB) and in 50 μM mb-SB2 in H_2O (mb-SB2).

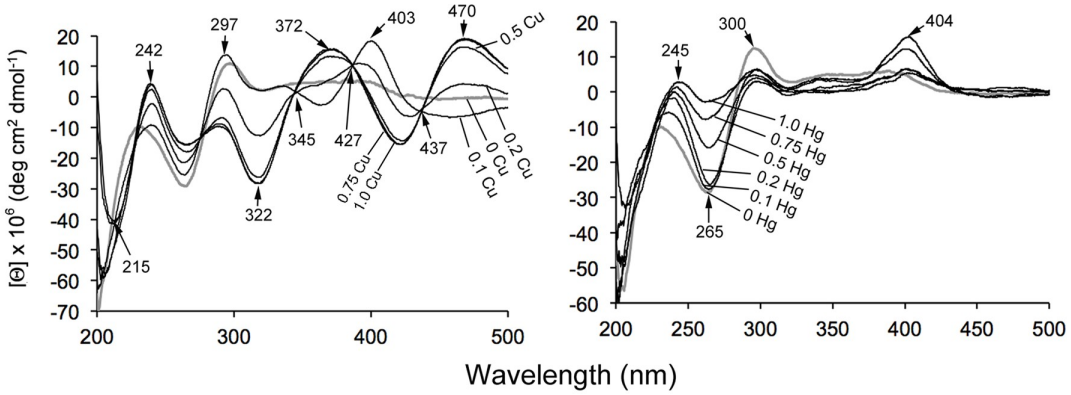

Fig. S4. UV---visible cirular dichroism spectra of mb-SB2 following acid hydrolysis of the oxazolone ring and following the addition of (A) 0.1, 0.2, 0.5 0.75, 1.0 and 2.0 $CuCl_2$ per mb-SB2 and (B) following the addition of 0.2, 0.5, 0.75, 1.0 and 2.0 $HgCl_2$ per mb-SB2.

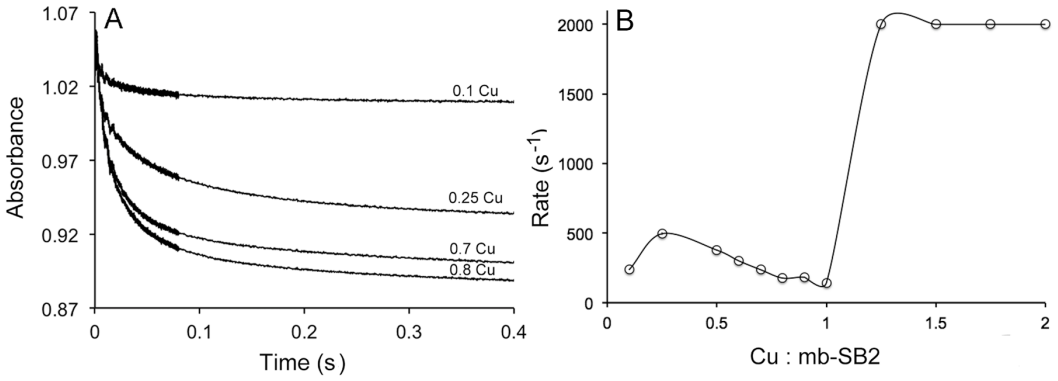

Fig. S5. Kinetics of Cu^{2+} binding by mb-SB2 at 4°C. A. Absorbance change monitored at 338 nm following the addition of 0.1, 0.25, 0.7 or 0.8 Cu^{2+} per mb-SB2. B. Rate of Cu^{2+} binding to to the oxazolone (OO) ring of mb-SB2 at 4°C as measured from the absorbance change at 341 nm. The rates for Cu^{2+} binding at Cu^{2+} to mb- SB2 molar ratios above 1.0 Cu^{2+} per mb-SB2 were >2000 s^{-1}, and were set at 2000 s^{-1} in the figure.

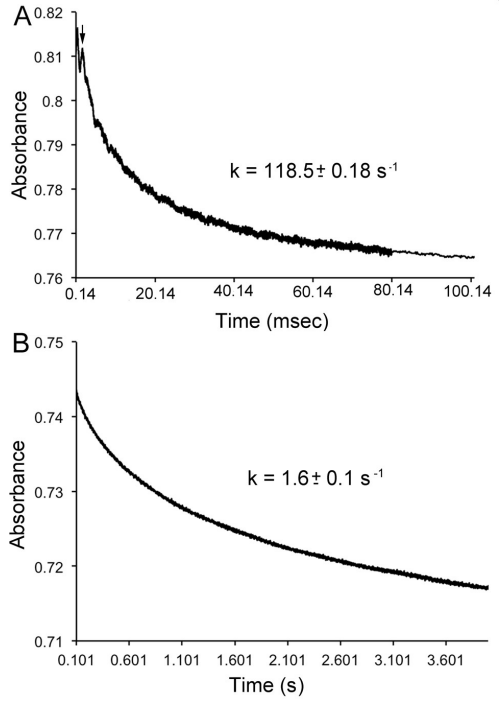

Fig. S6. Kinetics of Cu^{2+} displacement from Cu-mb-SB2 by Hg^{2+} at 4°C. A. Absorbance change monitored at 334 nm following the addition of an equimolar concentration of Hg^{2+} to Cu-mb-SB2. A. Kinetics of the fast phase representing approximately 25% of the reaction followed by (B) a slow phase representing the remaining 75% of the reaction. Arrow designates the end of sample mixing, 1.4 m.

References

1. **Choi DW, Do YS, Zea CJ, McEllistrem MT, Lee SW, Semrau JD, Pohl NL, Kisting CJ, Scardino LL, Hartsel SC, Boyd ES, Geesey GG, Shafe PH, Riedel TP, Kranski KA, Tritsch JR, Antholine WE and DiSpirito AA.** 2006. Spectral and thermodynamic properties of Ag(I), Au(III), Cd(II), Co(II), Fe(III), Hg(II), Mn(II), Pb(II), U(VI), and Zn(II) binding by methanobactin from *Methylosinus trichosporium* OB3b. J. Inorgan. Biochem. **100**: 2150 – 2161 DOI: 10.1016/j.inorgbio.2006.08.017.

2. **Choi, DW, Zea CJ, Do YS, Semrau JD, Antholine WA, Hargrove MS, Pohl NL, Boyd ES, Geesey GG, Hartsel SC, Shafe PH, McEllistrem MT, Kisting CJ, Campbell D, Rao V, de la Mora AM and DiSpirito AA.** 2006. Spectral, kinetic and thermodynamic properties of Cu(I)- and Cu(II)-binding by methanobactin from *Methylosinus trichosporium* OB3b. Biochemistry. **45:** 1142 – 1153.

CHAPTER 3

DETOXIFICATION OF MERCURY BY METHANOBACTIN FROM *Methylosinus trichosporium* OB3b

Alexey Vorobev, Sheeja Jagadevan, Bipin S. Baral, Alan A. DiSpirito, Brittani C. Freemeier, Brandt H. Bergman, Nathan L. Bandow, and Jeremy D. Semrau

Modified from the paper published in Journal of Applied Environmental Microbiology

Abstract

Many methanotrophs have been shown to synthesize methanobactin, a novel biogenic copper-chelating agent or chalkophore. Methanobactin binds copper via two heterocyclic rings with associated enethiol groups. The structure of methanobactin suggests that it can bind other metals, including mercury. Here we report that methanobactin from *Methylosinus trichosporium* OB3b does indeed bind mercury when added as $HgCl_2$ and, in doing so, reduced toxicity associated with Hg(II) for both *Alphaproteobacteria* methanotrophs, including *M. trichosporium* OB3b, *M. trichosporium* OB3b Δ*mbnA* (a mutant defective in methanobactin production), and *Methylocystis* sp. strain SB2, and a *Gammaproteobacteria* methanotroph, *Methylomicrobium album* BG8. Mercury binding by methanobactin was evident in both the presence and absence of copper, despite the fact that methanobactin had a much higher affinity for copper due to the rapid and irreversible binding of mercury by methanobactin. The formation of a gray precipitate suggested that Hg(II), after being bound by methanobactin, was reduced to Hg(0) but was not volatilized. Rather, mercury remained associated with methanobactin and was also found associated with methanotrophic biomass. It thus appears that although the mercury-methanobactin

complex was cell associated, mercury was not removed from methanobactin. The amount of biomass-associated mercury in the presence of methanobactin from *M. trichosporium* OB3b was greatest for *M. trichosporium* wild-type strain OB3b and the Δ*mbnA* mutant and least for *M. album* BG8, suggesting that methanotrophs may have selective methanobactin uptake systems that may be based on TonB-dependent transporters but that such uptake systems exhibit a degree of infidelity.

Introduction

It is well known that copper plays a key role in the physiology and activity of aerobic methanotrophs (1), a group of bacteria capable of utilizing methane as their sole carbon and energy source. The first step in methanotroph metabolism is the oxidation of methane to methanol and is catalyzed by one of two forms of methane monooxygenase: soluble methane monooxygenase (sMMO) and membrane-bound or particulate methane monooxygenase (pMMO). The concentration of copper in the growth medium determines which of these two forms is expressed : sMMO is produced only under conditions of copper starvation, whereas pMMO is expressed when copper is available, i.e., the phenomenological "copper-switch" (2-6). Copper has also been consistently found to enhance pMMO activity (7-9), and it is hypothesized that it composes the active site of pMMO (10), although some evidence also suggests iron is involved (11). It is generally agreed that at least in some methanotrophs, the copper requirement is approximately 10-fold higher than the Cu requirement observed in other microorganisms (5,8,12-14), possibly due to its role in the pMMO.

Given the important role of copper in methanotrophic metabolism, an effective copper acquisition system is crucial. To meet their high requirement for copper, methanotrophs appear to utilize multiple copper acquisition systems (15-21). One of the

copper acquisition systems utilized by methanotrophs involves the production and secretion of a copper chelating compound or chalkophore termed methanobactin (MB) (17). Methanobactin is a low molecular mass siderophore-like molecule, whose primary function is believed to be copper uptake, as well as possibly contributing to pMMO activity and being involved in regulating expression of sMMO and pMMO (6,17,22). Initially, MB was purified from *M. trichosporium* OB3b, and its crystal structure was characterized (15,17,18, 23-26). More recently, MB was isolated from four *Methylocystis* species: *Methylocystis* sp. strain SB2 (27), *Methylocystis hirsuta* CSC1, *Methylocystis* sp. strain M, and *Methylocystis rosea* (28). Comparison of these five forms of MB indicates that all have two heterocyclic rings, one of which is a five-member oxazolone ring, while the other ring is either a five member ring, either oxazolone or imidazolone, or a six-member pyrazinedione ring. Additionally, the rings of all known forms of MB have associated enethiol groups and are separated by 2 to 5 amino acids. Finally, all characterized forms of MB bind copper with extremely high affinity, $\geq 10^{21}$ M^{-1}.

Methanobactin from *M. trichosporium* OB3b has been shown to bind a variety of metals in addition to copper, including, Hg(II), Ag(I), Au(III), Co(II), Cd(II), Fe(III), Mn(II), Ni(II), Pb(II), U(VI), and some others (24). The binding of different metals by this form of MB, although with affinities orders of magnitude lower than that for copper, is intriguing and suggests that although MB preferentially binds copper, MB may play a role in controlling the speciation and bioavailability of other metals in situ, particularly mercury.

Microbial activities play an important role in modulating mercury toxicity in the environment. There are a number of resistance systems that are used by microorganisms to reduce the toxic effect of mercury. Some organisms use a detoxification mechanism that is

based on mercury reduction, which is specified by the *merA* gene (a part of the mercury resistance [*mer*] operon) (39). Another strategy of reducing mercury toxicity is to produce a compound capable of binding mercury in the environment. In this work, the primary focus was on the ability of MB produced by a methanotrophic bacterium, *Methylosinus trichosporium* OB3b, to bind mercury. Mercury is regarded as a "priority hazardous substance" by the Agency for Toxic Substances and Disease Registry (ATSDR) because of its toxicity, mobility, and long residence time in the atmosphere (29). Since mobilization and transport of heavy metals, including mercury, from hazardous waste sites are persistent and substantial problems, and methanotrophic bacteria are often present at these sites, it is important to understand the potential of this group of microorganisms to play a role in remediation of these ecosystems.

Materials and Methods

Bacterial strains and growth conditions.

Methylosinus trichosporium OB3b; a mutant defective in MB production, *Methylosinus trichosporium* OB3b Δ*mbnA*; *Methylomicrobium album* BG8; and *Methylocystis* sp. strain SB2, were used as model organisms. The *Methylosinus trichosporium* OB3b *ΔmbnA* mutant was constructed as previously described (6). Methanotrophic cultures were grown in NMS medium (30) at 30ºC in the dark without any added copper or with 1 μM copper as $CuCl_2$. For consideration of the impact of copper on mercury toxicity, *M. trichosporium* OB3b wildtype and ***Δ****mbnA* mutant were grown either in the absence of copper (to induce sMMO expression) and in the presence of 1 μM copper (to induce pMMO expression). *M. album* BG8 and *Methylocystis strain* SB2 were only grown

in the presence of 1 μM copper as these strains can only express pMMO. Furthermore, for growth of *M. trichosporium* OB3b **Δ***mbnA* mutant**,** 2.5 μg/ml gentamicin was added to the culture medium. Methanobactin was extracted and purified from *Methylosinus trichosporium* OB3b using previously described procedures (22). Mercury and MB were added to culture medium in the following concentrations: mercury (as $HgCl_2$) at 0 and 5 μM and MB at 0, 5 and 50 μM. Triplicate 200-ml serum vials (each with 35 ml of NMS medium) under each condition were capped with Teflon-coated butyl-rubber stoppers. For the growth of methanotrophs, CH_4 was added at a methane-to-air ratio of 1:2. The optical density at 600nm (OD_{600}) was measured in a Genesys 20 Visible spectrophotometer (Spectronic Unicam, Waltham, MA) at 12-hour intervals until the stationary phase was reached.

Protein measurement

Protein concentrations were measured using the Bradford assay (Bio-Rad Laboratories) after first concentrating 5 ml of the microbial cultures to 1 ml by centrifugation at 4500 X g for 10 min at room temperature. These cell suspensions were then digested in 2 M NaOH (0.4 ml 5 M NaOH per 1.0 ml of culture) at 98ºC for 15 minutes. The digested cell suspensions were then mixed with a 1X dye reagent, as suggested by the manufacturer. The samples were incubated for 5 min at room temperature, and the absorbance was measured at 595 nm using GENESYS 20 Visible spectrophotometer (Spectronic Unicam, Waltham, MA). The correlation between the protein concentration and the optical density (OD_{600}) was subsequently used to calculate the protein concentration for all cultures.

Measurement of mercury associated with biomass

Bacterial biomass was collected by centrifugation (4500 X g for 10 minutes) after the cultures reached the stationary phase of growth based on optical density measurements as described above. Supernatant samples were stored at -20ºC. The biomass was resuspended in 1 ml fresh NMS and also stored at -20ºC. To prepare samples for analysis on inductively coupled plasma mass spectrometry (ICP-MS) instrument (PerkinElmer, Waltham, MA), supernatant samples were diluted in NMS growth medium and 5% (vol/vol) HNO_3 to achieve a final concentration of 2.5 % (vol/vol) HNO_3). Cell suspensions were acidified in 1 ml 70% (vol/vol) HNO_3 and incubated at 95ºC for 2 h. The suspensions were mixed every 30 min by inverting the tubes 5 times. Two-milliliter plastic tubes with screw caps (Eppendorf) were used to prevent loss of sample during digestion. All measurements were performed in triplicate.

Binding of mixed metals by MB from *M. trichosporium* OB3b

To determine metal binding in the presence of 2- fold molar excess of both copper and mercury, 5 mM MB from *M. trichosporium* OB3b was mixed with 10 mM $HgCl_2$ and 10 mM $CuSO_4$. Following mixing, the reactants were incubated for 10 min, the solution run though a Sep-Pak column, washed with 30 ml of H_2O and MB eluted with 60% acetonitrile-40% H_2O. The Sep-Pak columns were subjected to a final wash with 5% HNO_3-5% HCl-90% H_2O solution. Mercury and copper concentrations were determined in the initial reaction mixture, in the water wash, in the 60% acetonitrile-40% H_2O wash, and in the 5% HNO_3-5% HCl-90% H_2O wash.

Kinetics and spectroscopy

UV-visible absorption spectroscopy, fluorescent spectroscopy and Hg(II) titrations were determined as previously described (Choi et al., 2006a; 2006b). $HgCl_2$ and $Hg(CN)_2$ stock solutions were made in double-distilled deionized H_2O, while CH_3ClHg stock solutions were made in 100% methanol. Kinetic measurements of mercury binding were made with a four-syringe Biologic SFM/400/S stopped-flow reactor coupled to a MOS-500 spectrophotometer (Bio-Logic Science Instrument SA, Claix, France). This four-syringe system has independent drives for each syringe, with a minimal dead time of 1.8 ms. Kinetics of mercury binding by MB from *M. trichosporium* OB3b was monitored at 340 or 394 nm. The reaction mixtures contained 250 μM MB and 50 to 500 μM $HgCl_2$ and the final pH following mixing was 6.7.

Mercury volatilization

Mercury volatilization was determined as previously described by Takeuchi *et al.* (31). Briefly, 2.5 μM MB solutions were incubated in sealed serum vials with shaking (200 rpm) in the presence of 2.5, 5.0 or 7.5 μM $HgCl_2$ for 0.5 to 24h at room temperature. The sealed serum vial contained a 0.6% $KMnO_4$ Hg (0) trap consisting of a test tube 0.5 cm shorter than the serum vial. Following the incubation period, the mercury in the reaction mixture and $KMnO_4$ trap was analyzed for mercury via vapor diffusion on an Agilent Technologies 55 AA atomic absorption spectrophotometer. Samples of the MB-Hg reaction mixture were also separated via Sep-Pak cartridges, as previously described, to determine the percentage of mercury bound to MB. Controls were determined as described above but with the exclusion of MB from the reaction mixture.

Nucleic acid extraction

Nucleic acid extraction was performed by first centrifuging cultures in late exponential phase at 4,500 x g for 10 min at 4ºC. Cell pellets were resuspended in 0.75 ml of RNA extraction buffer (0.2 M NaH_2PO4/Na_2HPO_4 buffer [pH 7.5] and 5% cetyltrimethylammonium bromide [CTAB] in 2.4 M NaCl). This sample was subjected to bead-beating (1 min at 4,800 rpm) in 2-ml plastic tubes containing 0.5 g of 0.1-mm zirconia-silica beads (Biospec Products), 35 µl of 20% SDS, 35 µl of 20% laurylsarcosine, and 750 µl of phenol-chloroform-isoamylic alcohol (25:24:1). The samples were then centrifuged at 14,000 rpm for 5 min at 4ºC. The aqueous phase was mixed with an equal volume of chloroform-isoamylic alcohol (24:1) and centrifuged at 14000 rpm for 5 min at 4ºC. RNA was precipitated by adding $MgCl_2$ (final concentration, 2.5 mM), 0.1 volume of 3 M sodium acetate, and 0.7 volumes of isopropanol and incubating overnight at -80 ºC. RNA was then recovered by centrifugation at 14,000 rpm for 30 min at 4ºC. The DNase treatment was carried out using the RNase free DNase set (Qiagen) in accordance with the manufacturer's instructions. The RNA samples were further purified using the RNeasy Plus Kit (Qiagen) using genomic DNA (gDNA) eliminator columns and RNeasy Mini Spin columns according to the manufacturer's instructions. To check for any DNA contamination, PCR was performed with extracted RNA as the template. RNA was reverse transcribed to obtain cDNA by using Superscript III Reverse Transcriptase (Invitrogen) according to the manufacturer's instructions.

Reverse transcription-PCR (RT PCR) was then performed to assay for the expression of *pmoA* (encoding the 26-kDa subunit of pMMO) and *mmoX* (encoding the α- subunit of the hydroxylase component of sMMO) in *M. trichosporium* OB3b wild-type and *M.*

trichosporium OB3b **Δ***mbnA* mutant cells grown with methane under varying copper, mercury and MB concentrations, using previously developed primers (32-34). A three-step cycle, with an initial denaturation at 94ºC for 2 min and 35 cycles of denaturation (94ºC for 1 min), annealing (55ºC for 1 min) and extension (72ºC for 1 min), was performed.

Results

Growth of methanotrophs in the presence of mercury and MB.

As shown in Fig. 1 and 2, the addition of as little as 5 μM mercury resulted in no growth of either *M. trichosporium* OB3b or the ***Δ****mbnA* mutant. The simultaneous addition of MB, however, allowed growth similar to that observed in the absence of mercury (Fig. 1A and B and 2A and B). It should be noted, however, that the concentration of MB required for growth in the presence of 5 μM mercury was different for the wild-type and *ΔmbnA* strains of *M. trichosporium* OB3b. Wild-type cultures of *M. trichosporium* OB3b were capable of growth in the presence of 5 μM mercury if as little as 5 μM MB was added to the growth medium, but the ***Δ****mbnA* mutant could grow in the presence of 5 μM mercury only if 50 μM MB was simultaneously added (Figure 1A and B and 2A and B). Interestingly, the addition of MB at a concentration of either **5** μM or 50 μM alone with no added copper or mercury had no effect on the growth of wild-type *M. trichosporium* OB3b but did improve the growth of the *ΔmbnA* mutant in both the absence and presence of copper**.** There was also no difference in the growth of either wildtype or ***Δ****mbnA* strain of *M. trichosporium* OB3b with different mercury and MB concentrations in the absence of copper or when 1 μM copper was added (see Fig. S1 and S2 in the supplemental material).

The ability of other methanotrophs to grow in the presence of mercury and MB from *M. trichosporium* OB3b was also examined. As can be seen in Fig. 3 and 4, MB from *M. trichosporium* OB3b at concentrations of 5 μM and 50 μM alone had no inhibitory effect on the growth of either *Methylomicrobium album* BG8 (a *Gammaproteobacteria* methanotroph) or *Methylocystis* strain SB2 (a Alphaproteobacteria methanotroph), and actually appeared to stimulate growth of *Methylocystis* strain SB2. The addition of as little as 5μM mercury resulted in no growth of either *M. album* BG8 or *Methylocystis* strain SB2, similar to what was observed with the *M. trichosporium* OB3b wildtype and the *ΔmbnA* mutant. Both *M. album* BG8 and *Methylocystis* strain SB2 were capable of growth in the presence of mercury if MB from *M. trichosporium* OB3b was added to the growth medium. Interestingly, *Methylocystis* strain SB2 could grow in the presence of 5μM mercury only if 50 μM MB was added (Fig. 3). *M. album* BG8 could grow under **5** μM mercury even if only 5 μM MB was added, although a long lag phase of growth was observed (Fig. 4).

Mercury associated with biomass

ICP-MS analysis of cell suspensions demonstrated that in the absence of any added mercury, the biomass-associated mercury concentration varied with an average 0.06 ± 0.03 μg mercury· mg protein^{-1}, for all methanotrophic strains. In the presence of 5 μM mercury, the amount of mercury associated with biomass for actively growing cultures (Table 1) was significantly larger than that in the absence of mercury for all tested strains at a 95% confidence interval. The ratio of mercury to biomass, however, did not change significantly in the presence of either 5 or 50 μM MB for the *M. trichosporium* OB3b wildtype. The *M. trichosporium* OB3b Δ*mbnA* mutant only grew in the presence of 50 μM MB and had a

greater amount of mercury associated with its biomass than did the *M. trichosporium* OB3b wild type under these conditions, but such a difference was not significantly different at a 95% confidence interval (Table 1). Interestingly, *M. album* BG8 had significantly less mercury associated with biomass from both the *M. trichosporium* OB3b wildtype and *ΔmbnA* mutant when either 5 or 50 μM MB from *M. trichosporium* OB3b was added (the difference was significant between *M. album* BG8 and *M. trichosporium* OB3b wildtype at 90% confidence and between *M. album* BG8 and *M. trichosporium* OB3b *ΔmbnA* mutant at a 95% confidence). *Methylocystis* strain SB2, which grew only in the presence of mercury with 50 μM MB added, had more mercury associated with biomass than *M. album* BG8 (significant at a 95% confidence interval), but had less than that found for both *M. trichosporium* OB3b wildtype and *ΔmbnA* mutant (the difference was not significant between *Methylocystis* strain SB2 and *M. trichosporium* OB3b wild type at either a 90 or 95% confidence interval, but was significant between *Methylocystis* strain SB2 and the *M. trichosporium* OB3b *ΔmbnA* mutant at a 95% confidence).

pmoA and mmoX expression in *M. trichosporium* OB3b wildtype and Δ*mbnA* mutant

Figure 5 shows that *pmoA* in the *M. trichosporium* OB3b wildtype was constitutively expressed regardless of the copper, mercury and MB concentrations with which the strain grew. *mmoX* expression was observed in *M. trichosporium* OB3b wild type in the absence of copper (Fig. 5B, lanes 1 to 5) but not in the presence of 1 μM copper (Fig. 5B, lane 6). Interestingly, however, the addition of either 5 or 50 μM MB simultaneously with 1 μM copper increased the *mmoX* expression in the *M. trichosporium* OB3b wild type in both the presence and absence of mercury (Fig. 5B, lanes 7 to 10).

For the *ΔmbnA* mutant, both *pmoA* and *mmoX* expressions were found under all conditions in which the culture grew (Figure 5C and D). *mmoX* expression, however, was significantly reduced in the presence of 1 μM copper (Fig. 5D, lane 6), and such expression increased with the simultaneous addition of MB (Fig. 5D, lanes 7, 9, and 10).

Hg (II) binding by MB from *M. trichosporium* OB3b

Previous studies by fluorescent and UV-visible absorption spectroscopy, isothermal titration calorimetry, as well as the development of a gray precipitate suggested that MB from *M. trichosporium* OB3b will reduce more Hg(II) to Hg(0) per MB (24). To extend our understanding of Hg(II) binding by MB, the spectral changes following Hg(II) binding, the pre-steady state kinetics of Hg(II) binding, and the potential of MB to volatilize mercury following reduction to Hg(0) were assayed. The UV-visible and fluorescent spectra of mercury binding by MB was complex and suggested the binding of 2 mercury per MB, as evidenced by by the requirement of 2Hg per MB-OB3b for saturation (Fig. 6 and 7). Major transitions in the spectral properties at 0.25, 0.5, 1.0 and 2.0 mercury per MB were evident in the emission spectra (Fig. 7). With the exception of the emissions in the 600- to 700 nm region, the fluorescent spectra of MB from *M. trichosporium* OB3b are associated with oxazolone ring A (27). The emissions associated with oxazolone ring A appear to be quenched at 0.9 mercury per MB (Fig. 7C and D), at which point emissions associated with oxazolone ring B increase dramatically (Fig. 7A and B), and new emissions associated with oxazolone A appear in the 400- to 430-nm region (Fig. 7C and D). The results suggest internal quenching or exciton transfer between the two rings, and this internal quenching or exciton transfer is disrupted at mercury-to -MB ratios above 1.0.

The spectral changes were similar to that observed with the binding and reduction of Au(III) to Au(0) and were similar to the spectral changes observed with metals that are reduced following binding by MB (23,24) . In general, metals that are reduced following binding are coordinated by both oxazolone rings, while metals that are not reduced are coordinated by only one of the oxazolone rings. To determine if Hg(II) is reduced to Hg(0) and either remained associated with MB or was volatilized, MB was incubated in the presence of 0,1,1 and 4 Hg(II) per MB in closed systems with permanganate to trap volatile mercury (31). Volatile mercury was never observed, suggesting that all mercury remained bound to MB.

The UV-visible absorption spectra of CH3ClHg and Hg(CN)2 suggested that methanobactin from M. trichosporium OB3b bound these forms of Hg (see Fig. S3 in the supplemental material). However, the spectra following the addition of CH_3ClHg and $Hg(CN)_2$ differed from the spectra following the addition of inorganic Hg(II), as did the saturation points where the spectra following the addition of CH_3ClHg and $Hg(CN)_2$ were saturated at 1.0 and 0.5 ligands per MB.

To estimate potential interactions that may occur in mixed metal environments, mercury and copper binding by MB was examined in the presence of 2-fold molar excess of both Cu(II) and Hg(II). The results showed that a copper-to-mercury molar ratio of 9.7 ± 7.6 copper to 1 mercury was bound to MB under these conditions. Based on reported binding constants (23), the binding of mercury in the presence of copper was unexpected. Hg(II) was found to be bound by MB with two affinities, a K_1 of 9.9×10^6 M^{-1} and $K_2 = 9.0 \times 10^5$ M^{-1}, which are 2 to 14 orders of magnitude lower than the Cu(II) binding constants of a K_1 of > 1.0×10^{21} M^{-1} and a K_2 of 2.6×10^8 M^{-1} (23,24).

Discussion

The ability to synthesize MB, a low-molecular-mass siderophore-like molecule, plays an important role in methanotrophic metabolism, given the central role of copper in methanotrophic physiology and gene expression (1). Methanobactin, while having a high affinity for copper, can also bind a variety of metals. We then decided to examine the ability and the effect of mercury binding by MB from *M. trichosporium* OB3b, particularly to determine if this form of MB reduced mercury toxicity to *M. trichosporium* OB3b as well as other methanotrophs.

This study demonstrated that the addition of as little as 5μM mercury to the growth medium resulted in no growth of *M. trichosporium* OB3b wild-type and *ΔmbnA* mutant cells. The addition of MB, however, allowed for growth similar to that observed in the absence of mercury, indicating that MB reduces its bioavailability. Interestingly, the amount of MB required to allow growth in the presence of mercury varied for the *M. trichosporium* OB3b wild-type and *ΔmbnA* mutant. Wild-type *M. trichosporium* OB3b was capable of growth in the presence of **5** μM mercury if as little as **5** μM mb was added to the growth medium (Fig.1A and B). The ***Δ****mbnA* mutant, however, could grow in the presence of 5 μM mercury only if 50 μM mb was added simultaneously (Fig. 2A and B). A possible explanation for this might be that while *M. trichosporium* OB3b wild type is capable of producing MB in addition to the MB added to the medium, the *ΔmbnA* mutant, defective in methanobactin production, cannot produce MB, resulting in higher requirements for MB for the *ΔmbnA* mutant to be able to grow in the presence of mercury.

An intriguing question is whether methanobactin produced by one microorganism can protect other microbes by binding toxic metals such as mercury. A simple experiment was

conducted in which MB isolated from *M. trichosporium* OB3b was added to cultures of *Methylomicrobium album* BG8 (a *Gammaproteobacteria* methanotroph) and *Methylocystis* strain SB2 (an *Alphaproteobacteria* methanotroph) grown with different concentrations of mercury. As can be seen in Fig. 3 and 4, it appears that MB was not toxic to either of these strains and actually enhanced the growth of *Methylocystis* strain SB2. Furthermore, the addition of as little as 5μM mercury in the absence of MB prevented any growth of *M. album* BG8 and *Methylocystis* strain SB2, as observed for the *M. trichosporium* OB3b wild type and *ΔmbnA* mutant. The addition of MB, however, allowed growth similar to that observed in the absence of mercury (Fig. 3 and 4).

It is noteworthy that the concentrations of MB needed to allow for growth were different for *M. album* BG8 and *Methylocystis* strain SB2. *Methylocystis* strain SB2 could not grow in the presence of **5** μM mercury if **5** μM MB was added, but did grow in the presence of **50** μM MB (Fig. 3), while *M. album* BG8 was capable of growth in the presence of **5** μM mercury if only **5** μM MB was added, but with a very long lag phase (Fig. 4). These data indicate that MB from *M. trichosporium* OB3b, when binding mercury, can act as a general prophylactic and protect the broader methanotrophic community from the toxic effects of mercury. At this time, it is unclear as to why *M. album* BG8 and *Methylocystis* strain SB2 required different amounts of MB to be able to grow in the presence of mercury. It can be speculated that mercury bound to MB from *M. trichosporium* OB3b is largely unavailable to *M. album* BG8, but that it is still bioavailable to *Methylocystis* strain SB2. It is known that both *M. album* BG8 and *Methylocystis* strain SB2 make different forms of MB but with very different affinities for metals, i.e., MB from *M. album* BG8 binds copper with an initial constant of ~10^5 M^{-1}, while MB from *Methylocystis* strain SB2 binds copper with an initial

constant of 7.6 X 10^{26} (15, 35). It may be that MB from *M. trichosporium* OB3b binds mercury to such a degree that it cannot be removed by MB from *M. album* BG8, while MB from *Methylocystis* strain SB2 can do so, increasing mercury bioavailability. In the presence of additional MB from *M. trichosporium* OB3b, it appears that such increased mercury bioavailability is reduced due to the greater likelihood of any released mercury to be re-associated with MB from *M. trichosporium* OB3b.

From the metal uptake analyses (Table 1), it is apparent that even in the presence of MB, mercury was found associated with the biomass of all tested strains whenever growth occurred. Thus, it appears that MB did not prevent the uptake of mercury, particularly for the *M. trichosporium* OB3b *ΔmbnA* mutant, but it did make mercury more unavailable, i.e., mercury associated with MB was not subsequently removed and thus could not interfere with microbial metabolism. It is interesting to note, however, that the amount of mercury associated with *M. album* BG8 and *Methylocystis strain* SB2 was smaller than that found for the *M. trichosporium* OB3b wildtype and *ΔmbnA* mutant. It appears that MB from *M. trichosporium* OB3b was not as easily taken up by *M. album* BG8 and *Methylocystis* strain SB2 suggesting that these strains have different systems for MB uptake than *M. trichosporium* OB3b. Genomic mining indicates that the putative uptake mechanism, a TonB-dependent transporter, varies between methanotrophs (36). These data, coupled with the mercury data shown here, indicate that methanotrophs may have some, but not complete selectivity for their own form of MB. This may also explain why less MB from *M. trichosporium* OB3b was needed to protect *M. album* BG8 from the toxic effects of mercury as than *Methylocystis* strain SB2, i.e., the canonic methanobactin biosynthesis and transport operon found in *M. trichosporium* OB3b and a variety of *Methylocystis* strains (6, 36, 37) is

not found in *M. album* BG8. As such, it may be that *M. album* BG8 is less able to take up MB from *M. trichosporium* OB3b and thus is less likely to be affected by mercury associated with it than *Methylocystis* strain SB2.

Expression levels of key genes involved in sMMO and pMMO were assayed for *M. trichosporium* OB3b wildtype and *ΔmbnA* mutant cells to determine if mercury toxicity was due to differential expression of the methane monooxygenases. As shown in Fig.5, for *M. trichosporium* OB3b wildtype, expression of *pmoA* (encoding for the 26-kDa subunit of pMMO) was found under all conditions in which cultures grew (i.e., all conditions but those where mercury was added in the absence of mb), but the addition of MB induced expression of *mmoX* (encoding for the 54-kDa subunit of the hydroxylase of sMMO). Furthermore, *M. trichosporium* OB3b *ΔmbnA* mutant expressed both *pmoA* and *mmoX* under all conditions in which it grew (i.e., all conditions but those where mercury was added in the absence of at least 50 μM MB). Such a finding indicates that MB plays a role in the copper switch of methanotrophs, as previously reported (6). Given that the *M. trichosporium* OB3b strains examined here grew in the presence of mercury while either expressing *pmoA* or both *pmoA* and *mmoX*, it appears that the toxicity of mercury in the absence of MB was not due to selectively inactivation of one form of the methane monooxygenase; rather, it was due to more general pleiotropic effects.

Collectively, these data raise several questions. First, how can MB from *M. trichosporium* OB3b detoxify mercury in the presence of copper, given that this form of MB has a much greater affinity for copper than mercury? Examination of the kinetics of mercury binding by MB provides a plausible explanation. At equimolar concentrations of mercury and MB, approximately 90% of the binding measured by spectral shifts at 341 nm and 394

nm (corresponding to the two oxazolone rings) was complete before the 1.8-ms dead time of the stopped flow system (see Fig. S4 in the supplemental material). Based on the remaining 10% of the reaction, an observed rate constant of, k_{obs}, of 640 ± 43 s^{-1} was determined for the binding of mercury to both rings of MB. This initial binding rate for mercury was similar to the observed rate constant for Cu(II) binding by oxazolone A and 5 times higher than the observed rate constant for Cu binding by oxazolone B (23). Further, previous studies demonstrated that Cu (II) cannot displace mercury bound to MB (24). In light of this finding, coupled with a comparable, if not higher rate, of Hg(II) binding by MB compared to that of copper, the observed binding of mercury in the presence of Cu(II) is not surprising. This binding ratio of mercury to copper also may explain the 10-fold-higher MB concentrations required to neutralize Hg(II) toxicity to *M. trichosporium* OB3b *ΔmbnA* mutant than to the *M. trichosporium* OB3b wildtype, as the *ΔmbnA* mutant is unable to make any methanobactin.

Second, in polluted environments, does MB produced by any methanotrophs serve to mitigate the toxicity of mercury to the general methanotrophic community? Does such detoxification extend to the broader microbial community, i.e., are nonmethanotrophs also protected from mercury toxicity through methanotrophic-mediated production of MB? Furthermore, given that mercury speciation *in situ* includes organic forms such as methyl-mercury, can MB bind these forms of mercury? UV-visible spectral data (see Fig. S3 in the supplemental material) indicate that organic forms of mercury can indeed be bound by MB, but the affinity for such forms of mercury is unknown. In addition, as speculated above, different forms of MB are known to above different affinities for copper- do they have different affinities for various forms of mercury? The detoxification of mercury by

methanotrophs *in situ* may be highly dependent on the composition of the methanotrophic community as well as the form(s) of mercury present.

Third, it was observed that the growth of *Methylocystis* strain SB2 was stimulated by the addition of MB of *M. trichosporium* OB3b in the absence of mercury (Fig. 3). As *Methylocystis* strain SB2 can express only pMMO (38), which required copper for high activity, it may be that MB from *M. trichosporium* OB3b increased the bioavailability of copper, thereby increasing the activity of pMMO in *Methylocystis* strain SB2. If so, this suggests that MB made by one methanotroph may actually be taken up by others (as also suggested by the mercury uptake data [Table 1]). This raises the following intriguing questions. Do all methanotrophs in a mixed community produce MB, or do some species act as "cheaters' and rely on MB made by other microbes to meet copper requirements for metabolism? How do methanotrophs that MB ensure that they are able to effectively compete with such cheaters for copper? As noted above, it appears that different methanotrophs selectively take up their own form of MB, by these uptake systems have some infidelity. It may be that *in situ,* such infidelity may be optimized as a general strategy for competition between methanotrophs. Such questions are beyond the scope of this research by clearly warrant more attention.

References

1. **Semrau JD, DiSpirito AA, Yoon S**. 2010. Methanotrophs and copper. FEMS Microbiol Rev. 34:469-531.

2. **Stanley SH, Prior SD, Leak DJ, Dalton H**. 1983. Copper stress underlies the fundamental change in intracellular location of methane monooxygenase in methane-oxidizing organisms: studies in batch and continuous cultures. Biotechnol Lett 5:487–492.

3. **Lontoh S, Semrau JD**. 1998. Methane and trichloroethylene degradation by *Methylosinus trichosporium* OB3b expressing particulate methane monooxygenase. Appl. Environ Microb 64:1106–1114.

4. **Lontoh S**. 2000. Substrate oxidation by methanotrophs expressing particulate methane monooxygenase (pMMO): a study of whole-cell oxidation of trichloroethylene and its potential use for environmental remediation. PhD Thesis. University of Michigan, Ann Arbor, MI.

5. **Choi DW, Kunz RC, Boyd ES, Semrau JD, Antholine WE, Han JI, Zahn JA, Boyd JM, de la Mora AM, DiSpirito AA**. 2003. The membrane-associated methane monooxygenase pMMO and pMMO-NADH:quinone oxidoreductase complex from *Methylococcus capsulatus*. Bath. J Bacteriol 185:5755− 5764.

6. **Semrau JD, Jagadevan S, DiSpirito AA, Khalifa A, Scanlan J, Bergman BH, Freemeier BC, Baral BS, Bandow NL, Vorobev A, Haft DH, Vuilleumier S, Murrell JC**. 2013. Methanobactin and MmoD Work in Concert to Act as the "Copper-Switch" in Methanotrophs. Environ Microbiol 15(11). 3077-3086.

7. **Semrau JD, Zolandz D, Lidstrom ME, Chan SI**. 1995. The role for copper in the pMMO of *Methylococcus capsulatus* Bath: a structural vs. catalytic function. J Inorg Biochem 58:235–244.

8. **Zahn JA, DiSpirito AA**. 1996. Membrane-associated methane monooxygenase from *Methylococcus capsulatus* (Bath). J Bacteriol 178:1018–1029.

9. **DiSpirito AA, Kunz RC, Choi DW, Zahn JA**. 2004. Respiration in methanotrophs. Respiration in Archaea and Bacteria, Ch. 7, Vol. 16 (Zannoni D, ed), pp. 149–168. Springer, Dordrecht, The Netherlands.

10. **Balasubramanian R, Smith SM, Rawat S, Stemmler TL, Rosenzweig AC**. 2010. Oxidation of methane by a biological dicopper centre. Nature 465:115−119.

11. **Martinho M, Choi DW, DiSpirito AA, Antholine WE, Semrau JD, Münck W**. 2007. Mössbauer studies of the membraneassociated methane monooxygenase from *Methylococcus capsulatus* Bath: evidence for a diiron center. J Am Chem Soc 129:15783–15785.

12. **Nguyen H-H, Shiemke AK, Jacobs SJ, Hales BJ, Lidstrom ME, Chan SI**. 1994. The nature of the copper ions in the membranes containing the particulate methane monooxygenase from *Methylococcus capsulatus* (Bath). J Biol Chem 269:14995–15005.

13. **Nguyen H-H, Nakagawa KH, Hedman B, Elliott SJ, Lidstrom ME, Hodgson KO, Chan SI**. 1996. X-ray absorption and EPR studies on the copper ions associated with the particulate methane monooxygenase from *Methylococcus capsulatus* (Bath). Cu(I) ions and their implications. J Am Chem Soc 118:12766–12776.

14. **Nguyen H-H, Elliott SJ, Yip JH-K, Chan SI**. 1998. The particulate methane monooxygenase from *Methylococcus capsulatus* (Bath) is a novel copper-containing three subunit enzyme: isolation and characterization. J Biol Chem 273:7957–7966.

15. **Choi DW, Bandow NL, McEllistrem MT, Semrau JD, Antholine WE, Hartsel SC, Gallagher W, Zea CJ, Pohl NL, Zahn JA, DiSpirito AA**. 2010. Spectral and thermodynamic properties of methanobactin from gammaproteobacterial methane oxidizing bacteria: a case for copper competition on a molecular level. J Inorg Biochem 104:1240–1247.

16. **DiSpirito AA, Zahn JA, Graham DW, Kim HJ, Larive CK, Derrick TS, Cox CD, Taylor A**. 1998. Copper-binding compounds from *Methylosinus trichosporium* OB3b. J Bacteriol 180:3606–3613.

17. **Kim HJ, Graham DW, DiSpirito AA, Alterman MA, Galeva N, Larive CK, Asunskis D, Sherwood PMA**. 2004. Methanobactin, a copper-acquisition compound from methane-oxidizing bacteria. Science 305:1612–1615.

18. **Kim HJ, Galeva N, Larive CK, Alterman M, Graham DW**. 2005. Purification and physical-chemical properties of methanobactin: a chalkophore from *Methylosinus trichosporium* OB3b. Biochemistry 44:5140–5148.

19. **Karlsen OA, Berven FS, Stafford GP, Larsen O, Murrell JC, Jensen HB, Fjellbirkeland A**. 2003. The surface-associated and secreted MopE protein of *Methylococcus capsulatus* (Bath) responds to changes in the concentration of copper in the growth medium. Appl Environ Microbiol 69:2386–2388.

20. **Helland R, Fjellbirkeland A, Karlsen OA, Ve T, Lillehaug JR, Jensen HB. 2008**. An oxidized tryptophan facilitates copper binding in *Methylococcus capsulatus* secreted protein MopE. J Biol Chem 283:13897–13904.

21. **Ve T, Mathisen K, Helland R, Karlsen OA, Fjellbirkeland A, Røhr ÅK, Andersson KK, Pedersen RB, Lillehaug JR, Jensen HB**. 2012. The *Methylococcus capsulatus* (Bath) secreted protein, MopE, binds both reduced and oxidized copper. PLoS One 7:e43146.

22. **Bandow NL, Gallagher WH, Behling L, Choi DW, Semrau JD, Hartsel SC, Gilles VS, DiSpirito AA.** 2011. Isolation of methanobactin from the spent media of methane-oxidizing bacteria. Methods Enzymol 495:259–269.

23. **Choi DW, Zea CJ, Do YS, Semrau JD, Antholine WE, Hargrove MS, Pohl NL, Boyd ES, Geesey GG, Hartsel SC, Shafe PH, McEllistrem MT, Kisting Cj, Campbell D, Rao V, de la Mora AM, DiSpirito AA.** 2006a. Spectal, kinetic, and thermodynamic properties of Cu(I) and Cu(II) binding by methanobactin from *Methylosinus trichosporium* OB3b. Biochemistry 45:1442-1453.

24. **Choi DW, Do YS, Zea CJ, McEllistrem MT, Lee SW, Semrau JD, Pohl NL, Kisting CJ, Scardino LL, Hartsel SC, Boyd ES, Geesey GG, Riedel TP, Shafe PH, Kranski KA, Tritsch JR, Antholine WE, DiSpirito AA.** 2006b. Spectral and thermodynamic properties of Ag(I), Au(III), Cd(II), Co(II), Fe(III), Hg(II), Mn(II), Ni(II), Pb(II), U(IV), and Zn(II) binding by methanobactin from *Methylosinus trichosporium* OB3b. J Inorg Biochem 100:2150-2161.

25. **Choi DW, Semrau JD, Antholine WE, Hartsel SC, Anderson RC, Carey J, Dreis Am, Kenseth EM, Renstrom JM, Scardino LL, Van Gorden GS, Volkert AA, Wingad AD, Yanzer PJ, McEllistrem MT, de la Mora AM, DiSpirito AA**. 2008. Oxidase, superoxide dismutase, and hydrogen peroxide reductase activities of methanobactin from type I and type II methanotrophs. J Inorg Biochem 102:1571-1580.

26. **Behling LE, Hartsel SC, Lewis DE, DiSpirito AA, Masterson LR, Veglia G, Gallgher WH**. 2008. NMR mass spectroscopy, and chemical evidence reveal a different chemical structure for methanobactin that contains oxazolone rings. J Am Chem Soc 130: 12604-12605.

27. **Krentz BD, Mulheron HJ, Semrau JD, DiSpirito AA, Bandow NL, Haft DH, Vuilleumier S, Murrell JC, McEllistrem MT, Hartsel SC, Gallagher WH**. 2010. A comparison of methanobactins from Methylosinus trichosporium OB3b and *Methylocystis* strain SB2 predicts methanobactins are synthesized from diverse peptide precursors modified to create a common core for binding and reducing copper ions. Biochemistry 49:10117-10130.

28. **El Ghazouani A, Baslé A, Gray J, Graham DW, Firbank SJ, Dennison C**. 2012. Variations in methanobactin structure influences copper utilization by methane-oxidizing bacteria. Proc Natl Acad Sci U.S.A. 109:8400-8404.

29. **Wang J, Feng X, Anderson CWN, Xing Y, Shang L**. 2012. Remediation of mercury contaminated sites - A review. J Hazard Mater 221/222:1-18.

30. **Whittenbury R, Phillips KC, Wilkinson JG**. 1970. Enrichment, isolation and some properties of methane-utilizing bacteria. J Gen Microbiol 61:205–218.

31. **Takeuchi F, Negishi A, Maeda T, Kamimura K, Sugio T**. 2003. Volatilization and recovery of mercury from mercury wastewater produced in the course of laboratory work using *Acidithiobacillus ferrooxidans* SUG 2-2 cells. J Biosci Bioeng 95: 239-244.

32. **Holmes AJ, Costello AM, Lidstrom ME, Murrell JC.** 1995. Evidence that particulate methane monooxygenase and ammonia monooxygenase may be evolutionarily related. FEMS Microbiol. Lett. 132**:**203-208.

33. **Costello AM, Lidstrom ME**. 1999. Molecular characterization of functional and phylogenetic genes from natural populations of methanotrophs in lake sediments. Appl. Environ Microbiol 65:5066-5074.

34. **Hutchens E, Radajewski S, Dumont MG, McDonald IR, Murrell JC**. 2004. Analysis of methanotrophic bacteria in Movile Cave by stable isotope probing. Environ Microbiol 6:111-120.

35. **Bandow N, Gilles VS, Freesmeier B, Semrau JD, Krentz B, Gallagher W, McEllistrem MT, Harstel SC, Choi DW, Hargrove MS, Heard TM, Chesner LN, Braunreiter KM, Cao BV, Gavitt MM, Hoopes JZ, Johnson JM, Polster EM, Schoenick BD, Umlauf AM, DiSpirito AA**. 2012. Spectral and copper binding properties of methanobactin from the facultative methanotroph *Methylocystis* strain SB2. J. Inorg Biochem 110:72-82.

36. **Kenney GE, Rosenzweig AC**. 2013. **Genome mining for methanobactins**. BMC Biol 11:0-17.

37. **Haft DH, Selengut JD, Richter RA, Harkins D, Basu MK, Beck E**. 2013. TIGRFAMs and Genome Properties in 2013. Nucleic Acids Res 41:D387-D395.

38. **Im J**, **Semrau JD**. 2011. Pollutant degradation by a *Methylocystis* strain SB2 grown on ethanol: bioremediation via facultative methanotrophy. FEMS Microbiol Lett 318:137-142.

39. **Osborn AM, Bruce KD, Strike P, Ritchie DA**. 1997. Distribution, diversity and evolution of the bacterial mercury resistance (mer) operon. FEMS Microbiol Rev. 19:239-262.

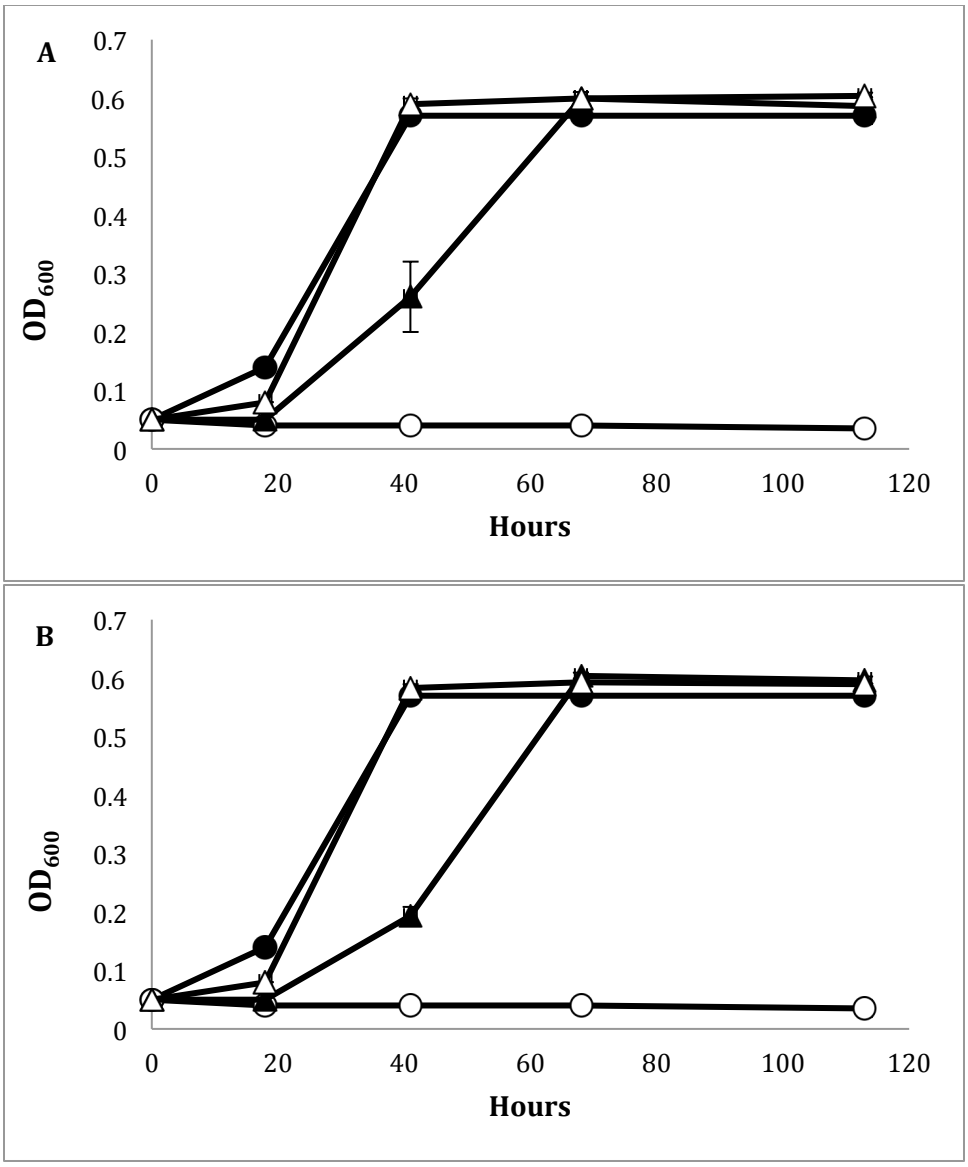

Figure 1. Growth of *M. trichosporium* OB3b WT on methane under (A) 0 µM Cu or (B) 1 µM Cu. 0 µM Hg + 0 µM MB (●), 5 µM Hg + 0 µM MB (○), 5 µM Hg + 5 µM MB (▲), 5 µM Hg + 50 µM MB (Δ). All data are means of triplicate samples. Error bars represent standard deviation (SD, n=3). When error bars are not visible, they are smaller than the size of the symbols.

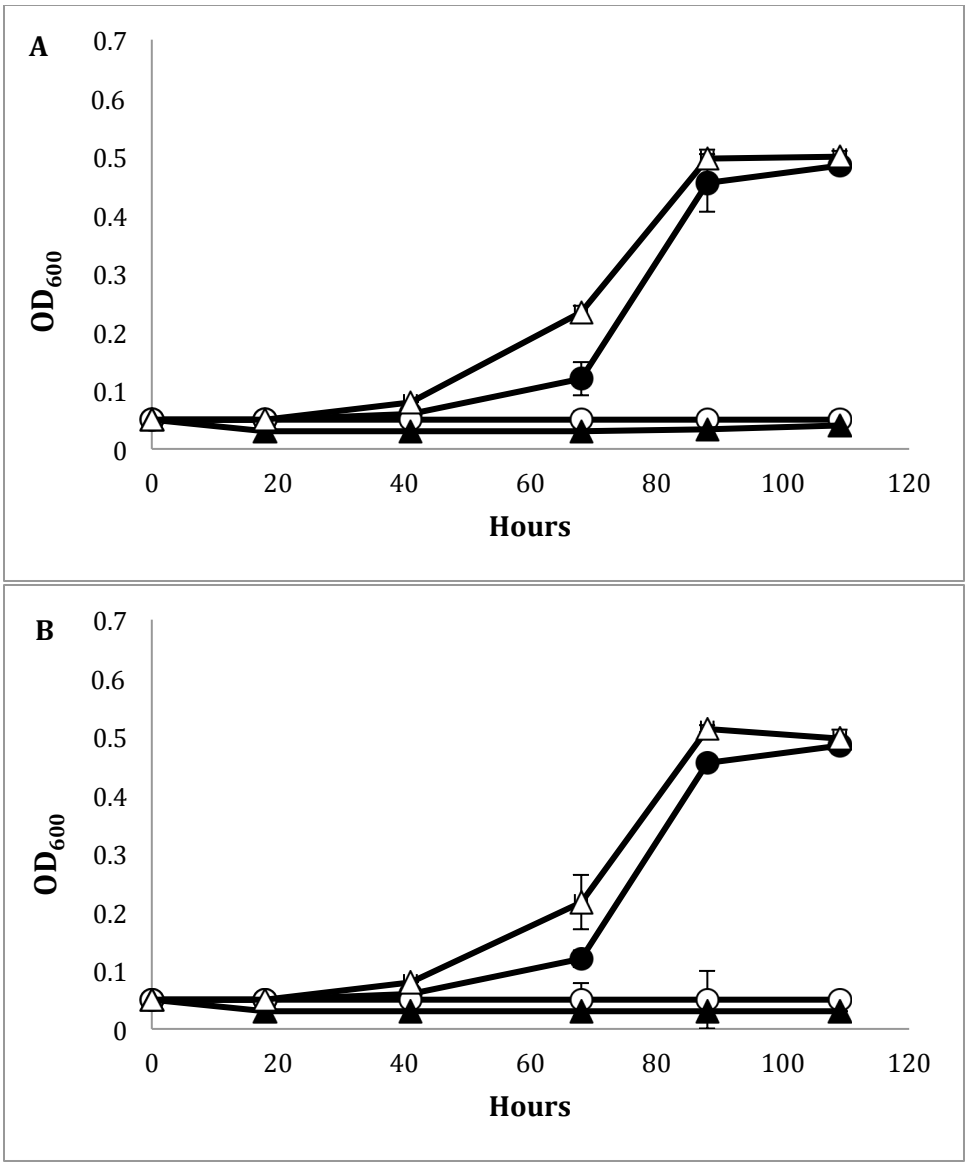

Figure 2. Growth of *M. trichosporium* OB3b *Δ**mbnA*** mutant on methane under (A) 0 µM Cu or (B) 1 µM Cu. 0 µM Hg + 0 µM MB (●), 5 µM Hg + 0 µM MB (○), 5 µM Hg + 5 µM MB (▲), 5 µM Hg + 50 µM MB (Δ). All data are means of triplicate samples. Error bars represent standard deviation (SD, n=3). When error bars are not visible, they are smaller than the size of the symbols.

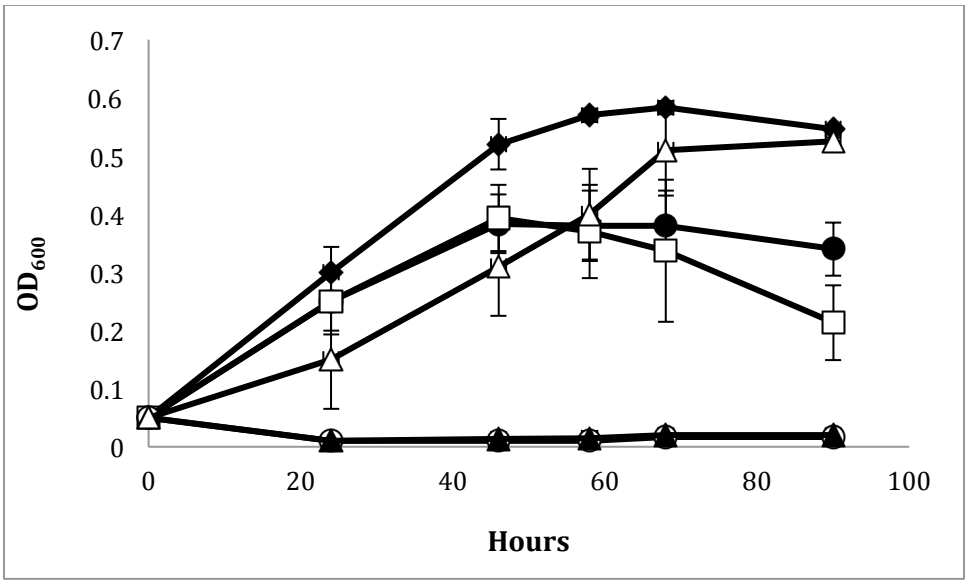

Figure 3. Growth of *Methylocystis* strain SB2 on methane under 1 µM Cu. 0 µM Hg + 0 µM MB (●), 5 µM Hg + 0 µM MB (○), 0 µM Hg + 5 µM MB (□), 5 µM Hg + 5 µM MB (▲), 0 µM Hg + 50 µM MB (♦), 5 µM Hg + 50 µM MB (Δ). All data are means of triplicates. Error bars represent standard deviation (SD, n=3). When error bars are not visible, they are smaller than the size of the symbols.

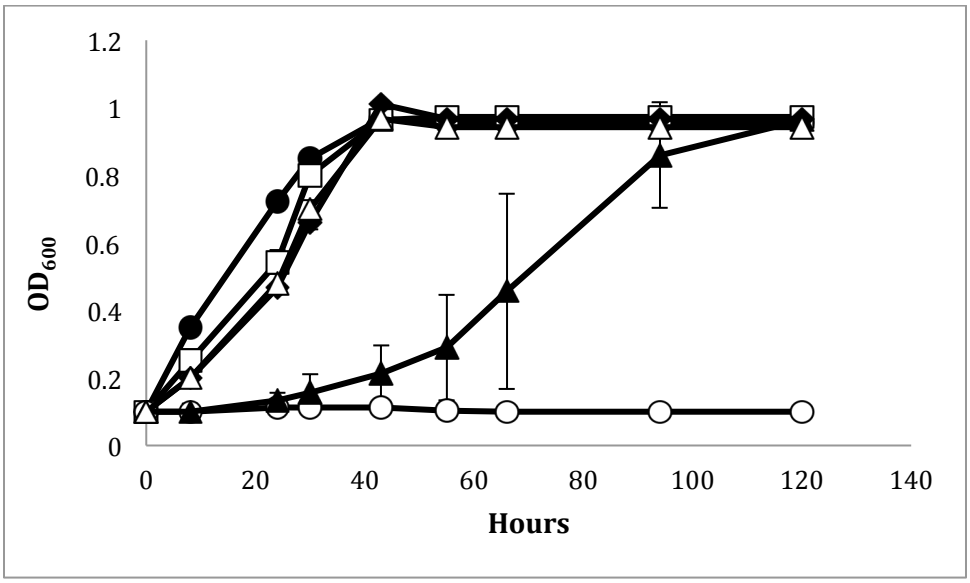

Figure 4. Growth of *M. album BG8* on methane under 1 µM Cu. 0 µM Hg + 0 µM MB (●), 5 µM Hg + 0 µM MB (○), 0 µM Hg + 5 µM MB (□), 5 µM Hg + 5 µM MB (▲), 0 µM Hg + 50 µM MB (♦), 5 µM Hg + 50 µM MB (Δ). All data are means of triplicates. Error bars represent standard deviation (SD, n=3). When error bars are not visible, they are smaller than the size of the symbols.

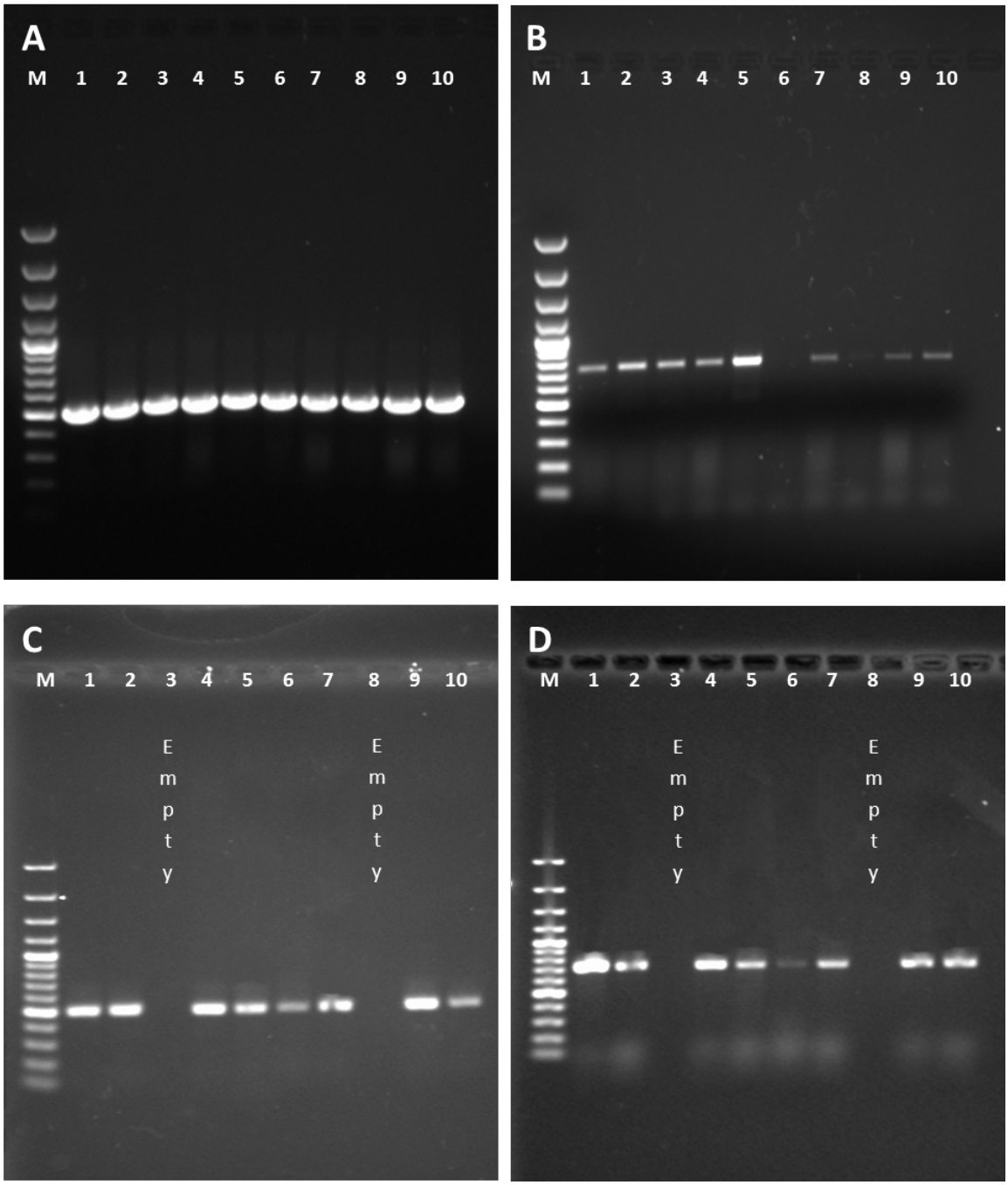

Figure 5. (A) RT-PCR of *M. trichosporium* OB3b wildtype for *pmoA* and (B) RT-PCR of *M. trichosporium* OB3b wildtype for *mmoX*; (C) RT-PCR of *M. trichosporium* OB3b *Δ**mbnA*** mutant for *pmoA* and (D) RT-PCR of *M. trichosporium* OB3b *Δ**mbnA*** mutant for *mmoX*; M – Marker, (1) 0 µM Cu + 0 µM Hg + 0 µM MB, (2) 0 µM Cu + 0 µM Hg + 5 µM MB, (3) 0 µM Cu + 5 µM Hg + 5 µM MB, (4) 0 µM Cu + 5 µM Hg + 50 µM MB, (5) 0 µM Cu + 0 µM Hg + 50 µM MB, (6) 1 µM Cu + 0 µM Hg + 0 µM MB, (7) 1 µM Cu + 0 µM Hg + 5 µM MB, (8) 1 µM Cu + 5 µM Hg + 5 µM MB, (9) 1 µM Cu + 5 µM Hg + 50 µM MB, (10) 1 µM Cu + 0 µM Hg + 50 µM MB. Note that no RT-PCR was attempted for either strain in the

presence of Hg and the absence of MB for *M. trichosporium* wildtype and for *M. trichosporium* OB3b *ΔmbnA* mutant in the presence of 5 µM Hg and 5 µM mb as no growth was observed in these conditions.

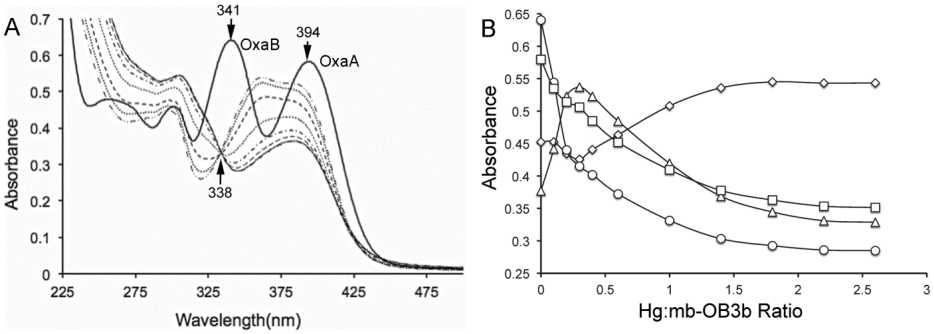

Figure 6. UV-visible absorption spectra of MB from M. trichosporium OB3b (——) as isolated and following the addition of 0.3 (—••—••), 0.4 (••••), 0.6 (– – –), 1.4 (·····) and 2.6 (——) Hg(II) per MB. B. Absorption at 304 (◇), 341 (△), 364 (O) and 391 (□) nm following Hg(II) additions.

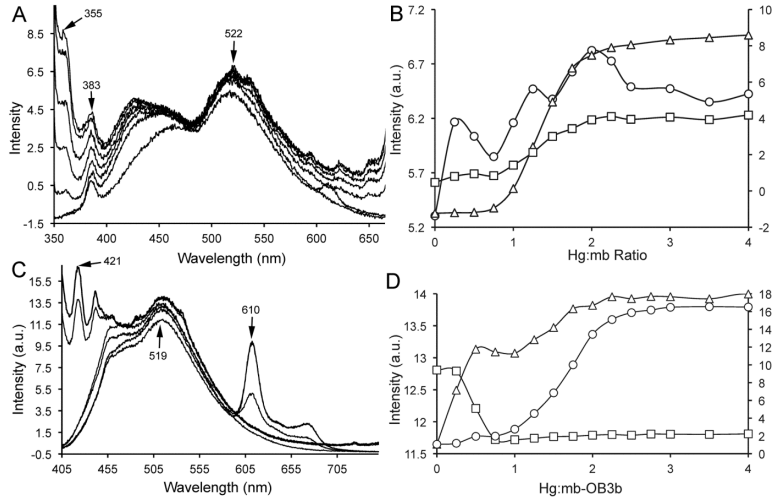

Figure 7. (A) Emission spectra of MB-OB3b with excitation at 341 nm and following the addition of 1.0, 1.25, 1.5, 2.0 and 4.0 Hg(II) per MB from *M. trichosporium* OB3b. (B) Intensity at 355 (△), 383 (□), and 521 (O) nm following excitation at 341 nm. (C) Emission spectra of MB with excitation at 394 nm and following the addition of 0.25, 0.5, 0.75, 2.0 and 3.0 Hg (II) per MB. (B) Intensity at 421 (△), 519 (O), and 610 (□) nm following excitation at 394 nm.

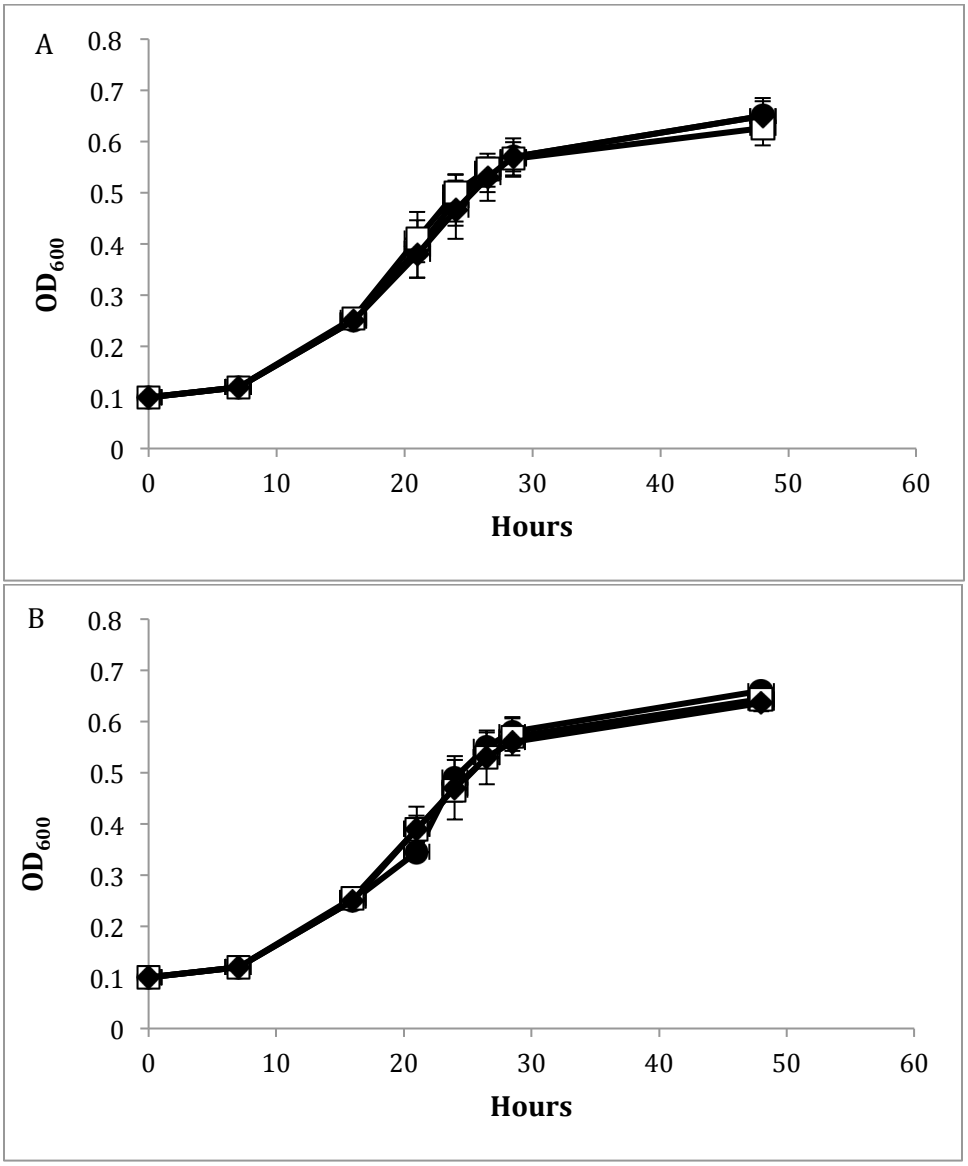

Supplementary Figure 1. Growth of strain *M. trichosporium* OB3b wildtype on methane under (A) 0 µM Cu or (B) 1 µM Cu. 0 µM Hg + 0 µM mb (●), 0 µM Hg + 5 µM mb (□), 0 µM Hg + 50 µM mb (♦). All data are means of triplicate samples. Error bars represent standard deviation (SD, n=3). When error bars are not visible, they are smaller than the size of the symbols.

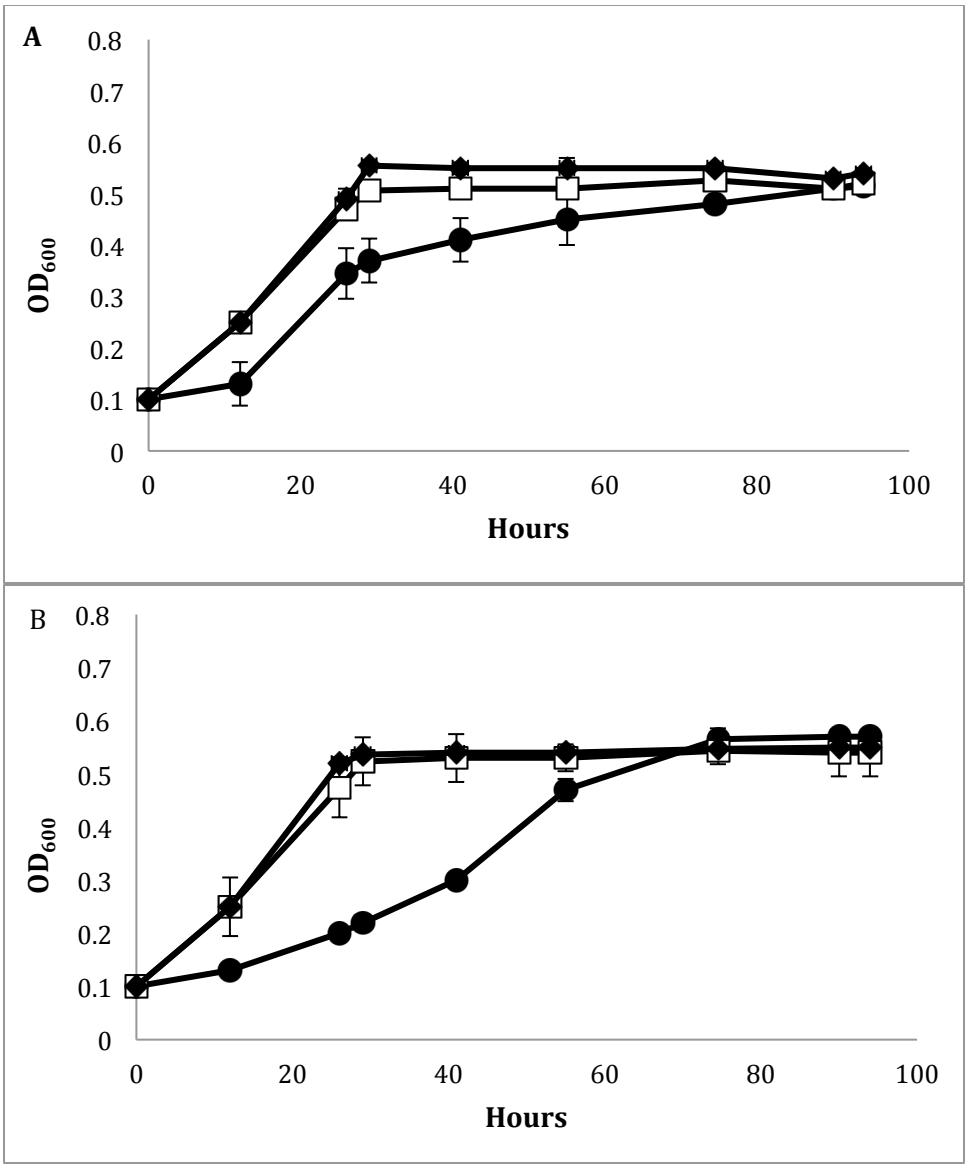

Supplementary Figure 2. Growth of strain *M. trichosporium* OB3b Δ***mbnA*** on methane under (A) 0 µM Cu or (B) 1 µM Cu. 0 µM Hg + 0 µM mb (●), 0 µM Hg + 5 µM mb (□), 0 µM Hg + 50 µM mb (♦). All data are means of triplicate samples. Error bars represent standard deviation (SD, n=3). When error bars are not visible, they are smaller than the size of the symbols.

CHAPTER 4

COMPETITION BETWEEN METALS FOR BINDING TO METHANOBACTIN ENABLES EXPRESSION OF SOLUBLE METHANE MONOOXYGENASE IN THE PRESENCE OF COPPER

Bhagyalakshmi Kalidass, Muhammad Farhan Ul-Haque, Bipin S. Baral, Alan A. DiSpirito, Jeremy D. Semrau

Modified from a paper published in Journal of Applied and Environmental Microbiology

Abstract

It is well known that copper is a key factor regulating expression of the two forms of methane monooxygenase found in proteobacterial methanotrophs. Of these forms, the cytoplasmic, or soluble, methane monooxygenase (sMMO) is expressed only at low copper concentrations. The membrane-bound, or particulate, methane monooxygenase (pMMO) is constitutively expressed with respect to copper, and such expression increases with increasing copper. Recent findings have shown that copper uptake is mediated by a modified polypeptide, or chalkophore, termed methanobactin. Although methanobactin has high specificity for copper, it can bind other metals, e.g., gold. Here we show that in *Methylosinus trichosporium* OB3b, sMMO is expressed and active in the presence of copper if gold is also simultaneously present. Such expression appears to be due to gold binding to methanobactin produced by *M. trichosporium* OB3b, thereby limiting copper uptake. Such expression and activity, however, was significantly reduced if methanobactin preloaded with copper was also added. Further, quantitative reverse transcriptase PCR (RT- qPCR) of transcripts of genes encoding polypeptides of both forms of MMO and SDS-PAGE results indicate that both sMMO and pMMO can be expressed when copper and gold are present, as gold effectively competes with copper for binding to methanobactin. Such findings suggest that under certain geochemical conditions, both forms of MMO may be expressed and active *in situ*. Finally, these findings

also suggest strategies whereby field sites can be manipulated to enhance sMMO expression, i.e., through the addition of a metal that can compete with copper for binding to methanobactin.

Introduction

The increased availability of methane through industrial practices such as hydraulic fracturing has enhanced interest in using methanotrophs, prokaryotes that thrive on methane as their sole source of carbon and energy, to convert methane to more valuable products, e.g., liquid biofuels, plastics, and protein to supplement animal feed (1–7). Methanotrophs have also received increasing attention given that methane is a very potent green- house gas, with a global warming potential 28 to 34 times that of carbon dioxide over a 100-year period (8), and methanotrophs are estimated to remove up to 90% of the methane produced in anaerobic soils (9). Methanotrophs are widespread in the environment, found in diverse locations such as landfill cover, forest, agricultural, and volcanic soils; freshwater and marine sediments; and sewage sludge (6, 10, 11). Many are amenable to genetic manipulation (12–18).

An important issue, however, in the use of methanotrophy for any purpose is that the first step in methane oxidation, the conversion of methane to methanol, is performed by two different forms of methane monooxygenase (MMO) with different oxidation kinetics and affinities for methane. One form, the soluble methane monooxygenase (sMMO), is found in the cytoplasm and has relatively high turnover (maximal whole-cell methane oxidation rate [V_{max}] of 730 nmol. min^{-1}. mg of $protein^{-1}$) but poor affinity (whole- cell binding constant [K_s] of 90 μM). The other form, the particulate methane monooxygenase (pMMO), is found in the intracytoplasmic membranes and has relatively low turnover ($V_{max,}$ ~80 nmol. min^{-1}. mg of $protein^{-1}$) but greater affinity (K_s, ~8 μM). The form of MMO expressed is of importance, as

the utility of methanotrophs for various applications, including methane oxidation and pollutant degradation, is strongly dependent on which form of MMO is expressed (19,20).

It is well known that copper plays a key role in the expression of the two forms of MMO. sMMO expression is evident only when copper concentrations in the growth medium are low (e.g., sub-micromolar). pMMO is constitutively expressed, however, with respect to copper, and its expression increases with increasing copper (21, 22). For the sequestration of copper, many methanotrophs have been found to synthesize different chalkophores for copper uptake, akin to siderophores used for iron uptake. These chalkophores, collectively called methanobactin, are small modified polypeptides (<1,200 Da) with two heterocyclic rings (one of which is an oxazolone ring and that other of which is either an oxazolone, imidazolone, or pyrazinedione ring) and associated enethiol groups (23-26). Copper is bound by methanobactin with very high affinity (reported affinities range from 10^{20} to 10^{34} M^{-1} [24,27-30]) using nitrogen from both heterocyclic rings and the sulfur of the enethiol groups.

The metal binding moieties of methanobactin, however, can bind many other metals, but generally with much lower affinities, ~10^{5} to 10^{7} M^{-1} (30). Detailed study of methanobactin from *Methylosinus trichosporium* OB3b indicated that these metals can be divided into two general groups. The first group, group A, are those metals that are bound to both heterocyclic rings of methanobactin (both being oxazolone rings) and are reduced following binding. These metals include Cu(II), Ag(I), Au(III), Hg(II), and Pb(II). The second group, group B, includes those metals that are bound to only one oxazolone ring and are not reduced after binding. These metals include Cd(II), Co(II), Fe(III), Mn(II), Ni(II), and Zn(II) (30).

Further, it has been found that at least one metal, Hg(II), binds to methanobactin with rapid kinetics, with most binding occurring in the dead time of the stopped-flow system used (1.8 ms). For the remainder, binding was observed to have a rate of 640 s^{-1} (31). Therefore, despite the presence of copper, mercury can be irreversibly bound to methanobactin. It may be that in the presence of copper, sMMO expression may be possible due to the inability of methanotrophs to collect copper via methanobactin because of the presence of competing metals. Here we report on the effects of various group A and B metals added in conjunction with copper on expression of sMMO and pMMO in *M. trichosporium* OB3b.

Materials and Methods

Bacterial strain and growth conditions

M. trichosporium OB3b was grown on nitrate mineral salt (NMS) medium (32) at 30°C in 250-ml sidearm Erlenmeyer flasks shaken at 200 rpm in the dark either with no added copper (creating a background copper concentration of 0.03 ± 0.01 μ,M) or with 2 μM copper (added as $CuCl_2$). For consideration of the effect of competing metals for binding to methanobactin, various concentrations of Ag as $AgNO_3$, Hg as $HgCl_2$, Au as $HAuCl_4$, Zn as $ZnSO_4 \cdot 7H_2O$, Mn as $MnCl_2 \cdot 4H_2O$, Mo as $Na_2MoO_4 \cdot 2H_2O$, Ni as $NiCl_2 \cdot 6H_2O$, and Co as $CoCl_2 \cdot 6H_2O$ were added from metal stock solutions of either 10 mM or 100 mM. All chemicals were of American Chemical Society grade or better. Specific concentrations and combinations of metals considered are shown in Table 1. Methanobactin from *M. trichosporium* OB3b was purified as described previously (33). Copper-methanobactin was then prepared by adding equimolar amounts of copper and methanobactin to create a 5 mM stock solution. Copper-methanobactin was freshly pre- pared at 30°C under constant mixing

at 200 rpm in the dark for 1 h before use. Copper-methanobactin was then added to some cultures at a concentration of 5 μM. All conditions were run using biological duplicates.

Protein measurements

The procedure outlined by Semrau et al. (34) was used to quantify protein concentrations. Briefly, protein was measured using the Bradford assay (Bio-Rad Laboratories) after concentration of 5 ml of the culture to 1 ml and digestion in 2 M NaOH (0.4 ml 5 M NaOH per 1.0 ml of culture) at 98°C for 15 min. A plot of protein concentrations of cultures of *M. trichosporium* OB3b cells at different optical densities at 600 nm (OD_{600}) yielded a linear regression of an OD_{595} value of 1.0, equal to 850 μg of protein per ml, with a coefficient of determination value (R^2) of 0.995. This correlation was used to calculate protein concentration for all cultures.

Metal measurements

Cultures were centrifuged at 5,000 X g for 10 min at 4°C. Supernatant samples were stored at -80ºC and cell pellets resuspended in 1 ml of fresh NMS medium before storage at -80ºC. Supernatant samples were then diluted in NMS medium with 5% (vol/vol) HNO_3 to achieve a final concentration of 2% (vol/vol) HNO_3. Cell suspensions were acidified in 1 ml of 70% (vol/vol) HNO_3 and incubated for 2h at 95°C (31). The acidified cell suspensions were mixed by inverting the tubes every 30 min. Copper and gold associated with biomass and supernatant were analyzed using an inductively coupled plasma mass spectrometry (ICP-MS) instrument (PerkinElmer, Waltham, MA). Duplicate biological samples were used for

each combination of copper, gold, and copper-methanobactin, with each replicate measured five times.

Measurement of sMMO activity

The activity of soluble methane monooxygenase (sMMO) was also monitored by performing a colorimetric assay as developed by Brusseau et al. (35). Briefly, a 2-ml aliquot of *M. trichosporium* OB3b under each growth condition was transferred to a 2-ml Eppendorf centrifuge tube and naphthalene was added. The cultures were then incubated for 1 h at 30°C and shaken at 200 rpm. Cells were pelleted by centrifugation for 5 min at 5,800 X g. Tetrazotized o-dianisidine (130 µl of 4.21 mM) was added to 1.3 ml of supernatant in a 1.5-ml cuvette. All experiments were performed using biological duplicates.

Nucleic acid extraction and real-time quantitative reverse transcriptase PCR (RT-qPCR)

RNA was extracted from *M. trichosporium* OB3b grown in 250-ml sidearm flasks as described previously (31, 34). Briefly, 2.5 ml of stop solution (5% buffer equilibrated phenol [pH 7.3] in ethanol) was added to individual cultures (22.5 ml each) to stop any new mRNA synthesis. Cell pellets were then collected by centrifugation at 5,000 X g for 10 min at 4°C. The cell pellet was then resuspended in 0.75 ml of extraction buffer, and subsequent steps were performed to extract RNA as described previously (31, 34). RNA was then subjected to RNase free DNase treatment until free of DNA contamination. RNA was checked for any DNA contamination via PCR amplification of the 16S rRNA gene, and the concentration of purified RNA was determined spectrophotometrically (NanoDrop ND1000; NanoDrop

Technologies, Inc., Wilmington, DE). RNA samples were stored at -80ºC and used for cDNA synthesis within 2 days of extraction. cDNA was prepared from DNA-free RNA samples (500 ng each) by reverse transcription using Superscript III reverse transcriptase (Invitrogen, Carlsbad, CA) according to the manufacturer's instructions.

Relative expression of the *pmoA*, *mmoX*, and *mbnA* genes in *M. trichosporium* OB3b grown at various concentrations of copper, gold, and/or copper-methanobactin was quantified by RT-qPCR. Amplifications of *pmoA*, *mmoX*, and *mbnA* and 16S rRNA genes were performed using primer pairs (5'-3') TTCTGGGGCTGGACCTAYTTC and CCGACAGCAGCAGGATGATG for *pmoA* (amplicon length, 94 bp), TCAACACCGATCTSAACAACG and TCCAGATTCCRCCCCAATCC for *mmoX* (amplicon length, 153 bp), TGGAAACTCCCTTAGGAGGAA and CTGCAC GGATAGCACGAAC for *mbnA* (amplicon length, 107 bp), and GCAGA ACCTTACCAGCTTTTGAC and CCCTTGCGGGAAGGAAGTC for 16S rRNA (amplicon length, 66 bp) (34). The threshold cycle (C_T) values were measured from cDNA preparations in 96-well PCR plates using the Mx3000P qPCR system (Stratagene, La Jolla, CA). Each RT-qPCR was carried out in a final volume of 20 µl containing 0.8 µl of cDNA, 1X Brilliant III SYBR green qPCR Mastermix (Agilent Technologies, Santa Clara, CA), 15 nM ROX dye, a 0.5 µM concentration each of gene-specific forward and reverse primers, and nuclease-free sterile water (Ambion, Life Technologies, Grand Island, NY). A three-step PCR program, with an initial denaturation at 95°C for 10 min and 40 cycles of denaturation (95°C for 30 s), annealing (58°C for 20 s), and extension (68°C for 30 s), was performed. The specificities of qPCR products were verified by melting curve, gel electrophoresis, and sequencing. Average C_T values obtained from MxPro software (Stratagene, La Jolla, CA)

were always in the linear range of amplification as determined by the standard curve for each gene (see Fig. S1 in the supplemental material). These C_T values were then used to calculate the relative gene expression levels with 16S rRNA as the housekeeping gene by the comparative threshold amplification cycle method ($2^{-\Delta\Delta CT}$), as described previously (36). Measurements were performed for two biological replicates for each growth condition.

Isolation of soluble and membrane fractions

M. trichosporium OB3b was also cultured for soluble and membrane fractions. Cells from NMS agar plates were used to inoculate four 250-ml Erlenmeyer flasks each with 50 ml of NMS medium with no added copper (i.e., a background concentration of 0.03 ± 0.01 μM copper) at 30°C. After an OD_{600} of ~0.7 was reached, these cultures were used to inoculate four 2-liter Erlenmeyer flasks each with 250 ml of NMS medium with no added cop- per. After these cultures subsequently grew to an OD_{600} of ~0.7, this combined 1 liter of cell culture was used to inoculate a 14-liter BioFlo and Celligen 310 fermenter (New Brunswick, Enfield, CT), again with no added copper. Growth was promoted by providing continuous methane-air feed rates of 70 ml min^{-1} for methane and 700 ml min^{-1} for air. After 24 h, the fermenter was filled with 8 liters of NMS medium, again with no added copper, and incubated for 24 h. Following the incubation period, 7 liters of culture was removed. The copper concentration in the remaining medium in the fermenter was then increased to 2 μM as $CuCl_2$, and an additional 7 liters of NMS medium amended with 2 μM copper as $CuCl_2$ was added. The culture was incubated for 24 h, and 7 liters of culture was then removed. The remaining medium was then amended with 5 μM Au as $HAuCl_4$, and the fermenter was filled with an additional 7 liters of NMS medium containing 2 μM copper as $CuCl_2$ plus 5 μM Au

as $HAuCl_4$. After another 24 h, 7 liters of culture was removed. The remaining medium was then amended with 5 μM copper-methanobactin, and the fermentor was filled with an additional 7 liters of NMS medium containing of 2 μM copper as $CuCl_2$, 5 μM Au as $HAuCl_4$, and 5 μM copper-methanobactin. After 24 h, the entire fermenter culture was harvested. Cells from the fermenter were collected by centrifugation at 4,550 x g for 30 min, and the cells were resuspended in minimal volume of 10 mM morpholinepropanesulfonic acid (MOPS) buffer (pH 7.3). The cell suspension was then centrifuged at 14,600 X g for 15 min and the pellet resuspended in 30 mM MOPS buffer (pH 7.3) to a final volume of 150 ml. The washed cell suspension was deoxygenated by 4 cycles of vacuum, followed by purging with argon. All manipulations after this were conducted in a type B Coy anaerobic chamber (95% argon and 5% hydrogen). Cells and subsequent fractions were kept at 4°C. The deoxygenated cell suspension was lysed with four passes on an Emulsiflex high-pressure homogenizer (Avestin, Ottawa, ON, Canada) at 25,000 to 30,000 $lb.in^{-2}$. The lysate was centrifuged at 14,600 X g for 15 min. The pellet was discarded, and the supernatant was centrifuged at 244,000 X g for 1.5 h. The supernatant was centrifuged a second time at 244,000 x g for 1.5 h to remove contaminating membranes, and the supernatant fraction was regarded as the soluble fraction. This supernatant was divided into smaller fractions and stored at -20ºC. The pellets from the centrifugations at 244,000 x g were resuspended using a Dounce homogenizer in 30 mM MOPS and 1 M KCl buffer (pH 7.3) and centrifuged at 244,000 X g for 1.5 h. The membrane pellet was resuspended in a minimal volume of 30 mM MOPS buffer (pH 7.3) and stored at -20ºC

Electrophoresis

Sodium dodecyl sulfate-polyacrylamide gel electrophoresis (SDS-PAGE) was performed on precast 12% Bis-Tris gels with MOPS-SDS running buffer as specified by the manufacturer (Invitrogen, NY). The gels were run at 60 V for 30 min and then at 100 V for another 3 h. Approximately 15-µg quantities of total protein from soluble and membrane fractions were loaded in the gels together with prestained broad-range SDS-PAGE standards (Bio-Rad, CA). Finally, the gels were stained with Coomassie brilliant blue R.

Prediction of metal speciation

Copper speciation in NMS medium amended with either copper or copper and gold was predicted using Visual Minteq version 3.0 (http://vminteq.lwr.kth.se/) using the assumption of equilibrium. pH and temperature were set at 6.8 and 30°C, respectively, to simulate growth conditions. The model parameter and interface model were set to the default hydrous ferric oxide model (37) and a 2-site protonation model (38), respectively.

Mixed-metal binding by methanobactin from M. trichosporium OB3b

Binding of gold and copper by methanobactin under mixed-metal conditions was determined in solutions containing $CuCl_2$, $HAuCl_4$, and methanobactin in molar ratios of 0.25:0.25:1, 0.5:0.5:1, 1:1:1, 1.5:1.5:1, and 2:2:1 as previously described for copper-mercury-methanobactin mixtures (39). Briefly, 100 µM methanobactin was added to various concentrations of gold and copper with a total volume of 20 ml and incubated with stirring (200 rpm) at room temperature for 5 min. Following this incubation period, the solution was loaded onto pre-equilibrated Sep-Pak cartridges (Millipore Corporation, Billerica, MA). Sep-

Pak cartridges were equilibrated by one wash with 3 ml of methanol, one wash of 3 ml of acetonitrile, one wash of 3 ml of methanol, and three washes of 3 ml of >18-MΩ·cm of H_2O. Once the reaction solution was loaded, the Sep-Pak cartridges were washed three times with 6 ml of >18 MΩ· cm H_2O and the methanobactin fraction was eluted with 60% acetonitrile - 40% H2O >18 MΩ· cm H_2O. Both the wash and eluted sample were diluted with a 5% trace-metal-grade HCl–5% trace-metal-grade HNO_3–90% >18MΩ · cm H_2O solution. Copper and gold concentrations in the wash solution and 60% acetonitrile eluent were determined on an Agilent 55 AA atomic absorption spectrometer (Agilent Technologies, Santa Clara, CA) run in flame mode. All measurements were done for triplicate samples, and each sample was measured five times.

Gold displacement of copper bound to methanobactin

Displacement of copper prebound to methanobactin was determined by monitoring changes in UV-visible (UV-Vis) absorption spectra following the addition of an equimolar concentration of gold as $HAuCl_4$. Briefly, a methanobactin concentration of 75 μM was incubated with an equimolar amount of copper as $CuCl_2$ as described above. Gold was then added at an equimolar amount as $HAuCl_4$, and the UV-Vis absorption spectra were measured immediately afterwards.

The kinetics for gold displacement of copper from methanobactin were determined by measuring absorption changes at 336 nm, using a four-syringe Biologic SFM/4000/S stopped-flow reactor coupled to a MOS-500 spectrophotometer (Biologic Science Instrument SA, Claix, France) at room temperature (23 to 24°C). Metal stock solutions of $CuCl_2$ or $HAuCl_4$ were prepared in >18 MΩ · cm of H_2O, followed by the addition of Cu(II) to

methanobactin in a molar ratio of Cu(II) to methanobactin of 1 to 1. The stock solutions for methanobactin were prepared by dissolving freeze-dried methanobactin in >18 MΩ·cm of H_2O. The stock solutions of $CuCl_2$, $HAuCl_4$, and copper-methanobactin were chilled on ice and then filtered through a 0.22-μm filter before being loaded into sample syringes. The final concentration of the stock copper- methanobactin solution after filtration was determined by UV-visible absorption spectroscopy (33). The path length for the cuvette used in the Biologic SFM/4000/S stopped-flow reactor was 1.5 mm. The dead time of the system was 1.4 ms. The reaction mixture contained 400 μM copper-methanobactin and 400 μM $HAuCl_4$. Rates obtained were an average of 5 traces, and the experiment was repeated four times. The rates were determined by fitting the traces to the exponential function in Bio-Kine operational software (Biologic Science Instrument SA).

Statistical analyses

Data were analyzed using unpaired, two-tailed Student's *t* tests assuming equal variance between groups to determine any significant differences in the response of *M. trichosporium* OB3b to different culture conditions.

Results

Growth and expression of sMMO in the presence of copper and various metals

An initial survey of both group A and B metals was performed to determine if, in the increased presence of these metals, sMMO expression was possible in the simultaneous presence of 2 μM copper. As shown in Table 1, *M. trichosporium* OB3b grew in the presence of many group B metals (Zn, Mn, Mo, Ni, and Co), either singly or in combination at

concentrations as high as 500 μM each. In no case, however, was any sMMO activity observed via the naphthalene assay. Given these results, further study of the effect of these metals on methanotrophic activity was not pursued. Of the three tested group A metals, mercury and silver were toxic at a concentration as low as 5 μM (i.e., no growth was observed) and were also not considered further. Growth, however, occurred in the presence of 5 μM gold, and despite the presence of 2 μM copper, sMMO activity was observed via the naphthalene assay. The impact of gold on methanotrophic activity and gene expression was thus explored in more detail.

pmoA, mmoX, and mbnA expression in *M. trichosporium* OB3b in the presence of copper, gold, and copper-methanobactin

Figure 1A shows that *pmoA* expression was constitutive in the presence of 2 μM copper regardless of the simultaneous presence of various amounts gold and copper-methanobactin, and such expression was not significantly different across all tested conditions ($P > 0.05$). As expected, in the presence of 2 μM copper, very little *mmoX* expression was observed (Fig. 1B). In the presence of 2 μM copper and 5 μM gold, however, *mmoX* expression increased over 10,000-fold (significant at a P value of <0.003). In the presence of 2 μM copper, 5 μM gold, and 5 μM copper-methanobactin, very little *mmoX* expression was observed, and it was not significantly different from that observed in the presence of only 2 μM copper ($P < 0.4$). Interestingly, *mmoX* expression was 5-fold greater in the presence of 2 μM copper and 5 μM gold than when the two metals were not added ($P < 0.007$). Expression of *mbnA* also varied in response to changing growth conditions, as shown in Fig. 1C. Specifically, *mbnA* expression increased significantly in the presence of 2

μM copper and 5 μM gold compared to that in the presence of 2 μM copper alone ($P < 0.03$) and was similar to that observed when neither copper nor gold was added ($P = 0.09$). When 5 μM copper-methanobactin was also added, expression of *mbnA* decreased but was not significantly different from the level of expression when *M. trichosporium* OB3b was grown either with 2 μM copper or with 2 μM copper and 5 μM gold ($P = 0.5$ and 0.12, respectively).

SDS-PAGE analyses of pMMO and sMMO polypeptides

To determine if sMMO polypeptides were formed in addition to gene expression, SDS-PAGE analyses were performed for both membrane and soluble fractions of *M. trichosporium* OB3b grown at various copper, gold, and copper-methanobactin concentrations. As shown in Fig. S2 in the supplemental material, it appears that polypeptides associated with sMMO and pMMO were present under all conditions but that sMMO expression was greatest in the absence of copper, gold, and copper-methanobactin and was lowest in the presence of 2 μM copper. When 5 μM gold was added in conjunction with 2 μM copper, expression of sMMO polypeptides appeared to increase, while pMMO polypeptides appeared to decrease. Finally, in the presence of 2 μM copper, 5 μM gold, and 5 μM copper-methanobactin, expression of sMMO polypeptides appeared to decrease compared to expression when *M. trichosporium* OB3b was grown in the presence of 2 μM copper and 5 μM gold, while pMMO polypeptides appeared to increase.

sMMO activity in the presence of copper, gold, and copper- methanobactin

To determine if sMMO was active as well as its genes expressed in the presence of gold, copper, and methanobactin pre-equilibrated with copper, the naphthalene assay was

used to monitor sMMO activity (35). As shown in Fig. 2, in the presence of 2 μM copper, no sMMO activity was observed. Clear evidence of naphthalene oxidation, however, was observed in cultures grown with no added copper, gold, or copper-methanobactin, as well as in the presence of both 2 μM copper and 5 μM gold, indicating that the genes for sMMO were expressed and active enzyme was produced under these conditions. When 5 μM copper-methanobactin was added in addition to 2 μM copper and 5 μM gold, no sMMO activity was observed, and this is in agreement with the results of RT-qPCR and SDS-PAGE analyses.

Copper and gold associated with biomass

As shown in Fig. 3, ICP-MS analyses of the biomass of *M. trichosporium* OB3b indicated that in the presence of gold, the amount of copper associated with biomass significantly decreased, -2.3-fold ($P < 0.03$). When copper was also added as copper-methanobactin, copper per unit biomass increased -40% compared to that in cultures grown only in the presence of copper, but such an increase was not statistically significant ($P < 0.2$). Approximately 85 times more gold was associated with biomass than copper when both were present in the growth medium (- 27 times more on a molar basis). In the simultaneous presence of 5 μM copper-methanobactin, the amount of gold per unit biomass was reduced by - 60% (significant at a P value of <0.03), but approximately 10 times more gold was associated with biomass than copper under these conditions (- 3 times more on a molar basis).

Metal speciation

The MINTEQ program was run for two conditions: (i) the presence of 2 μM copper and (ii) the presence of 2 μM copper and 5 μM gold. The results (see Table S1 in the supplemental material) show no differences in the distribution of Cu^{2+} between these conditions, indicating that the observed response of *M. trichosporium* OB3b in the presence of gold and copper versus copper alone was not due to the addition of gold causing copper speciation to change.

Mixed-metal binding and gold displacement of copper from copper-methanobactin

To estimate the extent of competition between copper and gold for binding to methanobactin from *M. trichosporium* OB3b, copper, gold, and methanobactin were incubated in the presence of both metals at different molar ratios of gold to copper to methanobactin. Surprisingly, methanobactin preferentially bound Au(III) over Cu(II) at all metal-to-methanobactin ratios tested (Fig. 4). Based on these results, the capacity of Au(III) to displace copper already bound to methanobactin was examined. The UV-visible absorption spectral changes following the addition of Au(III) to copper-methanobactin were consistent with the displacement of copper (Fig. 5A). To determine the displacement rate, the decrease in absorbance at 336 nm was measured (Fig. 5B). The displacement showed an initial high rate, 67.89 ± 0.12 s^{-1}, followed by a low rate, 23.19 ±0.014 s^{-1}, after 0.084 s.

Discussion

It is commonly stated that for those methanotrophs that can express both forms of MMO (i.e., the "switchover" strains), sMMO is expressed only when copper concentrations

are low. Such a conclusion is based on laboratory experiments that used simple culture conditions to identify the response of methanotrophs to various amounts of copper (for examples, see references 21, 22, and 40). Although these experiments provided insight into the role of copper in methanotrophic physiology, one should keep in mind that natural environments are intrinsically much more complex, with the geochemistry of many environments poorly understood. It should also be stressed that there are very few reported examples of sMMO expression in nature (for examples, see references 41 to 43), raising the question, "Under what conditions do methanotrophs express sMMO *in situ*?"

To answer this question, one must consider not only the geochemistry of various natural environments, i.e., whether copper is present or not, but also the mechanism(s) by which methanotrophs collect copper, i.e., methanobactin. This chalkophore is well known to have a very high affinity for copper ($>10^{20}$ M^{-1}), but it has also been recently found that methanobactin from *M. trichosporium* OB3b can bind other metals (e.g., group A metals such as mercury and gold) and that copper cannot displace these after they are bound to methanobactin (30). Further, at least for mercury, binding to methanobactin is very rapid, and as a result, substantial mercury binding can occur even in the presence of copper (31).

With this in mind, we chose to rephrase the question above to instead ask, "What happens to copper uptake and resulting MMO expression in methanotrophs when other metals are present along with copper?" From the data presented here, it is obvious that group B metals (those that bind to only one of the oxazolone rings of methanobactin from *M. trichosporium* OB3b and are displaced if copper is subsequently added) have no effect on expression of sMMO in *M. trichosporium* OB3b. Although it was not measured, it appears that the presence of these metals had little impact on the ability of *M. trichosporium* OB3b to

sequester copper (based on the lack of sMMO expression when these metals were added in excess). However, at least one group A metal, gold, can limit copper uptake by *M. trichosporium* OB3b. It appears that binding of gold by both oxazolone rings of methanobactin of *M. trichosporium* OB3b prevents copper from displacing gold once bound and, as a result, allows for sMMO expression and activity in the presence of copper. Further, substantially more gold than copper was found to be associated with biomass when both were added (Fig. 3).

Such a finding can be explained by considering the mixed-metal binding studies. It was found that in the presence of equimolar amounts of copper, gold, and methanobactin, more gold was associated with methanobactin than copper (Fig. 4). This is surprising, as the affinity of methanobactin for gold is reported to be many orders of magnitude lower than that measured for copper (30). It appears, as was found for mercury (31), that the kinetics of gold binding are rapid (Fig. 5) and possibly irreversible, and this may allow for the binding of gold in the presence of copper.

Thus, it should be stressed that it is inaccurate to predict, based on measurement of copper concentration alone, if sMMO will be expressed. Rather, it is expressed when methanotrophs are limited in their ability to sequester copper, e.g., through competition between metals for binding to methanobactin. This is supported by the finding that if methanobactin was preloaded with copper and added at a concentration of 5 μM, along with 2 μM copper and 5 μM gold, *mmoX* expression decreased significantly compared to expression in the presence of 2 μM copper and 5 μM gold (Fig. 1), expression of sMMO polypeptides decreased, and no sMMO activity was apparent (Fig. 2; see also Fig. S2 in the supplemental material). Further, the amount of copper associated with biomass increased

significantly (Fig. 3). It appears that under these conditions, *M. trichosporium* OB3b was able to sequester copper and, by doing so, to prevent sMMO expression and activity. It is interesting, however, that a substantial amount of gold was still associated with the biomass. It appears that the endogenous methanobactin produced by *M. trichosporium* OB3b bound gold under these conditions, but the uptake of gold itself did not allow for sMMO expression. Rather, it appears that the absence of copper-methanobactin complexes when only gold and copper were present enabled sMMO expression in the presence of copper. It is also interesting that the not only did *mmoX* expression increase in the presence of gold, but also expression of the gene encoding the precursor polypeptide of methanobactin, *mbnA*, increased, and such expression was not significantly different from that in cultures grown in the absence of copper and gold (Fig. 1C). It appears that *M. trichosporium* OB3b responded to the inability to collect copper in the presence of gold by increasing the production of methanobactin.

The addition of gold, although it clearly affected the expression and activity of sMMO as well expression of *mbnA*, had no discernible effect on the expression of *pmoA* in *M. trichosporium* OB3b. It is clear, then, that genes for both forms of MMO were expressed simultaneously in the presence of copper and gold, and it may be that both MMOs were active when *M. trichosporium* OB3b was grown in the presence of gold and copper. It is interesting that polypeptides of both sMMO and pMMO from the bacterial group of *Methylocystaceae* were found in the same sample of microbial communities as associated with the roots of field-grown rice (41). It may be that in many environments, both forms of MMO are simultaneously expressed, either by the same or by different mem- bers of the methanotrophic community. The data presented here suggest that such expression may be

due in part to the presence of copper and other group A metals. The finding that the presence of at least one group A metal, gold, can allow for expression and activity of sMMO in the presence of copper also suggests new strategies to manipulate methanotrophic activity in both natural and engineered environments. It may be desirable to have sMMO expressed due to its faster turnover rate, but inducing sMMO expression may be challenging if copper is present. It is difficult, if not practically impossible, to remove copper from a large complex environment. It may be much easier, however, to reduce copper uptake by adding a group A metal such that methanobactin binding of copper is limited. Certainly the use of gold for such a purpose is not feasible given its high cost. It may be that other group A metals, either singly or in combination, that provide an inexpensive means to selectively force methanotrophic communities to express sMMO can be identified. It is recommended that further field work be done integrating molecular and biochemical assays for detection of the expression and activity of both forms of MMO with more detailed geochemical characterization of metal speciation and concentra- tion. Such work will help determine if there is any correlation between the presence of other metals that can compete with copper for binding to methanobactin and sMMO expression and activity.

Finally, it should be kept in mind that it is unclear how widespread this phenomenon may be; i.e., do all switchover methanotrophs express sMMO in the presence of metals that compete for binding to methanobactin, thereby limiting copper uptake? Do all forms of methanobactin exhibit the same ability to bind gold or other group A metals? Given the significant similarity between the known forms of methanobactin (23–26), it is plausible to presume that they would all bind gold to some degree, but the resultant impact on MMO expression is less clear. For example, some non-switchover methanotrophs, i.e., those that

can express only pMMO, are known to produce methanobactin (24, 25). If these strains are challenged with gold, it may be that their growth and activity may be inhibited, as they cannot express sMMO and are unable to take up sufficient copper to allow for optimal pMMO activity. Therefore, the presence of competing metals may serve to stimulate the survival of switchover methanotrophs *in situ*. It is suggested that future work consider the impact of competing metals for binding to methanobactin in mixed methanotrophic cultures.

Acknowledgement

This research was supported by the Office of Science (BER), U.S. Department of Energy.

References

1. **Asenjo JA, Suk JS.** 1986. Microbial conversion of methane into poly-(3-hydroxybutyrate (PHB): growth and intracellular product accumulation in a type II methanotroph. J Ferment Technol **64:**271–278. http://dx.doi.org/10.1016/0385-6380(86)90118-4.

2. **Conrado RJ, Gonzalez R.** 2014. Envisioning the bioconversion of methane to liquid fuels. Science **343:**621– 62. http://dx.doi.org/10.1126/science.1246929.

3. **Haynes CA, Gonzalez R.** 2014. Rethinking biological activation of methane and conversion to liquid fuels. Nat Chem Biol 10: 331-339. http://dx.doi.org/10.1038/nchembio.1509.

4. **Pieja AJ, Rostkowski KH, Criddle CS.** 2011. Distribution and selection of poly-3-hydroxybutyrate production capacity in methanotrophic bacteria. Microb Ecol **62:**564 – 573. http://dx.doi.org/10.1007/s00248-011-9873-0.

5. **Pieja AJ, Sundstrom ER, Criddle CS.** 2012. Cyclic, alternating meth- ane and nitrogen limitation increases PHB production in a methanotrophic community. Bioresour Technol **107:**385–392. http://dx.doi.org/10.1016/j.biortech.2011.12.044

6. **Semrau JD, DiSpirito AA, Yoon S.** 2010. Methanotrophs and copper. FEMS Microbiol Rev **34:**496 –531.

7. **Wendlandt K-D, Stottmeister U, Helm J, Soltmann B, Jechorek M, Beck M.** 2010. The potential of methane-oxidizing bacteria for applications in environmental biotechnology. Eng Life Sci **10:**87–102. http://dx.doi.org/10.1002/elsc.200900093.

8. **Myhre G, Shindell D, Bréon F-M, Collins W, Fuglestvedt J, Huang J, Koch D, Lamarque J-F, Lee D, Mendoza B, Nakajima T, Robock A, Stephens G, Takemura T, Zhang H.** 2013. Anthropogenic and natural radiative forcing, p 659 –740. *In* Stocker TF, Qin D, Plattner G-K, Tignor M, Allen SK, Boschung J, Nauels A, Xia Y, Bex V, Midgley PM (ed), Climate change 2013: the physical science basis. Contribution of Working Group I to the Fifth Assessment Report of the Intergovernmental Panel on Climate Change. Cambridge University Press, Cambridge, United Kingdom.

9. **Chowdhury TR, Dick RP.** 2013. Ecology of aerobic methanotrophs in controlling methane fluxes from wetlands. Appl Soil Ecol 65:8 –22. http://dx.doi.org/10.1016/j.apsoil.2012.12.014.

10. **Op den Camp H, Islam T, Stott MB, Harhangi HR, Hynes A, Schouten S, Jetten MSM, Birkeland N-K, Pol A, Dunfield PF.** 2009. Environmental, genomic and taxonomic perspectives on methanotrophic *Verrucomicrobia*. Environ Microbiol Rep **1:**293–306. http://dx.doi.org/10.1111/j.1758-2229.2009.00022.x.

11. **Ho A, Vlaemunck SE, Ettwig KF, Schneider B, Frenzel P, Boon N.** 2013. Revisiting methanotrophic communities in sewage treatment plants. Appl Environ Microbiol **79:**2841–2846. http://dx.doi.org/10.1128/AEM.03426-12.

12. **Crombie A, Murrell JC.** 2011. Development of a system for genetic manipulation of the facultative methanotroph *Methylocella silvestris* BL2. Methods Enzymol **495:**119–133. http://dx.doi.org/10.1016/B978-0-12-386905-0.00008-5.

13. **Crombie AT, Murrell JC.** 2014. Trace-gas metabolic versatility of the facultative methanotroph *Methylocella silvestris*. Nature **510:**148 –151. http://dx.doi.org/10.1038/nature13192.

14. **Csáki R, Bodrossy L, Klem J, Murrell JC, Kovács KL.** 2003. Genes involved in the copper-dependent regulation of soluble methane monooxygenase of *Methylococcus*

capsulatus (Bath): cloning, sequencing and mutational analysis. Microbiology **149:**1785–1795.
http://dx.doi.org/10.1099/mic.0.26061-0.

15. **Murrell JC.** 1994. Molecular genetics of methane oxidation. Biodegradation **5:**145–159. http://dx.doi.org/10.1007/BF00696456.

16. **Smith TJ, Murrell JC.** 2011. Mutagenesis of soluble methane monooxygenase. Methods Enzymol **495:**136 –147.
http://dx.doi.org/10.1016/B978-0-12-386905-0.00009-7.

17. **Stafford G, Scanlan J, McDonald I, Murrell JC.** 2003. *rpoN*, *mmoR* and *mmoG*, genes involved in regulating the expression of soluble monooxygenase in *Methylosinus trichosporium* OB3b. Microbiology **149:**1771–1784.
http://dx.doi.org/10.1099/mic.0.26060-0.

18. **Welander PV, Summons RE.** 2012. Discovery, taxonomic distribution, and phenotypic characterization of a gene required for 3-methylhopanoid production. Proc Natl Acad SciUSA **109:**12905–12910.
http://dx.doi.org/10.1073/pnas.1208255109.

19. **Lee S-W, Keeney DR, Lim D-H, DiSpirito AA, Semrau JD.** 2006. Mixed pollutant degradation by *Methylosinus trichosporium* OB3b expressing either soluble or particulate methane monooxygenase: can the tortoise beat the hare? Appl Environ Microbiol **72:**7503–7509.
http://dx.doi.org/10.1128/AEM.01604-06.

20. **Yoon S, Carey JN, Semrau JD.** 2009. Feasibility of atmospheric methane removal using methanotrophic biotrickling filters. Appl Microbiol Biotechnol **83:**949 –956.
http://dx.doi.org/10.1007/s00253-009-1977-9.

21. **Choi D-W, Kunz R, Boyd ES, Semrau JD, Antholine WE, Han J-I, Zahn JA, Boyd JM, de la Mora A, DiSpirito AA.** 2003. The membrane-associated methane monooxygenase (pMMO) and pMMO-NADH:quinone oxidoreductase complex from *Methylococcus capsulatus* Bath. J Bacteriol **185:**5755–5764.
http://dx.doi.org/10.1128/JB.185.19.5755-5764.2003.

22. **Han J-I, Semrau JD.** 2004. Quantification of gene expression in methanotrophs by competitive reverse transcription-polymerase chain reaction. Environ Microbiol **6:**388 –399.
http://dx.doi.org/10.1111/j.1462-2920.2004.00572.x.

23. **Behling LA, Hartsel SC, Lewis DE, DiSpirito AA, Choi DW, Masterson LR, Veglia G, Gallagher WH.** 2008. NMR, mass spectrometry and chemical evidence reveal a different chemical structure for methanobactin that contains oxazolone rings. J Am Chem Soc **130:**12604 –12605.
http://dx.doi.org/10.1021/ja804747d.

24. **El Ghazouani A, Baslé A, Gray J, Graham DW, Firbank SJ, Dennison C.** 2012. Variations in methanobactin structure influences copper utilization by methane-oxidizing bacteria. Proc Natl Acad SciUSA **109:**8400 – 8404.
http://dx.doi.org/10.1073/pnas.1112921109.

25. **Krentz BD, Mulheron HJ, Semrau JD, DiSpirito AA, Bandow NL, Haft DH, Vuilleumier S, Murrell JC, McEllistrem MT, Hartsel SC, Gallagher WH.** 2010. A comparison of methanobactins from *Methylosinus tricho- sporium* OB3b and *Methylocystis* strain SB2 predicts methanobactins are synthesized from diverse peptide precursors modified to create a common core for binding and reducing copper ions. Biochemistry **49:**10117–10130. http://dx.doi.org/10.1021/bi1014375.

26. **Kim HJ, Graham DW, DiSpirito AA, Alterman MA, Galeva N, Larive CK, Asunskis D, Sherwood PMA.** 2004. Methanobactin, a copper- acquisition compound from methane-oxidizing bacteria. Science **305:** 1612–1615.
http://dx.doi.org/10.1126/science.1098322.

27. **Bandow N, Gilles VS, Freesmeier B, Semrau JD, Krentz B, Gallagher W, McEllistrem MT, Hartsel SC, Choi DW, Hargrove MS, Heard TM, Chesner LN, Braunreiter KM, Cao BV, Gavitt MM, Hoopes JZ, Johnson JM, Polster EM, Schoenick BD, Umlauf AM, DiSpirito AA.** 2012. Spectral and copper binding properties of methanobactin from the facultative methanotroph *Methylocystis* strain SB2. J Inorg Biochem **110:**72– 82.
http://dx.doi.org/10.1016/j.jinorgbio.2012.02.002.

28. **El Ghazouani A, Basle A, Firbank SJ, Knapp CW, Gray J, Graham DW, Dennison C.** 2011. Copper-binding properties and structures of methanobactins from *Methylosinus trichosporium* OB3b. Inorg Chem **50:**1378 – 1391.
http://dx.doi.org/10.1021/ic101965j.

29. **Choi DW, Zea CJ, Do YS, Semrau JD, Antholine WE, Hargrove MS, Pohl NL, Boyd ES, Geesey GG, Hartsel SC, Shafe PH, McEllistrem MT, Kisting CJ, Campbell D, Rao V, de la Mora AM, DiSpirito AA.** 2006. Spectral, kinetic, and thermodynamic properties of Cu(I) and Cu(II) binding by methanobactin from *Methylosinus trichosporium* OB3b. Biochemistry **45:**1442–1453. http://dx.doi.org/10.1021/bi051815t

30. **Choi DW, Do YS, Zea CJ, McEllistrem MT, Lee SW, Semrau JD, Pohl NL, Kisting CJ, Scardino LL, Hartsel SC, Boyd ES, Geesey GG, Riedel TP, Shafe PH, Kranski KA, Tritsch JR, Antholine WE, DiSpirito AA.** 2006. Spectral and thermodynamic properties of Ag(I), Au(III), Cd(II), Co(II), Fe(III), Hg(II), Mn(II), Ni(II), Pb(II), U(IV), and Zn(II) binding by methanobactin from *Methylosinus trichosporium* OB3b. J Inorg Biochem **100:**2150 –2161. http://dx.doi.org/10.1016/j.jinorgbio.2006.08.017.

31. **Vorobev A, Jagadevan S, Baral BS, DiSpirito AA, Freemeier BC, Berg- man BH, Bandow NL, Semrau JD.** 2013. Detoxification of mercury by methanobactin from *Methylosinus trichosporium* OB3b. Appl Environ Microbiol **79:**5918 –5926. http://dx.doi.org/10.1128/AEM.01673-13.

32. **Whittenbury R, Phillips KC, Wilkinson JF.** 1970. Enrichment, isolation and some properties of methane-utilizing bacteria. J Gen Microbiol **61:** 205–218.

33. **Bandow NL, Gallagher WH, Behling L, Choi DW, Semrau JD, Hartsel SC, Gilles VS, DiSpirito AA.** 2011. Isolation of methanobactin from the spent media of methane oxidizing bacteria. Methods Enzymol **495:**259 – 269. http://dx.doi.org/10.1016/B978-0-12-386905-0.00017-6.

34. **Semrau JD, Jagadevan S, DiSpirito AA, Khalifa A, Scanlan J, Bergman BH, Freemeier BC, Baral BS, Bandow NS, Vorobev A, Haft DH, Vuilleumier S, Murrell JC.** 2013. Methanobactin and MmoD work in concert to act as the "copper-switch" in methanotrophs. Environ Micro- biol **15:**3077–3086. http://dx.doi.org/10.1111/1462-2920.12150.

35. **Brusseau GA, Tsien HC, Hanson RS, Wackett LP.** 1990. Optimization of trichloroethylene oxidation by methanotrophs and the use of a colorimetric assay to detect soluble methane monooxygenase activity. Biodegradation **1:**19 –29. http://dx.doi.org/10.1007/BF00117048.

36. **Schmittgen TD, Livak KJ.** 2008. Analyzing real-time PCR data by the comparative CT method. Nat Protoc **3:**1101–1108. http://dx.doi.org/10.1038/nprot.2008.73.

37. **Dzombak DA, Morel FMM.** 1990. Surface complexation modeling: hydrous ferric oxide. John Wiley & Sons, New York, NY.

38. **Lützenkirchen J.** 1988. Comparison of 1-pK and 2-pK versions of surface complexation theory by goodness of fit in describing surface charge data of hydroxides. Environ Sci Technol **32:**3149 –3154.

39. **Baral BS, Bandow NL, Vorobev A, Freemeier BC, Bergman BH, Her- dendorf TJ, Fuentes N, Ellias L, Turpin E, Semrau JD, DiSpirito AA.** 2014. Mercury binding by methanobactin from *Methylocystis* strain SB2. J Inorg Biochem **141:**161–169. http://dx.doi.org/10.1016/j.jinorgbio.2014.09.004.

40. **Stanley SH, Prior SD, Leak DJ, Dalton H.** 1983. Copper stress underlies the fundamental change in intracellular location of methane monooxygenase in methane oxidizing organisms: studies in batch and continuous culture. Biotechnol Lett **5:**487–492. http://dx.doi.org/10.1007/BF00132233.

41. **Bao Z, Okubo T, Kubota K, Kasahara Y, Tsurumaru T, Anda M, Ikeda S, Minamisawa K.** 2014. Metaproteomic identification of diazotrophic methanotrophs and their localization in root tissues of field-grown rice plants. Appl Environ Microbiol **80:**5043–5052. http://dx.doi.org/10.1128/AEM.00969-14.

42. **Hazen TC, Chakraborty R, Fleming JM, Gregory IR, Bowman JP, Jimenez L, Pfiffner SM, Brockman FJ, Sayler GS.** 2009. Use of gene probes to assess the impact and effectiveness of aerobic in situ bioremediation of TCE. Arch Microbiol **191:**221–232. http://dx.doi.org/10.1007/s00203-008-0445-8.

43. **Liebner S, Svenning MM.** 2013. Environmental transcription of *mmoX* by methane-oxidizing *Proteobacteria* in a subarctic palsa peatland. Appl Environ Microbiol **79:**701–706. http://dx.doi.org/10.1128/AEM.02292-12.

Figure legeneds

Figure 1. RT-qPCR of *pmoA* (A), *mmoX* (B), and *mbnA* (C) in *M. trichosporium* OB3b grown in the presence of copper (Cu), gold (Au), and copper-methanobactin (Cu-mb). Bars within each plot labeled by different letters are significantly different ($P < 0.05$).

Figure 2. sMMO oxidation of naphthalene in *M. trichosporium* OB3b grown in the presence of various amounts of copper, gold, and copper-methanobactin, as follows: 2 μM copper (A); 2 μM copper and 5 μM gold (B); 2 μM copper, 5 μM gold, and 5 μM copper-methanobactin (C); and no added copper, gold, or copper-methanobactin (D).

Figure 3. Metals associated with the biomass of *M. trichosporium* OB3b grown in the presence of copper (Cu), gold (Au), and copper-methanobactin. (A) Copper. (B) Gold. Bars in each plot labeled by different letters are significantly different ($P < 0.05$).

Figure 4. Ratio of gold to copper bound to methanobactin following incubation of Cu(II), Au(III), and methanobactin in molar ratios of 0.25:0.25:1, 0.5:0.5:1, 1:1:1, 1.5:1.5:1, and 2:2:1. Error bars represent the standard deviations of triplicate samples each measured five times.

Figure 5. (A) UV-visible absorption spectra of copper-free methanobactin (dashed line), copper-methanobactin at a molar ratio of 1:1 (dotted line), and following the addition of an equimolar concentration of gold to copper-methanobactin (solid line). (B and C) Kinetics of copper displacement from copper-methanobactin by the addition of an equimolar concentration of gold. Absorbance changes were monitored at 336 nm following the addition of gold. The kinetics of copper displacement was biphasic, and the arrow indicates the transition from the initial high rate (k_1) to a secondary lower rate (k_2).

Table 1 Growth and sMMO activity of *M. trichosporium* OB3b in the presence of 2 μM copper and various concentrations of competing metals for binding to methanobactin.

Competing metal(s)	Metal (μM)	Growth of *M. trichosporium* OB3b[a]	sMMO activity[b]
None (2μM copper only)		Yes	No

Table 1 continued

Group A			
Hg	5	No	ND
Ag	5	No	ND
Au	5	Yes	Yes
Group B			
Zn	10	Yes	ND
Mn	10	Yes	ND
Mo	10	Yes	ND
Ni	10	Yes	ND
Co	10	Yes	ND
Zn+Ni+Mn+ Mo+Co	25,50,100,250 and 500	Yes	No

a Positive growth defined as OD_{600} of >0.2 within 3 days from an initial OD_{600} of -0.05.

b sMMO activity determined using the naphthalene assay (35). ND, not determined due to lack of growth

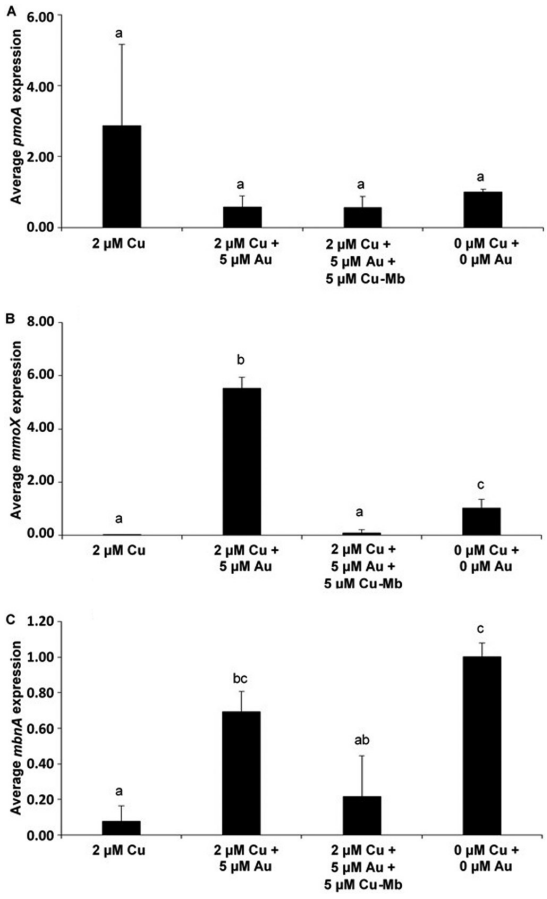

Figure 1

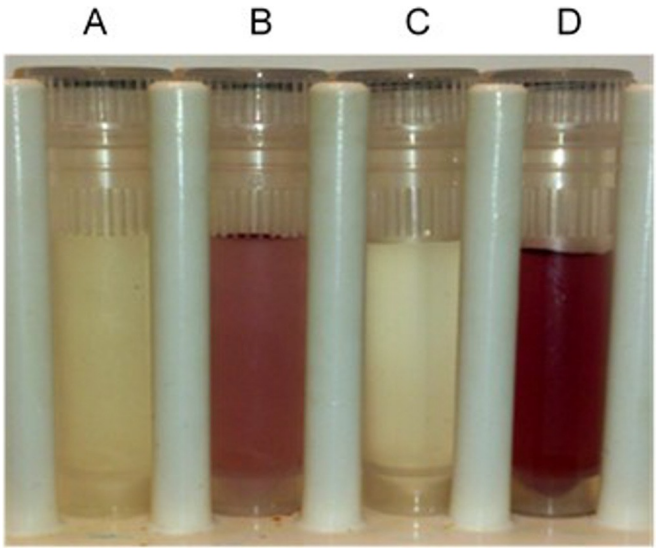

Figure 2

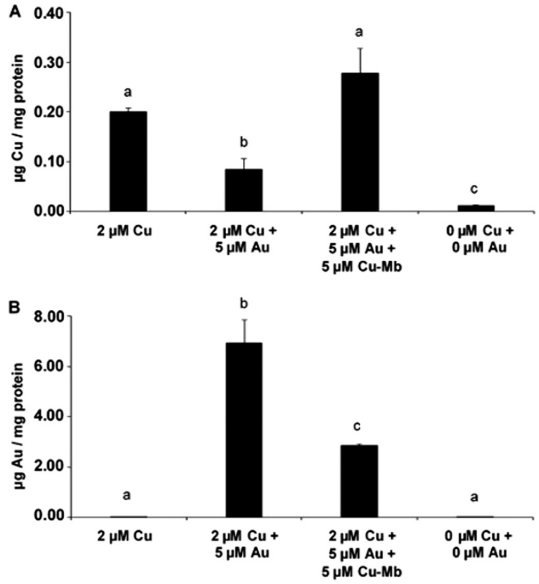

Figure 3

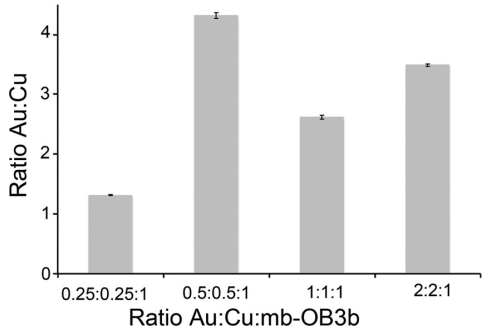

Figure 4

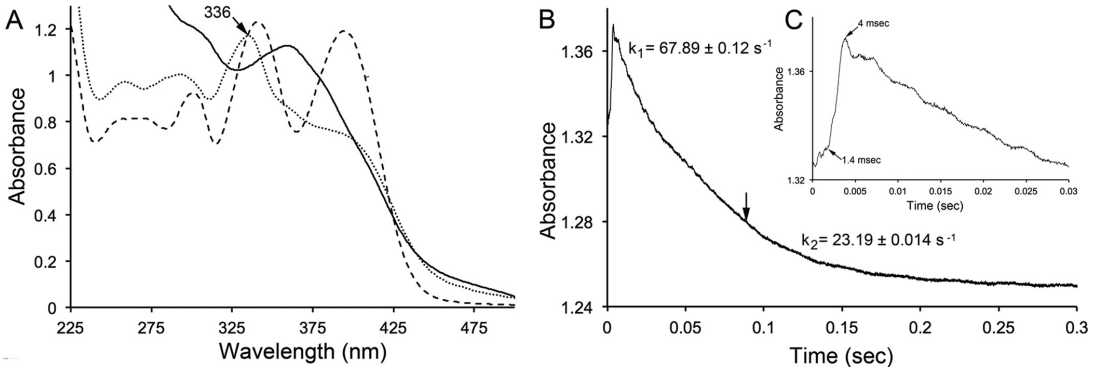

Figure 5

Supplemental Information

Table legends

Table S1. Predicted equilibrium speciation of copper in the presence and absence of gold.

Figure legends

Figure S1. qPCR standard curves for *pmoA*, *mmoX, mbnA* and 16S rRNA gene. Standards were prepared from the plasmids having *pmoA*, *mmoX mbnA,* and 16S rRNA inserts from *M. trichosporium* OB3b individually ligated into a cloning vector. Known copy numbers of the plasmid based standards were plotted against measured C_t. Each point represent the average of triplicate samples with error bars showing the standard deviation.

Figure S2. SDS-polyacrylamide gel electrophoresis of soluble (A, C, E, G) and membrane (B, D, F. H) fractions of *M. trichosporium* OB3b grown under carrying copper, gold, and copper-methanobactin concentrations. MW – molecular weight markers. A - soluble fraction of *M. trichosporium* OB3b grown with no added copper. B - membrane fraction of *M. trichosporium* OB3b grown with no added copper. C - soluble fraction of *M. trichosporium* OB3b grown with 2 µM copper. D - membrane fraction of *M. trichosporium* OB3b grown with 2 µM copper. E - soluble fraction of *M. trichosporium* OB3b grown with 2 µM copper + 5 µM gold. F - particulate fraction of *M. trichosporium* OB3b grown with 2 µM copper + 5 µM gold. G - soluble fraction of *M. trichosporium* OB3b grown with 2 µM copper + 5 µM gold + 5 µM copper-methanobactin. H - particulate fraction of *M. trichosporium* OB3b grown with 2 µM copper + 5 µM gold + 5 µM copper-methanobactin. Arrows on the left indicate the α- and γ– subunits of the hydroxylase component of sMMO (54 and 42 kDa, respectively) while arrows on the right indicate the α- and γ–subunits of pMMO (45 and 23 kDa, respectively).

Table S1. Predicted equilibrium speciation of copper in the presence and absence of gold.

	2 µM Cu	**2 µM Cu + 5 µM Au**
Species	% of total component	% of total component
Cu^{+2}	16	16
$CuOH^{+}$	2.9	2.9
$Cu(OH)_2$ (aq)	0.058	0.058
$Cu_2(OH)_2^{+2}$	0.074	0.074
$CuCl^{+}$	0.12	0.12
$CuSO_4$ (aq)	2.3	2.3
$CuNO_3^{+}$	0.27	0.27
$CuHPO_4$ (aq)	51	51
$CuEDTA^{-2}$	26	26

Figures

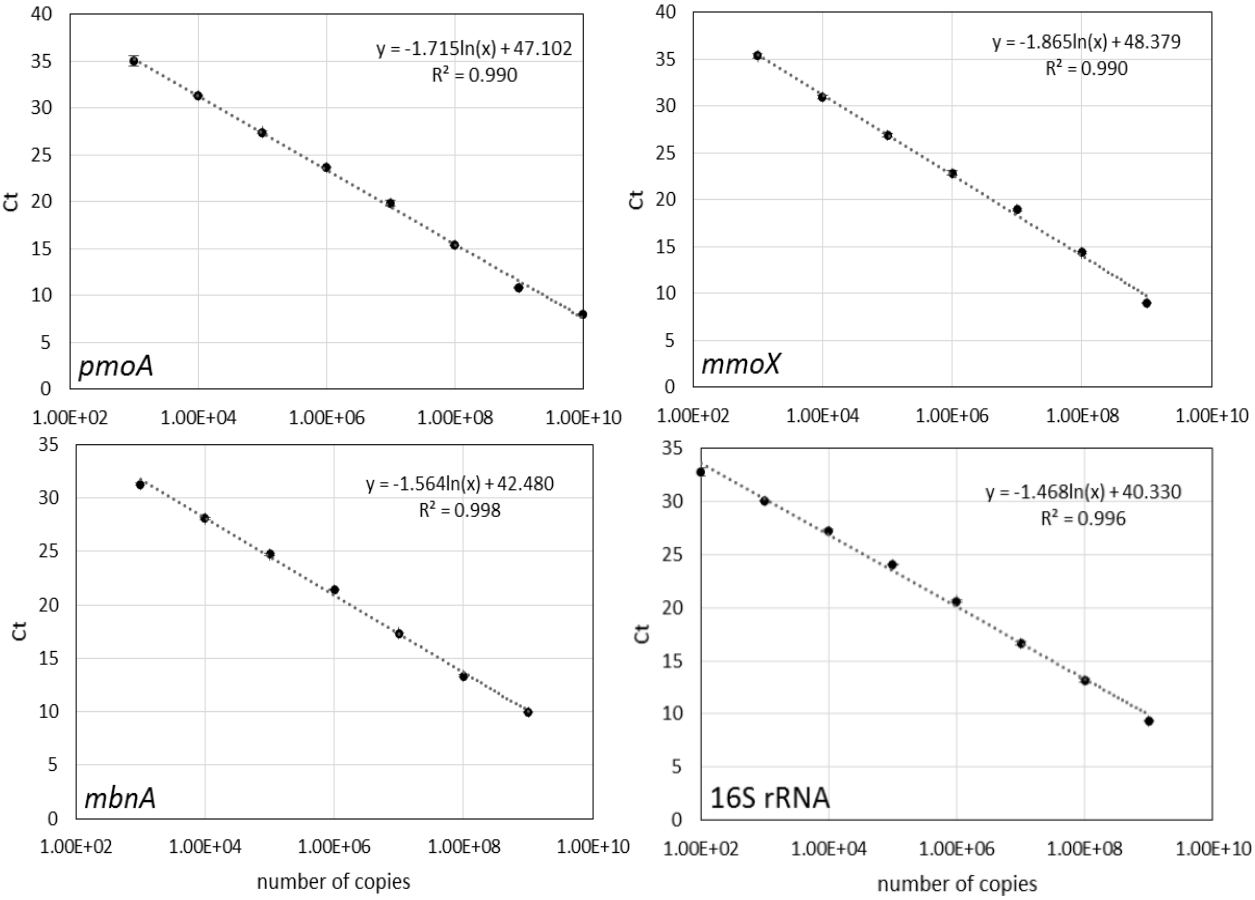

Figure S1

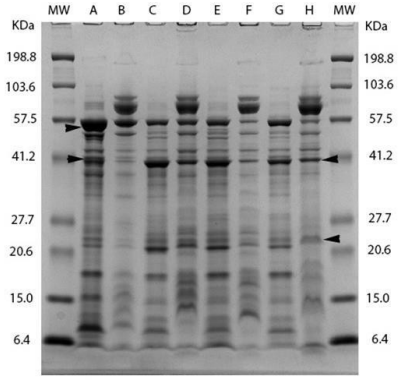

Figure S2

CHAPTER 5

A TONB-DEPENDENT TRANSPORTER IS RESPONSIBLE FOR METHANOBACTIN UPTAKE BY *Methylosinus trichosporium* OB3b

Wenyu Gu, Muhammad Farhan Ul Haque, Bipin S. Baral, Erick A. Turpin, Nathan L. Bandow, Josef Lichtmannegger, Elisabeth Kremmer, Hans Zischka , Alan A. DiSpirito and Jeremy D. Semrau

Modified from the article published in Journal of Applied and Environmental Microbiology

Abstract

Methanobactin, a small modified polypeptide synthesized by methanotrophs for copper uptake, has been found to be chromosomally encoded. The gene encoding for the polypeptide precursor of methanobactin, *mbnA*, is part of a gene cluster that also includes several genes encoding for proteins of unknown function (but speculated to be involved in methanobactin formation), as well as *mbnT*, encoding for a TonB-dependent transporter hypothesized to be responsible for methanobactin uptake. To determine if *mbnT* was truly responsible for methanobactin uptake, a knockout was constructed in *Methylosinus trichosporium* OB3b using marker exchange mutagenesis. The resulting *M. trichosporium mbnT::Gm*^{R} mutant was found to be able to produce methanobactin, but unable to internalize it. Further, if this mutant was grown in the presence of copper and exogenous methanobactin, copper uptake was significantly reduced. Expression of *mmoX* and *pmoA*, encoding polypeptides of the soluble methane monooxygenase (sMMO) and particulate methane monooxygenase (pMMO), respectively, also changed significantly when methanobactin was added, which indicates that the mutant was unable to collect copper under

these conditions. Copper uptake and gene expression, however, were not affected in wild-type *M. trichosporium* OB3b, indicating that the TonB-dependent transporter encoded by *mbnT* is responsible for methanobactin uptake, and that methanobactin is a key mechanism used by methanotrophs for copper uptake. When the *mbnT::Gm*^{R} mutant was grown under a range of copper concentrations in the absence of methanobactin, however, the phenotype of the mutant was indistinguishable from wild-type *M. trichosporium* OB3b, indicating that this methanotroph has multiple mechanisms for copper uptake.

Introduction

Methanotrophs, or methane-oxidizing bacteria, are a group of microbes with great environmental and industrial importance. For example, methanotrophs are well known to play a key role in controlling the net emission of methane from soils, a potent greenhouse gas with a global warming potential ~34 times that of carbon dioxide over a 100-year time frame (1). In fact, it is estimated that as much as 90% of methane generated in anaerobic soils via methanogenesis may be removed via methanotrophy (2). Further, methanotrophs oxidize methane under ambient temperatures and pressures, and thus, are attractive platforms for the valorization of methane to products such as single-cell protein, bioplastics, biofuels, and osmoprotectants (3-5).

Methanotrophs are fairly ubiquitous and are found in many different environments, including forest soils, landfill cover soils, agricultural soils, freshwater and marine sediments, and many other locations (4, 6, 7). Although methane oxidation is commonly associated with oxygen reduction, in the past 15 years, methane oxidation has also been shown to be coupled with sulfate, nitrite, and nitrate reduction (4,8-10). Methanotrophs also show remarkable

phylogenetic diversity, with aerobic methanotrophs grouping in the *Gammaproteobacteria* and *Alphaproteobacteria* as well as in the NC10 and *Verrucomicrobia* phyla (4,6,8).

A key issue affecting methanotrophic activity, particularly the activities in the *Gammaproteobacteria* and *Alphaproteobacteria*, is the availability of copper. It was first discovered >30 years ago that some methanotrophs exhibited a unique "copper-switch" where the form and activity of the methane monooxygenase (MMO) dramatically changes with changing copper availability. Specifically, it was found that under copper-limiting conditions, some methanotrophs synthesized a cytoplasmic, or soluble methane monooxygenase (sMMO). As copper levels increased, expression of sMMO decreased, while expression and activity of a membrane-bound, or particulate methane monooxygenase (pMMO) increased (4, 11, 12). The sMMO has a broad substrate range and as a result, has great versatility for use in biocatalysis and bioremediation, but it also has relatively poor affinity for methane. (4, 13-16). pMMO, conversely, has a relatively narrow substrate range and greater specificity for methane, suggesting that strategies to utilize methanotrophs to reduce methane emissions and/or remove methane from the atmosphere should target pMMO-expressing methanotrophs (14, 17, 18).

The mechanism underlying this "copper-switch" was recently found to involve a novel copper-binding compound, or chalkophore called methanobactin. Methanobactin is a small, modified polypeptide (< 1200 Da) with two heterocyclic rings, either an imidazole, oxazolone or pyrazinedione ring, each with an associated enethiol group, that together are responsible for copper binding (19-22). Biochemical analyses indicated that methanobactin may be formed from a polypeptide precursor with the heterocyclic rings derived from a –X—Cys dipeptide sequence (22). Interrogation of available methanotrophic genomes found one

possible candidate gene, *mbnA*. Deletion of *mbnA* in *Methylosinus trichosporium* OB3b showed that it is indeed the precursor of methanobactin and that it is part of a gene cluster (Fig. 1), with many genes of unknown function (possibly involved in methanobactin formation) as well as an aminotransferase (also possibly involved in methanobactin formation) and an extrusion protein (that may serve to secrete methanobactin). Upstream of *mbnA* is a gene encoding for a TonB-dependent transporter (*mbnT*), that has been suggested, but not shown, to be involved in methanobactin uptake (23).

To elucidate the role of *mbnT* in methanobactin uptake, we created mutants of *M. trichosporium* OB3b where *mbnT* has been selectively knocked out via marker exchange mutagenesis.

Materials and Methods

Growth conditions

Wild-type *Methylosinus trichosporium* OB3b and the *mbnT::Gm*^{R} mutant (constructed as described below) were grown on nitrate mineral salt (NMS) medium (24) at 30 °C with CH_4 added at a methane-to-air ratio of 1:2. Liquid cultures were grown in 250 mL side-arm Erlenmeyer flasks with 30 to 50 mL of medium shaken at 200 rpm. Copper (as $CuCl_2$) and methanobactin from *M. trichosporium* OB3b were filter sterilized and added to NMS medium as described earlier (25). Growth was monitored by measuring the optical density at 600 nm (OD_{600}) with a Genesys 20 Visible spectrophotometer (Spectronic Unicam, Waltham, MA) at 3- to 12-hour intervals. Cultures were grown in at least duplicate biological replicates and harvested at late-exponential phase for analysis of specific gene expression and metal distribution.

Knockout of *mbnT*

Marker-exchange mutagenesis was applied to create a knockout of *mbnT*, which encodes a TonB-dependent transporter using the protocol described in Semrau, et al. (23). Briefly, 3′ and 5′ DNA regions of *mbnT* (arms A and B, respectively) were selectively amplified by PCR using the primers listed in Table 1. These PCR products were then digested with BamHI, separated by gel electrophoresis, and were then purified using the QIAquick Gel Extraction Kit (Qiagen) by following the manufacturer's instructions. Arms A and B were ligated and were again PCR-amplified. The amplified product was digested with EcoRI and HindIII and inserted into pK18mobsacB, yielding the construct pWG01. The gentamycin resistance gene (Gm^R) was then excised from plasmid p34S-Gm using BamHI. This was then inserted into the BamHI site between arms A and B to give the construct pWG011. This was then used to transform *Escherichia coli* S17.1 (26). *E. coli* S17.1 was then conjugated with *M. trichosporium* OB3b as described by Martin and Murrell (27). Transconjugants were identified by plating cells onto NMS plates with 2.5 μg. ml^{-1} gentamicin. Residual contamination by *E. coli* S17.1 was then removed by subsequently growing the resulting *mbn::*Gm^R mutant of *M. trichosporium* OB3b in NMS medium with 2.5 μg. ml^{-1} gentamicin and 10 μg. ml^{-1} nalidixic acid. Successful knockout of *mbnT* via double homologous recombination was confirmed by screening of kanamycin-sensitive and sucrose-resistant phenotype, by PCR, and by sequencing.

RNA extraction and RT

RNA was isolated using the method described previously (23). Briefly, 2.5 ml of stop solution (5% buffer equilibrated phenol [pH 7.3] in ethanol) was first added to cultures (22.5

ml) to stop synthesis of new mRNA. Cell pellets were then collected by centrifugation at 4,300 × g for 15 min at 4 °C. The cells were re-suspended in 0.75 ml of extraction buffer [100 mM Tris-HCl [pH 8.0], 1.5 M NaCl, 1% [wt/v] hexadecyltrimethylammonium bromide (CTAB)] before lysis using 20 % SDS, 20% lauryl sarcosine, and bead beating. Subsequent steps of RNA extraction were then performed as described previously (23-25). Total RNA was then subjected to RNase-free DNase treatment until free of DNA contamination as proven via PCR amplification of the 16S rRNA gene. The purified RNA was quantified spectrophotometrically using NanoDrop (NanoDrop ND1000; NanoDrop Technologies, Inc., Wilmington, DE). RNA samples were stored at -80 °C and were used for cDNA synthesis within 2 days of extraction. DNA-free total RNA (500 ng) was treated with Superscript III reverse transcriptase for reverse transcription of mRNA to cDNA (Invitrogen, Carlsbad, CA) following the manufacturer's instructions.

RT-qPCR

Reverse transcription-quantitative PCR (RT-qPCR) analyses were performed to determine the relative expression of the *pmoA*, *mmoX*, and *mbnA* genes in *M. trichosporium* OB3b and in the *mbnT::Gm*^{R} mutant strains grown at various concentrations of copper and methanobactin. Gene specific primers (Table 1) were used for the RT-qPCR analyses, and their specificity was verified by sequencing and gel electrophoresis. Measurements were performed in 96-well PCR plates using CFX Connect Real Time PCR Detection System (Bio-Rad, Hercules CA). In each well, quantitative PCRs (qPCRs) reaction (20 µl) consisted of 0.8 µl cDNA, 1 x iTaq Universal SYBR Green Supermix (Bio-Rad, Hercules CA), 0.5 µM each of the forward and reverse primers, and nuclease-free sterile water (Ambion/Life

Technologies, Grand Island, NY). A three-step thermal cycler program, with an initial denaturation at 95°C for 3 min and 40 cycles of denaturation (94°C for 20 s), annealing (58°C for 20 s), and extension (68°C for 30 s), was performed. The specificity of qPCR products was again confirmed by melting curve analysis with temperature ranging from 55 °C to 95 °C after the completion of amplification cycles. The threshold amplification cycle (C_T) values were then imported from CFX Manager Software (Bio-Rad) into Microsoft Excel to quantify the relative levels of expression of different genes. The Comparative C_T method ($2^{-\Delta\Delta CT}$) (28) was used to calculate the relative gene expression levels using 16S rRNA as the housekeeping gene.

Metal analysis

Copper associated with the biomass of wild-type *M. trichosporium* OB3b and *mbnT::Gm*^{R} mutant was determined as described previously (29). Briefly, cultures were harvested by centrifugation at 4,300 X g for 15 min. The cell pellets were re-suspended in 1ml morpholinepropanesulfonic acid (MOPS) buffer before being stored at -80 □C. Before metal measurement, 1 mL of 70% nitric acid (vol/vol) was added to the cell suspension and incubated for 2 h at 95 □C with inversion every 20 min. Copper associated with biomass was subsequently analyzed using an inductively coupled plasma mass spectrometry (Agilent Technologies, Santa Clara, CA). At least triplicate biological samples for every condition were analyzed.

Methanobactin in spent medium and in cell extracts

For characterization of the location of methanobactin from wild-type *M. trichosporium* OB3b and the *mbnT::Gm*^{R} mutant, cells were cultured in 12 litres of NMS

medium amended with 0.2 μM $CuCl_2$ in a 15-liter New Brunswick fermenter at 30°C for 48 h. Following the incubation period, 10 liters of the culture was removed and 10 liters of fresh NMS medium was added to the fermentor, and the copper concentration increased to 5 μM. This sequence was then repeated with increasing copper concentration to 10 and 20 μM in subsequent fermenter turnovers.

The extracellular fraction and cells from each 10-liter sample were separated via tangential- flow filtration using a 10,000 Da molecular mass filter as previously described (30). The cells from the retentate were then harvested by centrifugation at 13,200 X g at 4°C. The pellet was re-suspended in 10 mM phosphate buffer, pH 7.3 and was centrifuged at 13,200 X g at 4°C. This cell pellet was then resuspended in a minimal volume of 10 mM phosphate buffer at a of pH 6.8 plus 1μg DNAase ml^{-1} and lysed by three passes through an EmlusiFex-C3 high-pressure homogenizer at 15,000 lb/in^2 (Avestin. Inc. Ottawa, ON, Canada) at 4°C. The cell extract was then centrifuged at 13,000 X g for 20 min to remove unlysed cells followed by filtration though 0.2-μm Millipore filters (Billerica, MA, USA)

Methanobactin antibody generation

Antibodies to methanobactin (Amb) from *M. trichosporium* OB3b were produced in LOU/c rats, which were immunized subcutaneously and intraperitoneally with a methanobactin-ovalbumin fusion protein (50 μg), 5 nmol CPG oligonucleotide (Tib Molbiol, Berlin, Germany), 500 μl phosphate-buffered saline and 500 μl incomplete Freund's adjuvant. A boost without adjuvant was given 6 weeks after the primary injection. Tissue culture supernatants (TCS) were tested in a solid-phase immunoassay with methanobactin coupled to bovine serum albumin (BSA) or an irrelevant peptide coupled to BSA-coated

enzyme-linked immunosorbent assay (ELISA) plates at a concentration of 4 $\mu g.ml^{-1}$. Monoclonal antibodies (MAbs) from TCS bound to methanobactin were detected with horseradish peroxidase (HRP)-conjugated MAbs against the rat IgG isotypes (TIB173 IgG2a, TIB174 IgG2b, TIB170 IgG1 [all from ATCC] and R-2c IgG2c [homemade]), thus avoiding MAbs of IgM class. HRP was visualized with ready to use 3,3‘ ,5,5‘ – tetramethylbenzidine (TMB) (1-Step Ultra TMB ELISA; Thermo Fisher, Waltham, MA). Hybridomas that reacted specifically with methanobactin were frozen, and the antibody containing TCS were used in subsequent blots.

Derivation of polyvinylidene difluoride membranes

The N terminus of methanobactin from *M. trichosporium* OB3b is lost during ring formation (19, 21), preventing methanobactin from binding to polyvinylidene difluoride (PVDF) membranes (31). Poly (allylamine) was therefore attached to PVDF membranes, which enables methanobactin binding via its C-terminus. Poly(allylamine) was attached to PVDF membranes by the derivatization procedure described by Rodrigues et al. (51). Briefly, PVDF sheets were etched in alcoholic KOH then reacted with poly(allylamine) under alkaline conditions. Next, the amino groups were reacted with 1,4-phenylene diisothiocyanate (DITC), converting the amino-modified PVDF to DITC-functionalized membranes (DITC-phosphonoacetic acid [PAA]-PVDF membranes).

Chemiluminescence western dot blots

DITC-PAA-PVDF transfer membranes were sized to fit an 8-by-12 well Bio-Dot dot blot (Bio-Rad Inc. Hercules, CA); they were washed with 20mM Tris-HCl plus 0.5M NaCl (Tris-buffered saline [TBS]) at pH 7.5 and were loaded with filter paper onto this dot blotter.

Samples (spent medium and cell extracts) were then loaded under vacuum and were dried for 30 min under vacuum. The membrane was then wetted with 50% CH_3OH-50% H_2O and washed twice in TBS at room temperature. The membrane was then incubated overnight in 0.2% nonfat dry milk in TBS overnight at 4°C with the TBS subsequently decanted. The membrane was then resuspended in TBS plus 0.1% Tween 20 (TTBS) at pH 7.5 and incubated for 10 min at room temperature. The membrane was then suspended in fresh TTBS and incubated at room temperature for 1 h. The TTBS was decanted and the membrane resuspended in the primary antibody buffer (TTBS plus 0.2% nonfat dry milk [antibody buffer] plus 5.7 µg Amb • ml^{-1} [primary antibody solution] and incubated overnight at 4°C. Following incubation, the primary antibody solution was decanted, and the membrane was resuspended in TTBS and incubated for 10 min with agitation, followed by one change in TTBS with incubations with incubation for an additional 10 min. The TTBS was decanted, and the membrane was resuspended in secondary antibody solution consisting of 33 µl of goat anti-rat Ig (H/L)-alkaline phosphatase from AbD Serotec (Atlanta, GA) to 100 ml of antibody buffer and incubated for 2 h. Following incubation, the secondary antibody solution was decanted, and the membrane washed three times with TTBS as described above. Visualization of the blot was done via Bio-Rad Immun-Star AP substrate for chemiluminescence (Hercules, CA, USA) by following the manufacturer's suggested procedure.

Results

Using marker exchange protocols, a transconjugant colony with a double homologous recombination event where *mbnT* was successfully knocked out was identified (Fig. 2). This

was confirmed by sequencing as well as by verifying that the mutant was gentamicin and sucrose resistant but sensitive to kanamycin (data not shown).

The phenotype of the *mbnT::Gm*^{R} mutant was then further examined and compared to that of wild-type *M. trichosporium*. When grown in various copper concentrations, both the *mbnT::Gm*^{R} mutant and the wild type had increasing amounts of copper associated with biomass (Fig. 3A). Further, gene expression in both the mutant and the wild type showed clear evidence of the copper-switch; i.e., as copper increased, expression of *mmoX* decreased by several orders of magnitude, while *pmoA* expression increased over an order of magnitude (Fig. 3B and C). Finally, expression of *mbnA*, encoding the precursor polypeptide of methanobactin, decreased substantially in wild-type *M. trichosporium* OB3b and in the *mbnT::Gm*^{R} mutant as copper increased, indicating that the knocking out of *mbnT* did not affect methanobactin expression (Fig. 3D).

These findings suggest either *mbnT* is not involved in copper uptake (i.e., binding of copper-methanobactin complexes) or tthat here are multiple mechanisms for copper uptake in *M. trichosporium* OB3b, such that the copper-switch is still operative. To differentiate between these possibilities, methanobactin in the spent medium and cell extracts of the *mbnT::Gm*^{R} mutant and wild-type strain of *M. trichosporium* OB3b was assayed for a wide range of copper concentrations using immunoblotting assays. As shown in Fig. 4, as the growth concentration of copper increased, the amount of methanobactin in the spent medium decreased in wild-type *M. trichosporium* OB3b, but was readily apparent in the spent medium of the *mbnT::Gm*^{R} mutant at all tested copper concentrations. Conversely, methanobactin was found in the cell extract of *M. trichosporium* OB3b under all conditions, indicating that methanobactin was taken up after secretion. No methanobactin was ever

observed in the cell extract of the *mbnT::Gm*^{R} mutant, indicating that the mutant produced and secreted methanobactin but was unable to subsequently take it up.

The *mbnT::Gm*^{R} mutant and wild-type strain of *M. trichosporium* OB3b were then grown in the presence of 1 μM copper and various amounts of copper-free methanobactin. As shown in Fig. 5A, in the presence of either 5 or 50 μM methanobactin, copper associated with the biomass of the *mbnT::Gm*^{R} mutant decreased >3-fold, while no significant change in the copper levels of wild-type *M. trichosporium* OB3b was observed. Further, expression of *mmoX* increased > 3 orders of magnitude in the *mbnT::Gm*^{R} mutant, while *pmoA* expression dropped by approximately 8-fold. No significant change in the expression of either *mmoX* or *pmoA* was observed, however, in wild-type *M. trichosporium* OB3b (Fig. 5B and C). Collectively, these data show that in the presence of a molar excess of methanobactin, copper was still bioavailable to wild-type *M. trichosporium* OB3b but was not for the *mbnT::Gm*^{R} mutant. Additionally, it was assayed whether the addition of exogenous methanobactin affected *mbnA* expression in wild-type *M. trichosporium* OB3b and in the *mbnT::Gm*^{R} mutant. As shown in Fig. 5D, as increasing amounts of methanobactin were added, *mbnA* expression increased in both wild-type and mutant strains.

Discussion

Since the discovery of the methanobactin gene cluster, it has been speculated that a TonB-dependent transporter encoded by *mbnT* is responsible for methanobactin uptake (23). Here, we show that methanobactin uptake is indeed mediated by *mbnT*, as (i) methanobactin was taken up by wild-type *M. trichosporium* OB3b but not by the *mbnT::Gm*^{R} mutant and (ii) the *mbnT::Gm*^{R} mutant of *M. trichosporium* OB3b was unable to take up copper if

methanobactin was exogenously added to bind copper, but wild-type *M. trichosporium* OB3b was able to take up copper.

The data also show, however, that *M. trichosporium* OB3b has an alternative mechanism(s) for copper uptake; i.e., in the absence of any exogenous methanobactin, the amounts of copper in the wild-type and *mbnT::Gm*^{R} strains of *M. trichosporium* OB3b were indistinguishable. The conclusion of multiple copper uptake systems, however, is not novel, as it was reported earlier that at least two pathways for copper uptake exist in *M. trichosporium* OB3b (33). Such redundancy in copper uptake systems in methanotrophs, although unusual compared to those of other microbes, can be explained when one considers the importance of copper in methanotrophic metabolism. That is, methanotrophs expressing pMMO have a strong need for copper, as it occupies at least two of three metal centers found in purified pMMO (4, 33-35).

An interesting issue is that, as found earlier in a mutant of *M. trichosporium* OB3b where *mbnA*, encoding the precursor polypeptide of methanobactin, was knocked out, the copper switch still existed in the *mbnT::Gm*^{R} mutant. Genomic analyses have found that *mbnT* is part of a FecIRA-like gene cluster; i.e., *mbnT* is preceded by *mbnR* and *mbnI*, encoding for a putative membrane sensor and an extracytoplasmic function sigma factor, respectively (36). Such a system is frequently found in siderophore synthesis where an outer membrane transporter binds a ferrisiderophore, transmitting a signal to a membrane sensor that then activates an extracytoplasmic function sigma factor. This ultimately induces the expression of genes required for siderophore synthesis, as well as, in some cases, genes unrelated to siderophore production or uptake, e.g., genes encoding for exotoxins and proteases (37-43). Given this similarity, it has been speculated that after MbnT binds copper-

methanobactin, a signal cascade results whereby methanobactin synthesis, and possibly expression of *mmo* and *pmo* operons is controlled (36).

The findings presented here, however, suggest that although such a signal cascade may exist after MbnT binds copper-methanobactin, such a regulatory scheme does not include the copper-switch between sMMO and pMMO. It is also difficult to conclude from our data that this signal cascade affects the expression of *mbnA*. That is, *mbnA* expression in *M. trichosporium* OB3b wild-type and in the *mbnT::Gm*^{R} mutant decreased significantly with increasing copper, but the magnitude of the drop in expression was greater in the wild-type strain (Fig. 3D). Further, in the presence of 1 μM copper and various amounts of exogenous methanobactin, *mbnA* expression in wild-type *M. trichosporium* OB3b and in the *mbnT::Gm*^{R} mutant responded in the same pattern (Fig. 5D). It appears that another regulatory circuit is involved in controlling expression of *mbnA*, but the possibility that such expression is also controlled to some extent by *mbnI*, which is indirectly activated by MbnT binding copper-methanobactin, cannot be excluded at this time.

In conclusion, here we report the successful knockout of *mbnT* and show that this is responsible for methanobactin uptake. The phenotype of the *mbnT::Gm*^{R} mutant, however, indicates that *M. trichosporium* OB3b has multiple systems for copper uptake. It is tempting to speculate that methanobactin may serve as a high affinity system to collect copper, but when copper is not limiting, an alternative lower-affinity system is used. Such a hypothesis is supported by the finding that expression of *mbnA* decreases with increasing copper both in wild-type *M. trichosporium* OB3b and in the *mbnT::Gm*^{R} mutant.

The nature of this imputed low-affinity copper uptake mechanism is still elusive, but clues from other methanotrophs, e.g., *Methylomicrobium album* BG8 and *Methylococcus*

capsulatus Bath, may provide some suggestions. That is, it has been shown that in *M. album* BG8, there exists an outer membrane protein, CorA, that is copper repressible and may serve to bind copper (44). Further, it has been found that *M. capsulatus* Bath synthesizes a similar outer membrane protein, MopE, as well as a secreted truncated form, MopE*, both bind Cu(II) (45-47). A gene encoding for a protein similar to CorA and MopE, *mbnP*, is adjacent to the methanobactin gene cluster in *M. trichosporium* OB3b (36), and it may be that this serves as an alternative copper uptake mechanism in *M. trichosporium* OB3b. To determine if this is indeed the case, it is recommended that the protein and lipid composition of the outer membrane of *M. trichosporium* OB3b be characterized under varying copper concentrations to see if any significant changes in MbnP occur. It may also be informative to create double knockouts, e.g., knockouts of both *mbnP* and *mbnT* or *mbnP* and *mbnA*, to determine if the resulting double mutants of *M. trichosporium* OB3b are severely inhibited in their ability to collect copper.

References

1. **Myhre G, Shindell D, Breon F-M, Collins W, Fuglestvedt J, Huang J, Koch D, Lamarque JF, Lee D, Mendoza B, Nakajima T, Robock A, Stephens G, Takamura T, Zhang H**. 2013. Anthropogenic and natural radiative forcing, p 659-740. In Stocker TF, Qin D, Plattner GK, Tignor MMB, Allen SK, Boschung J, Nauels A, Xia Y, Bex V, and Midgley PM (ed), Climate change 2013: the physical science basis. Cambridge University Press, Cambridge, United Kingdom.

2. **Chowdury TR, Dick RP**. 2013. Ecology of aerobic methanotrophs in controlling methane fluxes from wetlands. Appl Soil Ecol. **65**: 8-22.

3. **Khmelenina VN, ON Rozova, SY But, II Mustakhimov, AS Reshetnikov, AP Beschastnyl, Trotsenko YA**. 2015. Biosynthesis of secondary metabolites in methanotrophs: biochemical and genetic aspects (review). Appl Biochem Microbiol. (Russian) **51**: 150-158.

4. **Semrau JD, DiSpirito AA, Yoon S**. 2010. Methanotrophs and copper. FEMS Microbiol Rev **34**: 496-531.

5. **Strong PJ, S Xie, Clarke WP**. 2015. Methane as a resource: can the methanotrophs add value? Environ. Sci. Technol. **49**: 4001-4008.

6. **Op den Camp H, Islam T, Stott MB, Harhangi HR, Hynes A, Schouten S, Jetten MSM, Birkeland N-K, Pol A, Dunfield PF**. 2009. Environmental genomic and taxonomic prespectives on methanotrophic *Verrucomicrobia*. Environ Microbial Rep **1**: 293-306.

7. **Hanson RS, Hanson TE**. 1996. Methanotrophic bacteria. Microbiol Rev **60**: 439-471.

8. **Ettwig KF, Butler MK, Le Paslier D, Pelletier E, Mangenot S, Kuypers MM, Schreiber F, Dutilh BE, Zedelius J, de Beer D, Gloerich J, Wessels HJ, van Alen T, Luesken F, Wu ML, van de Pas-Schoonen KT, Op den Camp HJ, Janssen-Megens EM, Francoijs KJ, Stunnenberg H, Weissenbach J, Jetten MS, Strous M.** 2010. Nitrite-driven anaerobic methane oxidation by oxygenic bacteria. Nature **464**: 543-548.

9. **Knittel K, Boetius A.** 2009. Anaerobic oxidation of methane: progress with an unknown process. Annu Rev Microbiol **63**: 311-334.

10. **Haroon MF, Hu S, Shi Y, Imelfort M, Keller J, Hugenholtz P, Yuan Z, Tyson GW.** 2013. Anaerobic oxidation of methane coupled to nitrate reduction in a novel archaeal lineage. Nature **500**: 567-570.
11. **Choi D-W, Kunz R, Boyd ES, Semrau JD, Antholine WE, Han J-I, Zahn JA, Boyd JM, de la Mora A, DiSpirito AA**. 2003. The membrane-associated methane monooxygenase (pMMO) and pMMO-NADH:quinone oxidoreductase complex from *Methylococcus capsulatus* Bath. J Bacteriol **185**: 5755-5764.

12. **Stanley SH, Prior SD, Leak DJ, Dalton H**. 1983. Copper stress underlies the fundamental change in intracellular location of methane monooxygenase in methane-oxidising organisms: Studies in batch and continuous cultures. Biotechnol Lett **5**: 487-492.

13. **Kalyuzhnaya MG, Puri AW, Lidstrom ME**. 2015. Metabolic engineering in methanotrophic bacteria. Metabol Eng **29**: 142-152.

14. **Lee SW, DR Keeney, DH Lim, AA DiSpirito, Semrau JD**. 2006. Mixed pollutant degradation by *Methylosinus trichosporium* OB3b expressing either soluble or particulate methane monooxygenase: can the tortoise beat the hare? Appl Environ Microbiol **72**: 7503-7509.

15. **Semrau JD**. 2011. Bioremediation via methanotrophy: overview of recent findings and suggestions for future research. Front Microbiol **2**:209.

16. **Trotsenko YA, Murrell JC**. 2008. Metabolic aspects of aerobic obligate methanotrophy. Adv Appl Microbiol **63**:183-229.

17. **Lontoh S, Semrau JD**. 1998. Methane and trichloroethylene degradation by *Methylosinus trichosporium* expressing particulate methane monooxygenase. Appl Environ Microbiol **64**: 1106-1114.

18. **Yoon S, Carey JN, Semrau JD**. 2009. Feasibility of atmospheric methane removal using methanotrophic biotrickling filters. Appl Microbiol Biotechnol **83**:949-956.

19. **Behling LA, Hartsel SC, Lewis DE, DiSpirito AA, Choi DW, Masterson LR, Veglia G, Gallagher WH**. 2008. NMR, mass spectrometry and chemical evidence reveal a different chemical structure for methanobactin that contains oxazolone rings. J. Amer. Chem. Soc **130**:12604-12605.

20. **El Ghazouani A, Baslé A, Gray J, Graham DW, Firbank SJ, Dennison C**. 2012. Variations in methanobactin structure influences copper utilization by methane-oxidizing bacteria. Proc. Natl. Acad. Sci U S A **109**: 8400-8404.

21. **Kim HJ, Graham DW, DiSpirito AA, Alterman MA, Galeva N, Larive CK, Asunskis D, Sherwood PMA**. 2004. Methanobactin, a copper-acquisition compound from methane-oxidizing bacteria. Science **305**: 1612–1615.

22. **Krentz BD, Mulheron HJ, Semrau JD, DiSpirito AA, Bandow N, Haft DH, Vuilleumier S, Murrell JC, McEllistrem MT, Hartsel SC, Gallagher W**. 2010. A

comparison of methanobactins from *Methylosinus trichosporium* OB3b and *Methylocystis* strain SB2 predicts they are synthesized from diverse ribosomally produced peptide precursors modified to create a common core for binding and reducing copper ions. Biochemistry **49**: 10117-10130.

23. **Semrau JD, Jagadevan S, DiSpirito AA, Khalifa A, Scanlan J, Bergman BH, Freemeier BC, Baral BS, Bandow NS, Vorobev A, Haft DH, Vuilleumier S, Murrell JC**. 2013. Methanobactin and MmoD work in concert to act as the "copper-switch" in methanotrophs. Environ Microbiol **15**: 3077-3086.

24. **Whittenbury R, Phillips KC, Wilkinson JF**. 1970. Enrichment, isolation and some properties of methane-utilizing bacteria. J Gen Microbiol **61**: 205-218.

25. **Vorobev A, Jagadevan S, Baral BS, DiSpirito AA, Freemeier BC, Bergman BH, Bandow NL, Semrau JD.** 2013. Detoxification of mercury by methanobactin from *Methylosinus trichosporium* OB3b. Appl Environ Microbiol **79**: 5918-5926.

26. **Simon R**. 1984. High frequency mobilization of gram-negative bacterial replicons by the *in vitro* constructed Tn5-Mob transposon. Molecul Gen Genet **196**: 413-420.

27. **Martin H, Murrell JC**. 1995. Methane monooxygenase mutants of *Methylosinus trichosporium* OB3b constructed by marker-exchange mutagenesis. FEMS Microbiol Lett **127**: 243–248.

28. **Schmittgen TD, Livak KJ**. 2008. Analyzing real-time PCR data by the comparative C_T method. Nat Protoc **3**: 1101–1108.

29. **Kalidass B, Ul-Haque MF, Baral BS, DiSpirito AA, Semrau JD**. 2015. Competition between metals for binding to methanobactin enables expression of soluble methane monooxygenase in the presence of copper. Appl Environ Microbiol **81**: 1024-2031.

30. **Bandow NL, Gallagher WH, Behling L, Choi DW, Semrau JD, Hartsel SC, Gilles VS, Dispirito AA**. 2011. Isolation of methanobactin from the spent media of methane-oxidizing bacteria. Methods Enzymol **495**:259-269.

31. **Zahn JA, Dispirito AA**. 1996. Membrane-associated methane monooxygenase from *Methylococcus capsulatus* (Bath). J Bacteriol **178**: 1018-1029.

32. **Rodrigues JD, Combrink J, Brandt WF.** 1994. Derivatization of polyvinylidene diflluoride membranes for solid-phase sequencing analysis of a phosphorylated sea urchin embryo histone H1 peptide. Anal Biochem **216**:365-372.

33. **Balasubramanian R, Smith SM, Rawat S, Yatsunyk LA, Stemmler TL, Rosenzweig AC**. 2010. Oxidation of methane by a biological dicopper centre. Nature. **465**: 115-119.

34. **Hakemian AS, Kondapalli KC, Tesler J, Hoffman BM, Stemmler TL, Rosenzweig AC**. 2008. The metal centers of particulate methane monooxygenase from *Methylosinus trichosporium* OB3b. Biochemistry **47**: 6793-6801.

35. **Martinho, M, Choi DW, DiSpirito AA, Antholine WE, Semrau JD, Münck E**. 2007. Mössbauer studies of the membrane-associated methane monooxygenase from *Methylococcus capsulatus* Bath: Evidence for a dinuclear iron center. J Am Chem Soc. **129**:15783 – 15785.

36. **Kenney GE, Rosenzweig AC**. 2013. Genome mining for methanobactins. BMC Biology **11**:17.

37. **Braun V, Mahren S, Sauter A**. 2006. Gene regulation by transmembrane signaling. BioMetals **19**: 103-113.
38. **Brooks BE, Buchanan SK**. 2008. Signaling mechanisms for activation of extracytoplasmic function (ECF) sigma factors. Biochim Biophys Acta **1778**: 1930-1945.

39. **Crosa JH**. 1997. Signal transduction and transcriptional and posttranscriptional control of iron-regulated genes in bacteria. Microbiol Mol Biol Rev **61**: 319-336.

40. **Grosse C, Friedrich S, Nies DH**. 2007. Contribution of extracytoplasmic function sigma factors to transition metal homeostasis in *Cupriavidus metallidurans* strain CH34. J Mol Microbiol Biotechnol **12**: 227-240.
41. **Lamont IL, Beare PA, Ochsner U, Vasil AI, Vasil ML**. 2002. Siderophore-mediated signaling regulates virulence factor production in *Pseudomonas auerginosa*. Proc Natl Acad Sci U S A **99**: 7072-7077.

42. **Mahren S, Braun V**. 2003. The FecI extracytoplasmic-function sigman factor of *Escherichia coli* interacts with the β' subunit of RNA polymerase. J Bacteriol **185**: 1796-1802.

43. **Visca P, Leoni L, Wilson MJ, Lamont IL**. 2002. Iron transport and regulation, cell signaling and genomics: lessons from *Escherichia coli* and *Pseudomonas*. Mol Microbiol **45**: 1177-1190.

44. **Berson O, Lidstrom ME**. 1997. Cloning and characterization of *corA*, a gene encoding for a copper-repressible polypeptide in the type I methanotroph, *Methylomicrobium albus* BG8. FEMS Microbiol Lett **148**: 169-174.

45. **Karlsen OA, Berven FS, Stafford GP, Larsen Ø, Murrell JC, Jensen HB, Fjellbirkeland A**. 2003. The surface-associated and secreted MopE protein of *Methylococcus capsulatus* (Bath) corresponds to changes in the concentration of copper in the growth medium. Appl. Environ. Microbiol **69**: 2386-2388.

46. **Helland R, Fjellbirkeland A, Karlsen OA, Ve T, Lillehaug JR, Jensen HB**. 2008. An oxidized tryptophan facilitates copper binding in *Methylococcus capsulatus*-secreted protein MopE. J Biol Chem **283**: 13897-13904.

47. **Ve T, Mathisen K, Helland R, Karlsen OA, Fjellbirkeland A, Røhr Å, Andersson KK, Pedersen R-B, Lillehaug JR, Jensen HB**. 2012. The *Methylococcus capsulatus* (Bath) secreted protein, MopE* binds both reduced and oxidized copper. PLoS One **7**(8)e43146.

48. **Knapp CW, Fowle DA, Kulczycki E, Roberts JA, Graham DW**. 2007. Methane monooxygenase gene expression mediated by methanobactin in the presence of mineral copper sources. Proc. Natl Acad Sci U S A **104**: 12040-12045.

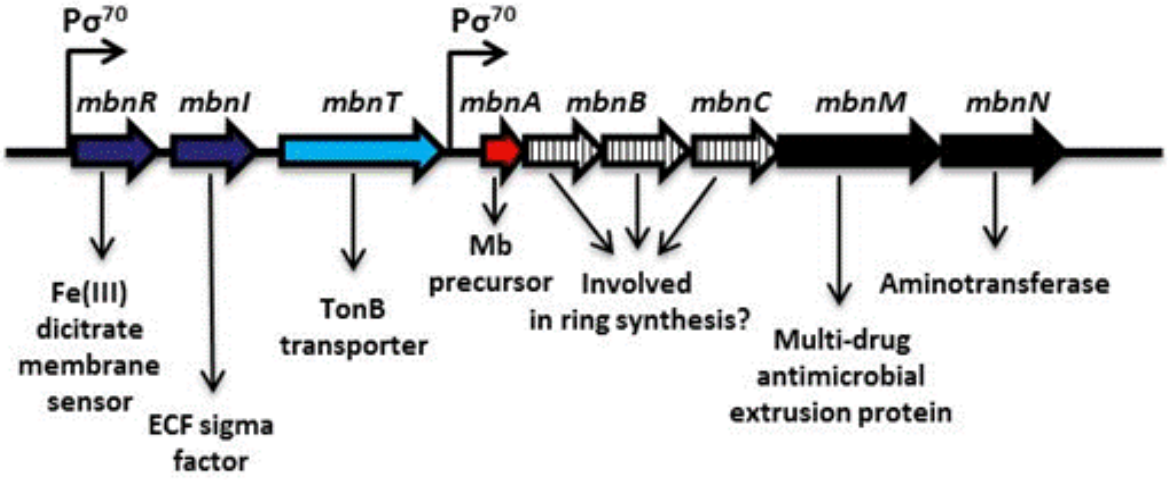

Figure 1. Methanobactin gene cluster in *M. trichosporium* OB3b, ECF, extracytoplasmic function; Mb, methanobactin.

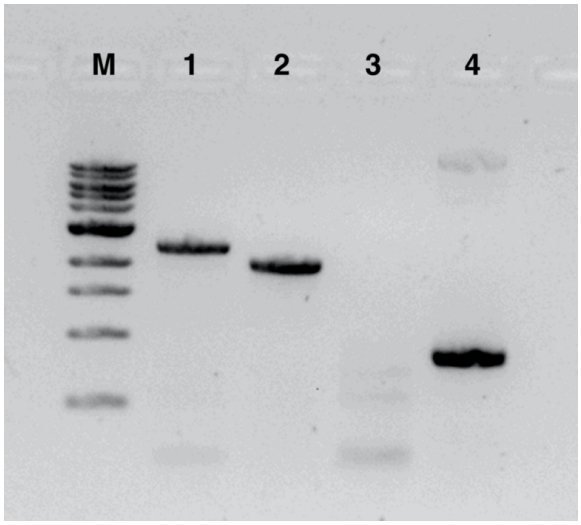

Figure 2. Verification of knockout of *mbnT* in *M. trichosporium* by PCR. M, molecular weight markers; lane 1, PCR of *mbnT* from the *M. trichosporium* OB3b *mbnT::Gm*^{R} mutant; lane 2, PCR of *mbnT* from wild-type *M. trichosporium* OB3b; lane 3, PCR of pK18*mobsacB* backbone in *M. trichosporium* OB3b *mbnT::Gm*^{R}; lane 4, PCR of pK18*mobsacB* backbone in pWG011.

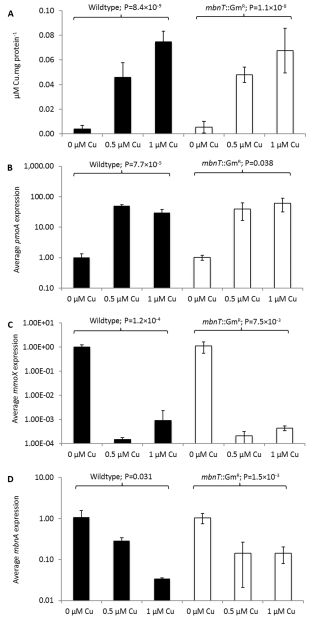

Figure 3. Characterization of wild-type *M. trichosporium* OB3b (black bars) and the *mbnT::Gm*^{R} mutant (white bars) grown in the presence of various amounts of copper. (A) Copper associated with biomass; (B). RT-qPCR of *pmoA*; (C) RT-qPCR of *mmoX*; (D) RT-qPCR of *mbnA*. Error bars indicate standard deviations from at least duplicate biological replicates. Indicated *P* values are from one-way analysis of variance (ANOVA).

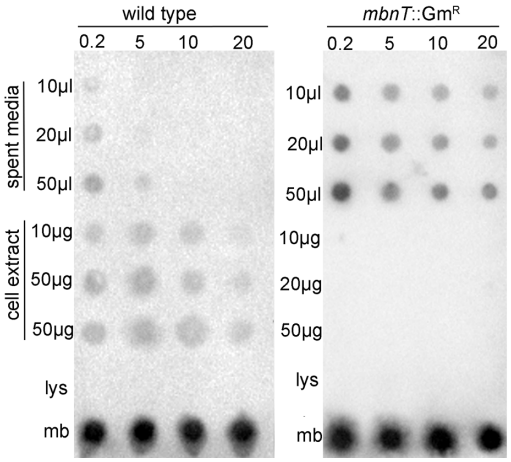

Figure 4. Immuno-blotting assays for location of methanobactin in wild-type *M. trichosporium* OB3b and in the *mbnT::Gm*^{R} mutant as a function of the concentration of copper in the growth medium (0.2, 5, 10, 20 μM copper). Fifty nanomoles lysozyme (lys) and 50 nmol methanobactin (mb) were used as negative and positive controls, respectively.

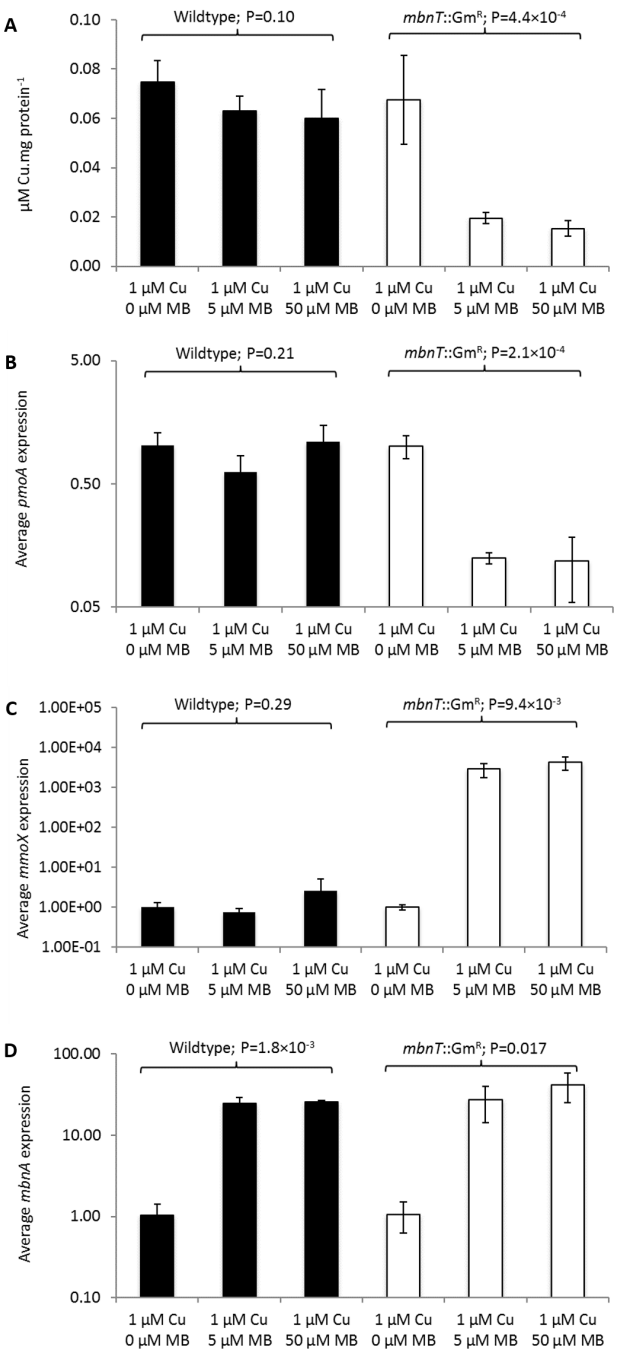

Figure 5. Characterization of wild-type *M. trichosporium* OB3b wildtype (black bars) and the *mbnT::Gm*^{R} mutant (white bars) grown in the presence of 1 µM copper and various amounts of methanobactin (MB). (A) Copper associated with biomass; (B) RT-qPCR of *pmoA*; (C) RT-qPCR of *mmoX*; (D) RT-qPCR of *mbnA*. Error bars indicate standard deviations from at least duplicate biological replicates. Indicated *P* values are from one-way analysis of variance (ANOVA).

CHAPTER 6

AN AMINOTRANSFERASE IS RESPONSIBLE FOR THE DEAMINATION OF THE N-TERMINAL LEUCINE AND REQUIRED FOR FORMATION OF OXAZOLONE RING A IN METHANOBACTIN OF *Methylosinus trichosporium* OB3b

Wenyu Gu, Bipin S. Baral, Alan A. DiSpirito and Jeremy D. Semrau

Modified from the paper published in Journal of Applied and Environmental Microbiology

Abstract

Gene expression in methanotrophs has been shown to be affected by the availability of a variety of metals, most notably copper-regulating expression of alternative forms of methane monooxygenase. A copper-binding compound or chalkophore, called methanobactin plays a key role in copper uptake in methanotrophs. Methanobactin is a, ribosomally synthesized and posttranslationally modified peptide (RiPP) with two heterocyclic rings with an associated thioamide for each ring, formed from X-Cys dipeptide sequences that bind copper. The gene encoding for the precursor polypeptide of methanobactin, *mbnA*, is part of a gene cluster, but the role of other genes in methanobactin biosynthesis is unclear. To begin to elucidate the function of these genes, we constructed an unmarked deletion of *mbnABCMN* in *Methylosinus trichosporium* OB3b, and then homologously expressed *mbnABCM* off a broad-host-range cloning vector to determine the function of *mbnN*, annotated as coding for an aminotransferase. Methanobactin produced by this strain was found to be substantially different from wild-type methanobactin in that the C-terminal methionine was missing, and only one of the two oxazolone rings was formed. Rather, in the place of the N-terminal 3-methylbutanoyl-oxazolone-thioamide group, a leucine and a thioamide-containing glycine (Gly-Ψ) were found, indicating that MbnN is used for deamination of the N-terminal leucine of methanobactin, and that this posttranslational modification is critical for closure of the N-terminal oxazolone ring in *M.*

trichosporium OB3b. These studies provide new insights into methanobactin biosynthesis, and also provide a platform for understanding the function of other genes in the methanobactin gene cluster.

Introduction

Methanotrophs utilize a novel modified peptide termed methanobactin for copper uptake (1-4). Methanobactin is the first example of a chalkophore, or copper-specific chelating agent, and is akin to the siderophores used for iron sequestration by many microbes. Methanobactins are characterized as being small (< 1200 Da) polypeptides with two heterocyclic rings each with an adjacent thioamide group. The N-terminal ring is an oxazolone, while the other is either another oxazolone or an imidazolone or pyrazinedione group (5). Perhaps the best-characterized methanobactin is that from *Methylosinus trichosporium* OB3b (Figure 1). Methanobactin from this methanotroph has several interesting features, including that the N-terminal leucine has been deaminated and that the two heterocyclic rings are both oxazolones (1, 2, 6).

The genetics underlying methanobactin synthesis are slowly being unraveled. Given the unique structure of methanobactin from *M. trichosporium* OB3b, it was initially speculated that it was synthesized via a non-ribosomal peptide synthase (7). Subsequent investigation, however, suggested that it may be a ribosomally synthesized and post-translationally modified peptide (RiPP), with a gene – *mbnA* – possibly coding for the polypeptide precursor of methanobactin identified that includes a 19-amino-acid leader sequence and a 11-amino-acid core sequence (8). When *mbnA* was knocked out in *Methylosinus trichosporium* OB3b, this microbe was unable to synthesize methanobactin,

providing evidence that methanobactin is a RiPP (4). With these data, the core polypeptide sequence of methanobactin from *M. trichosporium* OB3b was shown to be **Leu-Cys**-Gly-Ser-Cys-Tyr-**Pro-Cys**-Ser-Cys-Met, where the heterocyclic rings shown in Figure 1 are formed from the two X-Cys dipeptide sequences highlighted in bold (5).

mbnA is part of a gene cluster in *M. trichosporium* OB3b as shown in Figure 2. Upstream of *mbnA* is *mbnT*, encoding for TonB-dependent transporter. Recently, *mbnT* was successfully knocked out in *M. trichosporium* OB3b, with the resultant mutant able to synthesize methanobactin but unable to take it back up, showing that *mbnT* encodes the mechanism of methanobactin uptake (9). Immediately upstream of *mbnT* are *mbnR* and *mbnI*, coding for a putative membrane sensor and an extracytoplasmic function sigma factor, respectively. Collectively, these genes appear to be under the control of a σ^{70}-dependent promoter as predicted using BPROM (10). Downstream of *mbnA* are several other genes, some of which have unknown function but are likely involved in methanobactin biosynthesis (*mbnB* and *mbnC*), as well as genes annotated as encoding either an extrusion protein that may be responsible for methanobactin secretion (*mbnM*) or an aminotransferase that may play a role in methanobactin biosynthesis (*mbnN*). These genes also appear to be part of an operon under the control of a σ^{70}-dependent promoter as predicted using BPROM. Two additional genes, *mbnP* and *mbnH*, encoding a putative diheme cytochrome *c* peroxidase and its partner, are adjacent to *mbnN* but look to be under the control of a separate σ^{70}-dependent promoter (again predicted using BPROM). The function of *mbnP* and *mbnH* is unclear, although they may be involved in ring formation in methanobactin, or may be part of a secondary copper uptake system (5,9).

There is increasing interest in understanding the methanobactin biosynthetic pathway ; e.g., it has been recently shown that methanobactin from *M. trichosporium* OB3b has the potential to treat individuals afflicted with Wilson disease (11-13). Wilson disease is an autosomal recessive disorder in which the body is unable to correctly assimilate copper, with copper accumulating in the liver and brain, and can result in severe and irreversible damage (14,15). Current treatment therapies include prescription of chelating agents such as penicillamine and trientine, but it is not uncommon for serious side effects to occur, and in any case, when using these compounds, copper is excreted through the urine and not the bile, which is the preferred or normal physiological route. Methanobactin, however, was found to bind copper quite strongly in a rat model of Wilson disease. Copper was then quickly removed via the bile, and animals treated with methanobactin had sustained clinical recovery (11). Such findings indicate that methanobactin has the potential to be an alternative treatment for Wilson disease, particularly for those patients with acute liver failure (16).

Here we describe the role of *mbnN* in production of methanobactin from *M. trichosporium* OB3b by comparing and contrasting methanobactin produced by a mutant where *mbnN* has been deleted versus that made by *M. trichosporium* OB3b with the complete methanobactin gene cluster.

Materials and Methods

Bacterial strains, growth media, and culture conditions

Plasmid construction was accomplished using *Escherichia coli* strain TOP10 (Invitrogen, Carlsbad, CA). Plasmids used and constructed during this study are shown in

Table 2. The donor strain for conjugation of plasmids into *Methylosinus trichosporium* OB3b was *E. coli* S17-1 (17). *E. coli* strains were cultivated at 37°C in Luria broth medium (Dot scientific, Burton, MI). Strains of *M. trichosporium* OB3b were cultivated at 30°C on nitrate mineral salts (NMS) medium (20) either in 250-ml flasks with side-arms at 200 rpm or in a 15-liter New Brunswick Bioflow and Cellgen 310 fermenter (Eppendorf, Hauppauge, NY,USA) using methane as the sole carbon and energy source. Where necessary, filter-sterilized solutions of copper, as $CuCl_2$, or antibiotics (Sigma-Aldrich, St. Louis, MO), were added to culture media aseptically. The working concentrations of antibiotics were as follows: ampicillin, 100 $\mu g \bullet ml^{-1}$; kanamycin, 25 $\mu g \bullet ml^{-1}$ (for *E.coli*) or 5 $\mu g \bullet ml^{-1}$ (for *M. trichosporium* OB3b transconjugants) nalidixic acid, 15 $\mu g \bullet ml^{-1}$; spectinomycin - 20 $\mu g \bullet ml^{-1}$. Chemicals were purchased from Fisher Scientific (Waltham, MA) or Sigma-Aldrich (St. Louis, MO) and were of American Chemical Society reagent grade or better.

General DNA Methods, transformation and conjugation

DNA purification and plasmid extraction were performed using QIAquick and QIAprep kits from Qiagen following the manufacturer's instruction. DNA cloning, preparation of chemically competent cells, and plasmid transformation with *E. coli* were performed according to Sambrook and Russell (21). Enzymes used for restriction digestion and ligation were purchased from New England Biolabs (Ipswich, MA). PCR of DNA for cloning purposes was accomplished using iProof-High Fidelity polymerase (Bio-Rad, Hercules, CA). PCR for general purposes was accomplished using GoTaq DNA polymerase (Promega, Fitchburg, WI). PCR programs were set according to manufacturers' suggestions.

Plasmids were conjugated into methanotrophic strains with *E. coli* S17.1 as the donor strain as described by Martin and Murrell (22).

Construction of a new methanobactin-defective methanotrophic strain

A *M. trichosporium mbnA:*:Gm^r mutant was constructed previously where *mbnA* was knocked out via marker-exchange mutagenesis (4). While this mutant was unable to synthesize methanobactin, it does not allow easy mutation of other genes in the *mbn* operon. We therefore constructed a new *M. trichosporium* Δ*mbnAN* mutant, in which *mbnABCMN* was deleted by counterselection technique. Specifically, a 1-kb DNA fragment from upstream of *mbnA* and a 1-kb fragment spanning the 3' region of *mbnN* were amplified using dmbnaF/dmbnaR and dmbnbF/dmbnbR (Table 2) primer sets, respectively. The amplified fragments were ligated together using *KpnI* site and then cloned into pK18mob*sacB* at *BamHI* and *HindIII* sites to create pWG012. pWG012 was then conjugated into the *M. trichosporium* OB3b wild type strain. Counterselection of mutants followed the procedure described by Puri et al (23). First, transconjugants were first selected by resistance to kanamycin for successful single homologous recombination and nalidixic acid to remove donor *E. coli*. Second, selected transconjugants were grown on NMS medium with no added copper and with 2.5% (mass/vol) sucrose for counterselection of double homologous recombination. Resulting colonies were then checked for kanamycin sensitivity and genotype via sequencing. A 3.5-kb region containing all of *mbnABCM* and 490 bp of the 5' region of *mbnN* (>40%) was thus deleted.

Back complementation of the *M. trichosporium ΔmbnAN* mutant and construction of the *ΔmbnN* mutant

The suitability of mutant Δ*mbnAN* as a host for expression of recombinant methanobactin-synthesizing genes was established by introducing pWG101, an expression vector containing the wild-type *mbn* operon (*mbnABCMN*) with its native promoter, into Δ*mbnAN* for back-complementation. pWG101 was constructed by cloning a 4.8-kb DNA fragment amplified by mbnANf/mbnANr primers (Table 2) into the pTJS140 vector (19) at the KpnI site.

To characterize the function of *mbnN*, a *ΔmbnN* mutant was constructed by introducing pWG102 expression vector into the Δ*mbnAN* mutant. pWG102 was constructed by cloning a 3.7-kb DNA fragment of *mbnABCM,* leaving out *mbnN,* amplified by mbnANf/mbnAMr primers (Table 2) into the pTJS140 vector (19) at the KpnI site. Both Δ*mbnAN* + pWG101 and Δ*mbnAN* + pWG102 *M. trichosporium* strains were maintained on NMS medium containing 20 $\mu g \bullet ml^{-1}$ spectinomycin and with no added copper. Figure S1 in the supplemental material graphically illustrates the composition of the Δ*mbnAN* strain as well as the insertions into pWG101 and pWG102.

Extraction of RNA and reverse transcription-PCR (RT-PCR)

To check the expression of various genes from plasmid and chromosome of different *M. trichosporium* OB3b strains and their response to copper, RNA from different cultures were collected, purified, and reverse transcribed to cDNA to perform RT-PCR. Total RNA was isolated from cells grown to exponential phase using a phenol-chloroform method modified from that of Griffiths et al (24). Details have been described previously (4,9).

Following isolation, RNA was purified using Zymo RNA Clean & Concentrator kit (Zymo Research, Irvine, CA) with combination of at least two DNase treatments using Qiagen RNase-free DNase (Qiagen, Germany). Removal of DNA was confirmed by the absence of 16S rRNA PCR product from PCRs. The purified RNA was quantified using a NanoDrop instrument (NanoDrop ND-1000; NanoDrop Technologies, Inc., Wilmington, DE). The same amount of RNA (500 ng) was used for reverse transcription with SuperScript III reverse transcriptase (Invitrogen, Carlsbad, CA) for all reactions. RT-PCR analyses were performed to confirm the expression of *mbnPH* (primers mbnPH-F/mbnPH-R) in the *M. trichosporium* Δ*mbnAN* mutant and *mbnA* (qmbnA_FO/qmbnA_RO), *mbnM* (mbnM-F/mbnM-R), and *mbnN* (mbnN-F/mbnN-R) in *M. trichosporium* strains *ΔmbnAN* + pWG101 and *ΔmbnAN* + pWG102. To compare the expression levels of select genes in response to the copper level, the same amount of cDNA was used as a PCR template, and the same amount of PCR mix was loaded for gel analysis.

Isolation of methanobactin

Methanobactin was isolated from the spent media of wild-type *M. trichosporium* OB3b, Δ*mbnAN* + pWG101, and Δ*mbnAN* + pWG102 strains as previously described by Bandow et al (25) with the following modifications. Following freeze-drying, the samples were dissolved in pre-filtered (0.22-µM-pore-size filter) H_2O (>18MΩ▪cm) and loaded onto a 2.2-cm-by-25-cm Vydac Protein and Peptide C18 column (The Separations Group, CA, USA). The sample was washed with one column volume of H_2O (>18MΩ▪cm) and one column volume of 5% methanol/ 95% H_2O (>18MΩ▪cm). Methanobactin from *M. trichosporium* Δ*mbnAN* + pWG102 was eluted in one column volume of 10% methanol/

90% H_2O (>18MΩ▪cm), and methanobactin from the *M. trichosporium* OB3b wild-type and Δ*mbnAN* + pWG101 strains was eluted with 15% methanol/85% H_2O (>18MΩ▪cm).

Mass spectroscopy

Molecular masses of methanobactin from the *M. trichosporium* Δ*mbnAN* + pWG101 and Δ*mbnAN* + pWG102 strains were initially screened using a Voyager DE Pro matrix-assisted laser desorption ionization-time of flight (MALDI-TOF) mass spectrometer (JBI Scientific, Hunstville, TX USA). Samples (10 to 20 $\mu g \cdot \mu l^{-1}$) were mixed in a 1:1 ratio with matrix Super dihydroxybenzoic acid (Super DHB) and 1µl of this mixture was loaded on a plate V700666 (from JBI Scientific) and allowed to dry at room temperature. Super DHB was prepared from 9 parts 2,5-dihydroxybenzoic acid (DHB) and 1 part 2-hydroxy-5-methoxybenzoic acid (Sigma Aldrich, St. Louis, MO), both prepared in 70% acetonitrile-29.9% H_2O-0.1% trifluoroacetic acid.

Exact molecular masses were determined on a Q Exactive Hybrid Quadrupole-Orbitrap mass spectrometer (Thermo Fisher Scientific, Waltham MA, USA) coupled with an 1260 Infinity liquid chromatography system (Agilent Technologies, Santa Clara, CA, USA) in either the MS mode (LC-MS) or the MS/MS mode (LC-MS/MS). Samples were separated on a 0.5-mm-by-150-mm Zorbax SB C_{18} column (Agilent Technologies, Santa Clara CA, USA) with a linear gradient of buffer A (0.1 % formic acid, 99.9% H_2O) and buffer B (0.1% formic acid, 99.9% acetonitrile).

Molecular masses of methanobactin from *M. trichosporium* Δ*mbnAN* + pWG101 and Δ*mbnAN* + pWG102 were also determined by direct injection on a Bruker SolariX Fourier transform-ion cyclotron resonance (FT-ICR) mass spectrometer (Bruker, MA, USA) in

positive electron spray ionization-mode. Masses of methanobactin samples digested with with 100 mM HCl for 12 h were also measured using LC-MS.

Amino acid sequence and composition analyses

The N-terminal amino acid sequence of methanobactin from *M. trichosporium* Δ*mbnAN* + pWG101 and Δ*mbnAN* + pWG102 was determined by Edman degradation on a model 494 protein/peptide sequencer (Applied Biosystems, Carlsbad, CA USA). The amino acid composition of methanobactin from *M. trichosporium mbnAN* + pWG101 and Δ*mbnAN* + pWG102 was also determined by the Experiment Station Chemical Laboratories University of Missouri-Columbia using acid hydrolysis and performic acid oxidation methods as previously described (26). Amino acids were separated by cation exchange chromatography-high-performance liquid chromatography (cIEC-HPLC) coupled with postcolumn ninhydrin derivitization and quantified on an L8900 amino acid analyzer (Hitachi, Tokyo, Japan).

UV-visible absorption spectroscopy

UV-visible absorption spectroscopy, acid hydrolysis of oxazolone rings, and copper titration experiments were determined as described earlier (1, 2, 8).

Thiol determination

The concentration of thiol groups in methanobactin from *M. trichosporium* Ob3b wild-type, Δ*mbnAN* + pWG101 and Δ*mbnAN* + pWG102 strains [as isolated and following reduction with tris(2-carboxyethyl)phosphine (TCEP)] was determined using a thiol fluorometric detection kit from Creative BioMart (Shirley, NY, USA). For detection of

thiols after reduction, methanobactin was first placed in a Coy anaerobic chamber (95% argon/ 5% hydrogen atmosphere). Reaction mixtures for reduction contained 100 µl of 1 mM methanobactin from each strain and 200 µl of 8 mM TCEP and were incubated for 30 min at room temperature. Following reduction, samples were transferred to a 96-well microplate and sealed with microplate adhesive film (USA scientific Inc., Ocala, FL, USA). Microplates were then removed from the anaerobic chamber and read immediately on Tecan Safire fluorescence, absorbance and luminescence reader (Tecan Group, Ltd., Männedorf, Switzerland).

Results

Using sucrose counterselection techniques, a markerless deletion of *mbnA* through *mbnN* was constructed in *M. trichosporium* OB3b. This was confirmed by PCR amplification of *mbnA* through *mbnN* and verification of the loss of plasmid backbone (Figure S2). This was further confirmed by sequencing as well as by the finding that the *M. trichosporium* OB3b Δ*mbnAN* strain was kanamycin sensitive and sucrose resistant (data not shown). The construction of this deletion mutant had no effect on expression of *mbnPH* as confirmed by reverse transcription-PCR (RT-PCR) (Figure S3). Interestingly, expression of *mbnPH* was dependent on copper as found earlier for *mbnA* (4), suggesting that *mbnA, mbnP,* and *mbnH* utilize a shared regulatory element for expression.

After verification of the deletion of *mbnA* through *mbnN* from the chromosome, methanobactin production was examined in this mutant. The absence of color in the culture medium suggested that no methanobactin was being produced by this mutant even when it was cultured under low-copper conditions (Figure S4). The lack of methanobactin

production in the Δ*mbnAN* mutant was confirmed via UV/visible light absorption spectral analyses of the spent medium (which was concentrated more than 50-fold in using an HP20 Dianion column; Figure 3).

The Δ*mbnAN* strain was then back complemented with *mbnA* through *mbnN* via insertion of these genes into pTJS140 to generate pWG101. Expression of these back-added genes was suggested by the color of the culture medium (Figure S4), and was confirmed via RT-PCR (Figure S5). Methanobactin production was clearly visible via UV-visible light absorption spectroscopy (Figure 3), and was approximately 75% of that observed from wild-type *M. trichosporium* OB3b. The mass of methanobactin from this back-complemented mutant (*M. trichosporium* Δ*mbnAN* + pWG101) was found to be 1154.27 Da by both liquid chromatography-tandem mass spectrometry (LC-MS/MS) (Figure S6) and Fourier transform-ion cyclotron resonance-mass spectrometry (FT-ICR-MS) (Figure S7) and was identical to the mass of methanobactin from wild-type *M. trichosporium* OB3b, indicating that *M. trichosporium* Δ*mbnAN* + pWG101 produced the same form of methanobactin.

The native σ^{70}-dependent promoter upstream of *mbnA* was also incorporated into pWG101, and based on earlier findings showing that *mbnA* expression decreased with increasing copper in *M. trichosporium* OB3b wild-type strain (4), similar results were expected in *M. trichosporium* Δ*mbnAN* + pWG101. Indeed, expression of *mbnA* and *mbnN* was visibly reduced in *M. trichosporium* Δ*mbnAN* + pWG101 in the presence of copper compared to the results seen in the growth medium in the absence of copper (Figure S5). Comparable results were seen for methanobactin production, i.e., the level of methanobactin in the spent medium was markedly reduced when *M. trichosporium* Δ*mbnAN* + pWG101 was grown in the presence of copper (Figure 3).

The role of *mbnN* in methanobactin biosynthesis was then investigated by inserting *mbnA* through *mbnM* (again under the control of the native σ^{70}-dependent promoter) into pTJS140, creating pWG102, and then conjugating this into *M. trichosporium* Δ*mbnAN*. Expression of *mbnA* and *mbnM* was evident (Figure S8), and the methanobactin produced by *M. trichosporium* Δ*mbnAN* + pWG102 was isolated and characterized. The molecular mass of methanobactin produced by this strain was found to be 999.47 Da by LC-MS/MS (Figure S6) and 999.46 Da by FT-ICR MS (Figure S7), 154.7 Da less than that of methanobactin isolated from *M. trichosporium* OB3b wild-type strain (6). The difference suggests that one or both heterocyclic rings did not form and that an amino acid residue was missing. Subsequently, methanobactin from *M. trichosporium* Δ*mbnAN* + pWG102 was subjected to Edman degradation and was found to have a polypeptide backbone with a sequence consisting of Leu-?-Gly-Ser-?-Tyr-Pro-?-Ser-? (question marks suggest moieties with sulfhydryl groups, e.g., cysteines or non-amino acid moieties). It should be noted that the C-terminal methionine is missing from Δ*mbnAN* + pWG102 methanobactin, and this can explain 131.2 Da of the difference in mass in comparing methanobactin from the wild-type strain to that from *M. trichosporium* Δ*mbnAN* + pWG102. More importantly, successful amino acid sequencing of methanobactin from *M. trichosporium* Δ*mbnAN* + pWG102 was surprising, as previous attempts to sequence wild-type methanobactin via Edman degradation resulted in the non-methanobactin sequence of Ser-Met-Tyr-Pro-? Ser-?-Met. The modification of the N-terminal leucine and the presence of the adjacent oxazolone ring A alter or disrupt N-terminal amino acid sequencing in wild-type methanobactin. The successful collection of methanobactin sequence data from *M. trichosporium* Δ*mbnAN* +

pWG102 indicates that the N-terminal leucine had not been modified, and raises the possibility that oxazolone ring A might also have been missing.

To help identify the unknown residues found in the initial amino acid sequence of methanobactin from *M. trichosporium* Δ*mbnAN* + pWG102, the compositions of acid-digested methanobactin from *M. trichosporium* Δ*mbnAN* + pWG101 and Δ*mbnAN* + pWG102 were determined and compared. Methanobactin from *M. trichosporium* Δ*mbnAN* + pWG101 was found to have 0 leucines, 1.9 serines, 2.1 glycines, 0.8 prolines, 1.8 cysteines, and 0.8 methionines per tyrosine (used as an internal standard). The presence of proline and one more glycine than expected from the structure of wild-type methanobactin (Figure 1) indicates that under these conditions, oxazolone ring B underwent hydrolysis and decarboxylation to form proline and a glycine (likely containing thioamide or Gly-Ψ), but oxazolone ring A was not degraded. Such a result is not unprecedented as it was shown earlier that when methanobactin from *M. trichosporium* OB3b was subjected to acid digestion, oxazolone ring B was hydrolyzed and decarboxylated to proline and a thioamide-containing glycine before ring A was converted to an α–oxo-leucine and a thioamide-containing glycine (8).

Methanobactin from *M. trichosporium* Δ*mbnAN* + pWG102 was found to have a different composition, i.e., 1.0 leucines, 1.8 serines, 3.3 glycines, 0.7 prolines and 1.6 cysteines per tyrosine. The absence of a Met was consistent with the N-terminal sequencing results. The presence of leucine and a third glycine is remarkable and is unlikely to be the result of the degradation of oxazolone ring A, as methanobactin from *M. trichosporium* Δ*mbnAN* + pWG102 was prepared in the same fashion as that from *M. trichosporium* Δ*mbnAN* + pWG101. Rather, the finding of these residues supports the possibility that

oxazolone ring A was not present in methanobactin from *M. trichosporium* Δ*mbnAN* + pWG102 methanobactin.

To consider this further, UV/visible light absorption spectral analyses of *M. trichosporium* Δ*mbnAN* + pWG102 methanobactin were performed and the results were compared to those from methanobactin produced by *M. trichosporium* Δ*mbnAN* + pWG101 (Figure 4). The presence of only one major absorption peak at 337 nm indicates that *M. trichosporium* Δ*mbnAN* + pWG102 methanobactin has only oxazolone ring B, and not oxazolone ring A, as a second major absorption peak would be expected at 394 nm. Further, copper titration of *M. trichosporium* Δ*mbnAN* + pWG102 methanobactin demonstrated copper binding, but the sample saturated at a copper/methanobactin molar ratio of ~0.5, compared to 1.0 for wild-type methanobactin (1,2) and for methanobactin from *M. trichosporium* Δ*mbnAN* + pWG101 (Figure 4A). The impaired copper binding by methanobactin from *M. trichosporium* Δ*mbnAN* + pWG102 again suggests that oxazolone ring A is missing. Finally, acid digestion of methanobactin produced by *M. trichosporium* Δ*mbnAN* + pWG102 followed the hydrolysis pattern observed for oxazolone B from both wild-type *M. trichosporium* (8) and *M. trichosporium* Δ*mbnAN* + pWG101. In wild-type *M. trichosporium* and *M. trichosporium* Δ*mbnAN* + pWG101 methanobactin, oxazolone ring B is hydrolyzed before oxazolone ring A, as evidenced by the decrease in absorption at 340 nm but the minimal change at 394 nm (Figure S9). The mass changes for methanobactin from *M. trichosporium* Δ*mbnAN* + pWG101 (24.98 Da) and Δ*mbnAN* + pWG102 (25.99, 27 and 28 Da) (Figure S10) after acid digestion were consistent with the 25.98-Da change predicted following hydrolysis of the oxazolone ring B (8).

Considering the mass spectral, amino acid sequence, composition, and UV/visible light absorption data *in toto*, we propose that the metal-free form of methanobactin from *M. trichosporium* Δ*mbnAN* + pWG102 has the molecular structure shown in Figure 5. This structure, with a mass of 999.26 Da, agrees well with that measured via mass spectroscopy (Figure S6 and S7). In particular, we predict that leucine is adjacent to a thioamide-containing glycine (Gly-Ψ), and that oxazolone ring B is also present. To verify the presence of this modified glycine in methanobactin, we assayed for the presence of thiol groups before and after reduction performed using tris(2-carboxyethyl)phosphine (TCEP). Before reduction, no thiol groups were measured in methanobactin from the *M. trichosporium* OB3b wild-type, Δ*mbnAN* + pWG101, and Δ*mbnAN* + pWG102 strains (Table 1), suggesting that the thioamide groups associated with the oxazolone rings are not detectable using this methodology and the cysteine thiol groups were oxidized. After reduction, however, the methanobactins from the *M. trichosporium* OB3b wild-type and Δ*mbnAN* + pWG101 strains had 1.7 ± 0.3 and 2.1 ±0.1 thiols per methanobactin, respectively (Table 1), and were likely created from the reduction of the disulfide bond connecting Cys 3 and Cys 6 (Figure 1). Methanobactin from *M. trichosporium* Δ*mbnAN* + pWG102 had 3.1 ± 0.3 thiols per methanobactin after reduction with TCEP. The finding of an additional thiol after reduction indicates that despite the lack of oxazolone ring A, the sulfur group remains and, as such, supports the conclusion that a thioamide-containing glycine exists in place of oxazolone ring A.

Discussion

Since the discovery that the precursor polypeptide of methanobactin was chromosomally encoded and that the gene is part of a gene cluster that includes genes encoding for an extrusion protein and for a putative diheme cytochrome *c* peroxidase and its partner protein, as well genes of unknown function, it has been accepted that methanobactin is a RiPP, but the roles of genes in the methanobactin gene cluster other than *mbnT* (encoding for a TonB-dependent transporter required for uptake of the copper-methanobactin complex (9), have not been explicitly determined. Here we show through the construction of markerless deletion of *mbnABCMN* and expression of *mbnABCM* from a plasmid that the product of *mbnN* is necessary for the deamination of the N-terminal leucine. Further, *M. trichosporium* Δ*mbnAN* + pWG102 is unable to construct oxazolone ring A in methanobactin, but oxazolone ring B is formed, indicating that these two rings are made independently. At this time, it is unclear if oxazolone rings A and B are formed via the same or different modifying enzyme(s), but from the data collected, it appears that the modifying enzyme(s) responsible for formation of oxazolone ring A can bind and/or modify the N-terminal cysteine only after the deamination of the adjacent leucine.

In our earlier proposed pathway for methanobactin biosynthesis (5), we speculated that ring closure occurred before changes in connectivity of the peptide backbone. On the basis of the findings reported here, however, it appears that deamination of the N-terminal acid must occur before formation of oxazolone ring A in *M. trichosporium* OB3b, and we present in Figure 6 an alternative scheme for formation of methanobactin. We stress that we do not know whether, in wild-type methanobactin, rearrangement of the peptide backbone

occurs before leucine deamination (or vice-versa)-only that both are required for formation of oxazolone ring A.

It should be noted that all methanobactins characterized to date have an oxazolone ring near the C-terminus, but the N-terminal heterocyclic ring is either an oxazolone ring, a pyrazinedione ring, or an imidazolone ring. In our earlier proposal of a pathway for methanobactin biosynthesis (5), we speculated that pyrazinedione and imidazolone rings are formed from modification of an oxazolone ring, but further consideration of available bioinformatic data juxtaposed with the findings reported here suggests that pyrazinedione and imidazolone rings can be created without an oxazolone ring platform. That is, in our original model of ring formation, deamination of the amino acid residue adjacent to the cysteine converted to an oxazolone ring was not necessary for ring formation. The data presented here, however, show such deamination is required for the formation of oxazolone ring A. Methanobactin of *Methylocystis rosea* and methanobactin of *Methylocystis* strain SB2 have an N-terminal pyrazinedione and imidazolone ring, respectively, but the methanobactin gene clusters of these two strains do not show any clear evidence of an encoded aminotransferase (5). Given that the N-terminal oxazolone ring in methanobactin of *M. trichosporium* OB3b is only formed when *mbnN* is expressed, it is possible that the creation of the alternative rings found in other forms of methanobactin does not require an oxazolone ring be formed first. Rather, the formation of a pyrazinedione and imidazolone rings may be due to the concerted activity of a suite of modifying enzymes, including a putative flavin adenine dinucleotide (FAD)-dependent oxidoreductase found in the methanobactin gene clusters of *Methylocystis rosea* and *Methylocystis* strain SB2 but not in *M. trichosporium* OB3b (5). As noted earlier, however, formation of imidazolone or

pyrazinedione rings without an oxazolone intermediate would likely necessitate multiple changes in the connectivity of the peptide backbone (5).

It thus appears that different strategies have been developed by different methanotrophs for the formation of methanobactin, and creation and characterization of more mutants are clearly required to fully reconstruct these different biosynthetic pathways. That *M. trichosporium* OB3b is the only methanotroph known to produce methanobactin with a validated system for generation of mutants represents a challenge, however. Similar approaches may be possible in other methanotrophs that produce methanobactin, but in the event that working genetic systems are difficult to construct in these strains, it may be useful to pursue efforts whereby methanobactin genes from other strains are heterologously expressed in either *E. coli* or methanobactin-defective mutants of *M. trichosporium* OB3b.

In conclusion, through the construction and back-complementation of a deletion mutant defective in methanobactin production, we have elucidated the function of *mbnN* and can now utilize the deletion mutant platform to unravel the role of other genes in the methanobactin gene cluster. With such data, we can develop a better mechanistic understanding of the methanobactin biosynthesis pathway and also create strategies to modify methanobactin for enhanced treatment of copper-related diseases such as Wilson disease.

Funding Information

This research was supported by the Office of Science (Biological and Environmental Research), U.S. Department of Energy, Grant #DE-SC0006630 to JDS and AAD. Use of the Q Exactive™ Hybrid Quadrupole-Orbitrap™ mass spectrometer was made possible

through a generous gift from the Roy J. Carver Charitable Trust (Muscatine, Iowa). The funders had no role in study design, data collection and interpretation, or the decision to submit the work for publication.

References

1. **Choi DW, Do YS, Zea CJ, McEllistrem MT, Lee SW, Semrau JD, Pohl NL, Kisting CJ, Scardino LL, Hartsel SC, Boyd ES, Geesey GG, Riedel TP, Shafe PH, Kranski KA, Tritsch JR, Antholine WE, DiSpirito AA**. 2006a. Spectral and thermodynamic properties of Ag(I), Au(III), Cd(II), Co(II), Fe(III), Hg(II), Mn(II), Ni(II), Pb(II), U(IV), and Zn(II) binding by methanobactin from *Methylosinus trichosporium* OB3b. J Inorg Biochem **100**:2150-2161.

2. **Choi DW, Zea CJ, Do YS, Semrau JD, Antholine WE, Hargrove MS, Pohl NL, Boyd ES, Geesey GG, Hartsel SC, Shafe PH, McEllistrem MT, Kisting CJ, Campbell D, Rao V, de la Mora AM, DiSpirito AA**. 2006b. Spectral, kinetic, and thermodynamic properties of Cu(I) and Cu(II) binding by methanobactin from *Methylosinus trichosporium* OB3b. Biochemistry **45**:1442-1453.

3. **Kim HJ, Graham DW, DiSpirito AA, Alterman MA, Galeva N, Larive CK, Asunskis D, Sherwood PM**. 2004. Methanobactin, a copper-acquisition compound from methane-oxidizing bacteria. Science **305**:1612-1615.

4. **Semrau JD, Jagadevan S, DiSpirito AA, Khalifa A, Scanlan J, Bergman BH, Freemeier BC, Baral BS, Bandow NS, Vorobev A, Haft DH, Vuilleumier S, Murrell JC**. 2013. Methanobactin and MmoD work in concert to act as the 'copper-switch' in methanotrophs. Environ Microbiol **15**:3077–3086.

5. **DiSpirito AA, Semrau JD, Murrell JC, Gallagher WH, Dennison C, Vuilleumier**. 2016. Methanobactin and the link between copper and bacterial methane oxidation. Microbiol Mol Biol Rev **80**:287-409.

6. **Behling LA, Hartsel SC, Lewis DE, DiSpirito AA, Choi DW, Masterson LR, Veglia G, Gallagher WH**. 2008. NMR, mass spectrometry and chemical evidence reveal a different chemical structure for methanobactin that contains oxazolone rings. J Am Chem Soc **130**:12604-12605.

7. **Kim HJ, Galeva N, Larive CK, Alterman M, Graham DW**. 2005. Purification and physical-chemical properties of methanobactin: a chalkophore from *Methylosinus trichosporium* OB3b. Biochemistry **44**:5140-5148.

8. **Krentz BD, Mulheron HJ, Semrau JD, Di Spirito AA, Bandow NL, Haft DH, Vuilleumier S, Murrell JC, McEllistrem MT, Hartsel SC, Gallagher WH**. 2010. A comparison of methanobactins from *Methylosinus trichosporium* OB3b and *Methylocystis strain* SB2 predicts methanobactins are synthesized from diverse peptide precursors modified to create a common core for binding and reducing copper ions. Biochemistry **49**:10117-10130.

9. **Gu W, Haque MF, Baral BS, Turpin EA, Bandow NL, Kremmer E, Flatley A, Zischka H, DiSpirito AA, Semrau JD**. 2016. A TonB-Dependent Transporter Is Responsible for Methanobactin Uptake by *Methylosinus trichosporium* OB3b. Appl Environ Microbiol **82**:1917-23.

10. **Solovyev V, Salamov A**. 2011. Automatic annotation of microbial genomes and metagenomic sequences, p 61-78. *In* Li RW (ed), Metagenomics and its applications in agriculture, biomedicine and environmental Studies. Nova Science Publishers, Hauppauge, NY.

11. **Lichtmannegger J, Leitzinger C, Wimmer R, Schmitt S, Schulz S, Kabiri Y, Eberhagen C, Rieder T, Janik D, Neff F, Straub BK, Schirmacher P, DiSpirito AA, Bandow N, Baral BS, Flatley A, Kremmer E, Denk G, Reiter FP, Hohenester S, Eckardt-Schupp F, Dencher NA, Adamski J, Sauer V, Niemietz C, Schmidt HHJ, Merle U, Gotthardt DN, Kroemer G, Weiss KH, Zischka H**. 2016. Methanobactin reverses acute liver failure in a rat model of Wilson disease. J. Clinic Invest **126**:2721-2735.

12. **Summer KH, Lichtmannegger J, Bandow N, Choi DW, DiSpirito AA, Michalke B**. 2011. The biogenic methanobactin is an effective chelator for copper in a rat model for Wilson disease. J Trace Elem Med Biol **25**:36-41.

13. **Zischka H, Lichtmannegger J, Schmitt S, Jagemann N, Schulz S, Wartini D, Jennen L, Rust C, Larochette N, Galluzzi L, Chajes V, Bandow N, Gilles VS, DiSpirito AA, Esposito I, Goettlicher M, Summer KH, Kroemer G**. 2011. Liver mitochondrial membrane crosslinking and destruction in a rat model of Wilson disease. J Clin Invest **121**:1508-1518.

14. **Ala A, Walker AP, Ashkan A, Dooley JS, Schilsky M**. 2007. Wilson's disease. Lancet **369**:397 - 408.

15. **Roberts EA**. 2011. Wilson's disease. Medicine **39**:602 - 604.

16. **Kaler SG**. Microbial peptide de-coppers mitochondria: implications for Wilson disease. J. Clinic Invest **126**: 2412-2414.

17. **Simon R**. 1984. High frequency mobilization of gram-negative bacterial replicons by the in vitro constructed Tn5-Mob transposon. Mol Gen Genet **196**:413– 420.

18. **Schäfer A, Tauch A, Jäger W, Kalinowski J, Thierbach G & Pühler A**. 1994. Small mobilizable multipurpose cloning vectors derived from the Escherichia coli plasmids pK18 and pK19: selection of defined deletions in the chromosome of *Corynebacterium glutamicum*. Gene **145**: 69-73.

19. **Smith TJ, Slade SE, Burton NP, Murrell JC, Dalton H**. 2002. Improved system for protein engineering of the hydroxylase component of soluble methane monooxygenase. Appl Environ Microbiol **68**:5265-73.

20. **Whittenbury R, Phillips KC, Wilkinson JF**. 1970. Enrichment, isolation and some properties of methane-utilizing bacteria. J Gen Microbiol **61**:205-218.

21. **Sambrook J, Russell DW**. 2001. Molecular cloning: a laboratory manual 3rd edition. Coldspring-Harbour Laboratory Press, UK.

22. **Martin H, Murrell JC**. 1995. Methane monooxygenase mutants of *Methylosinus trichosporium* constructed by marker-exchange mutagenesis. FEMS Microbiol Lett **127**:243–248.

23. **Puri AW, Owen S, Chu F, Chavkin T, Beck DA, Kalyuzhnaya MG, Lidstrom ME**. 2015. Genetic tools for the industrially promising methanotroph Methylomicrobium buryatense. Appl Environ Microbiol **81**(5):1775-81.

24. **Griffiths RI, Whiteley AS, O'Donnell AG, Bailey MJ**. 2000. Rapid method for coextraction of DNA and RNA from natural environments for analysis of ribosomal DNA- and rRNA-based microbial community composition. Appl Environ Microbiol **66**:5488-91.

25. **Bandow NL, Gallagher WH, Behling L, Choi DW, Semrau JD, Hartsel SC, Gilles VS, Dispirito AA**. 2011. Isolation of methanobactin from the spent media of methane-oxidizing bacteria. Meth Enzymol **495**:259-269.

26. **AOAC International**. Official Methods of Analysis. 77, 1362 (1994). Gaithersburg, MD, USA, Official Method 994.12.

Table 1. Strains and plasmids used in this study.

Strains	Genotype/Description	Source
E. coli		
TOP10	F– *mcr*A Δ(*mrr-hsd*RMS-*mcr*BC) Φ80*lac*ZΔM15 Δ*lac*X74 *rec*A1 *ara*D139 Δ(*ara leu*) 7697 *gal*U *gal*K *rps*L (StrR) *end*A1*nup*G	Invitrogen
S17.1	*recA1 thi pro hsdR*- RP4-2Tc::Mu Km::Tn*7*	17
M. trichosporium OB3b	wild type	
Δ*mbnAN*	*mbnABCMN* deleted	this study
Δ*mbnAN* + pWG101	Δ*mbnAN* back-complemented by pWG101	this study
Δ*mbnAN* + pWG102	*mbnN* deleted, constructed by Δ*mbnAN* carrying pWG102	this study
Plasmids	**Description**	**Source**
pK18mob*sacB*	Mobilizable suicide vector; *oriT* Km^r*lacZ sacB*	26
pWG012	pK18mob*sacB* carrying 2-kb ligated arms used to knockout *mbnABCMN*	this study
pTJS140	Broad host-range cloning vector; Mob Ap^{r}Sp^{r}Sm^r*lacZ*	22
pWG101	pTJS140 carrying 5-kb *mbnABCMN* with its native promoter	this study
p102	pTJS140 carrying 4-kb *mbnABCM* with its native promoter	this study

Table 1 continued

Primers	**Sequence (5'-3')***	**Restriction sites**	**Source**
dmbnaF	ATTTTTggatccCGAAGGACAATAACAAGGCG	BamHI	this study
dmbnaR	ATTTTAggtaccACTCCAAACAgcatgcGATA	KpnI/SphI	this study
dmbnbF	ATTTTAggtaccATCCTTCTATGTCTGCAGCC	KpnI	this study
dmbnbR	ATTTTTaagcttGATCCTCCTCGAATTCCCTC	HindIII	this study
mbn21	GACGTTCGGGTCTTCTTCGC		this study
mbn22	CGCCTCTAGATCATTCCGAC		this study
pK18-bb-F	CTCTGGTAAGGTTGGGAAGC		this study
pK18-bb-R	GCAATACACGGGTAGCCAA		this study
mbnANf	ATTTTTggtaccGACGTTCGGGTCTTCTTCGC	KpnI	this study
mbnANr	ATTTTTggtaccCGCCTCTAGATCATTCCGAC	KpnI	this study
mbnAMr	ATTTTTggtaccTTCGTTTCACATGGGATCGC	KpnI	this study
mbnPH-F	TTCGTGACGATCGAGGTC		this study
mbnPH-R	GGTGCGTCCGTCGGTAAA		this study
qmbnA_FO	TGGAAACTCCCTTAGGAGGAA		4
qmbnA_RO	CTGCACGGATAGCACGAAC		4
mbnN-F	GCTCGGAATTCTCGCTTTCC		this study
mbnN-R	CGCCTCTAGATCATTCCGAC		this study
mbnM-F	GTTCGGCTATTTCCTGACGC		this study
mbnM-R	CTAGGCGCATCATCATCACA		this study

* Restriction sites are shown in lower case letters.

Table 2. Quantification of thiol groups in methanobactin from *M. trichosporium* OB3b Δ*mbnAN* + pWG101 and Δ*mbnAN* + pWG102 strains as isolated and following reduction by tris(2-carboxyethyl)phosphine under anaerobic conditions. Values are the average ± standard deviation of duplicate samples.

	Thiol per methanobactin	
Methanobactin	**As Isolated**	**Reduced**
Δ*mbnAN* + pWG101	$3.7 \times 10^{-3} \pm 3.2 \times 10^{-4}$	2.02 ± 0.2
Δ*mbnAN* + pWG102	$2.2 \times 10^{-3} \pm 1.1 \times 10^{-4}$	3.1 ± 0.3

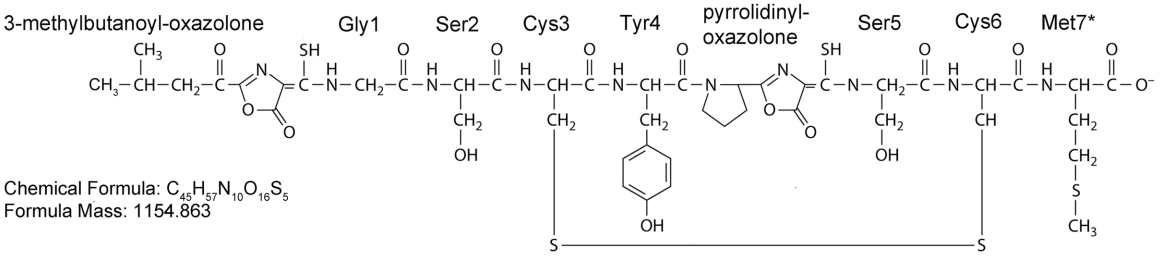

Figure 1. Primary structure of methanobactin from *M. trichosporium* OB3b (modified from 8). * indicates a methionine that is observed in some but not all samples.

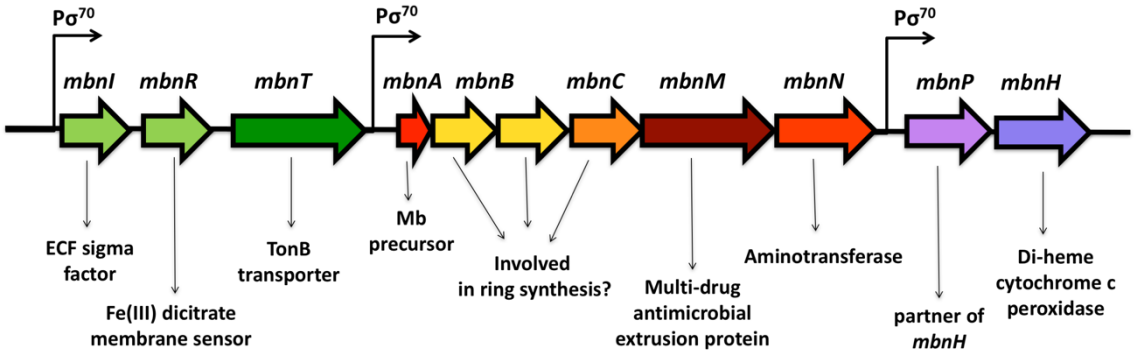

Figure 2. Methanobactin gene cluster of *M. trichosporium* OB3b.

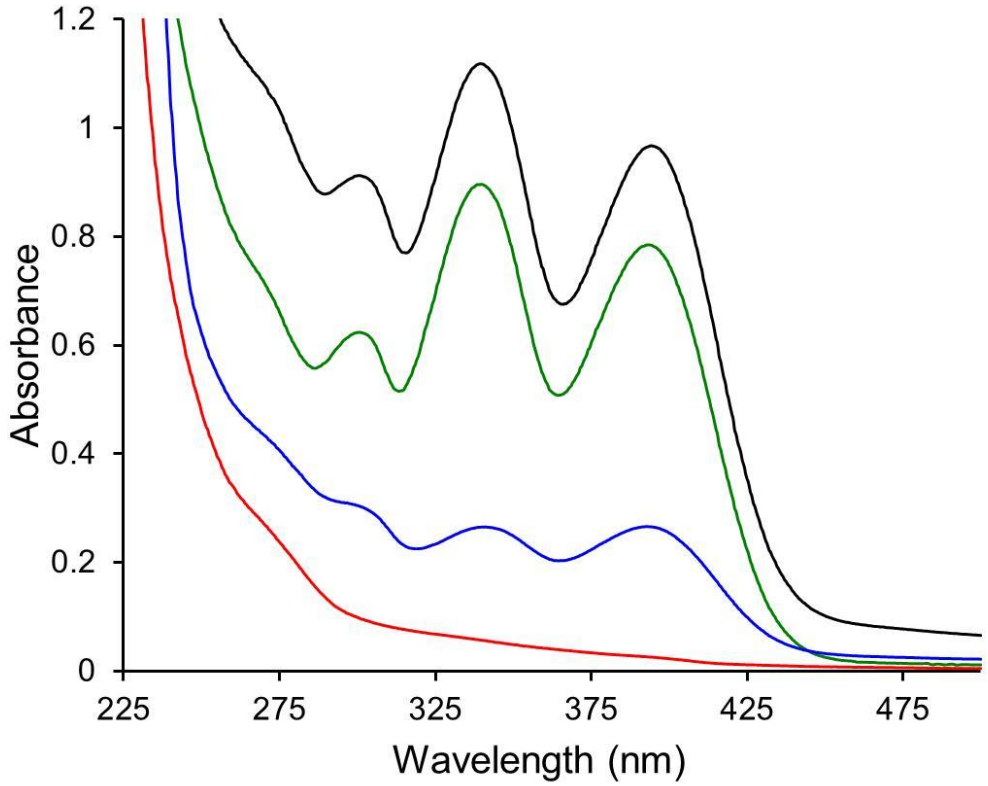

Figure 3. UV-visible absorption spectra of the spent media from wild type *M. trichosporium* OB3b, (black trace) Δ*mbnAN* mutant (red trace), and Δ*mbnAN* + pWG101 (green trace). Cells were cultured on NMS medium amended with 0.2 μM $CuCl_2$ (black and red traces) or on NMS medium amended with 0.2 μM $CuCl_2$ and 20 μg▪ml^{-1} spectinomycin (green trace). The blue trace shows methanobactin production in and Δ*mbnAN* + pWG101 when grown on NMS medium amended with 5.0 μM $CuCl_2$ and 20 μg▪ml^{-1} spectinomycin.

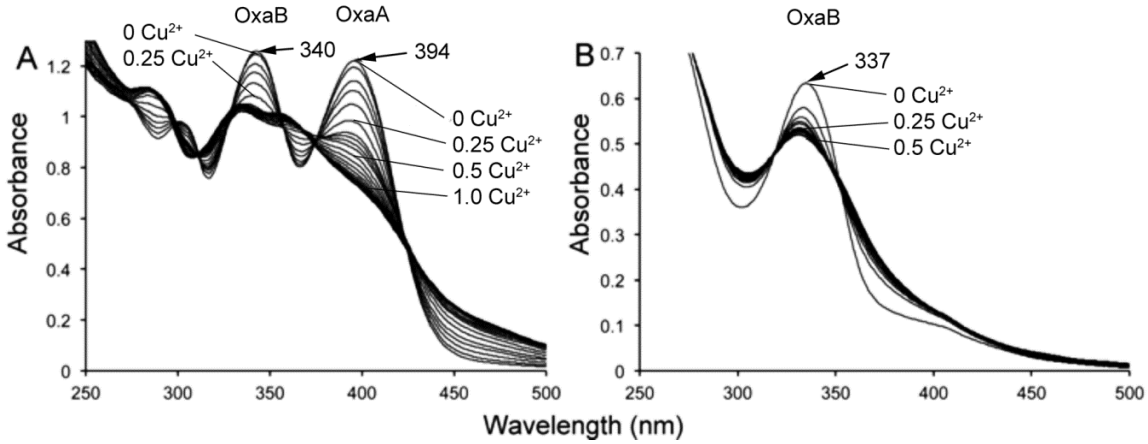

Figure 4. Comparison of the UV/visible absorption spectra of methanobactin from (A) *M. trichosporium* OB3b Δ*mbnAN* + pWG101 and (B) *M. trichosporium* OB3b Δ*mbnAN* + pWG102 with the addition of 0.0 to 1.0 Cu(II) per methanobactin in 0.05 increments.

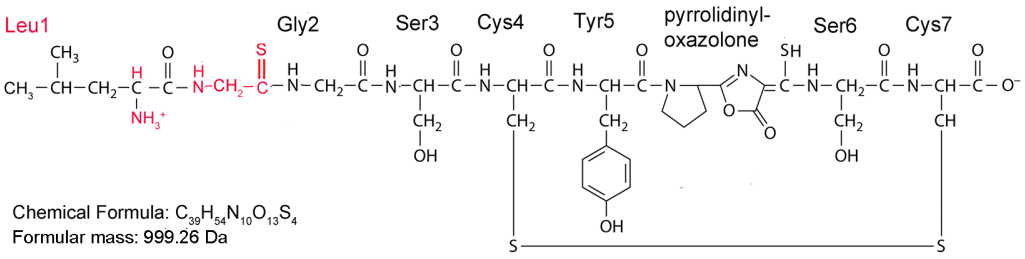

Figure 5. Proposed structure of methanobactin from *M. trichosporium* Δ*mbnAN* + pWG102. Major differences from wildtype methanobactin are shown in red.

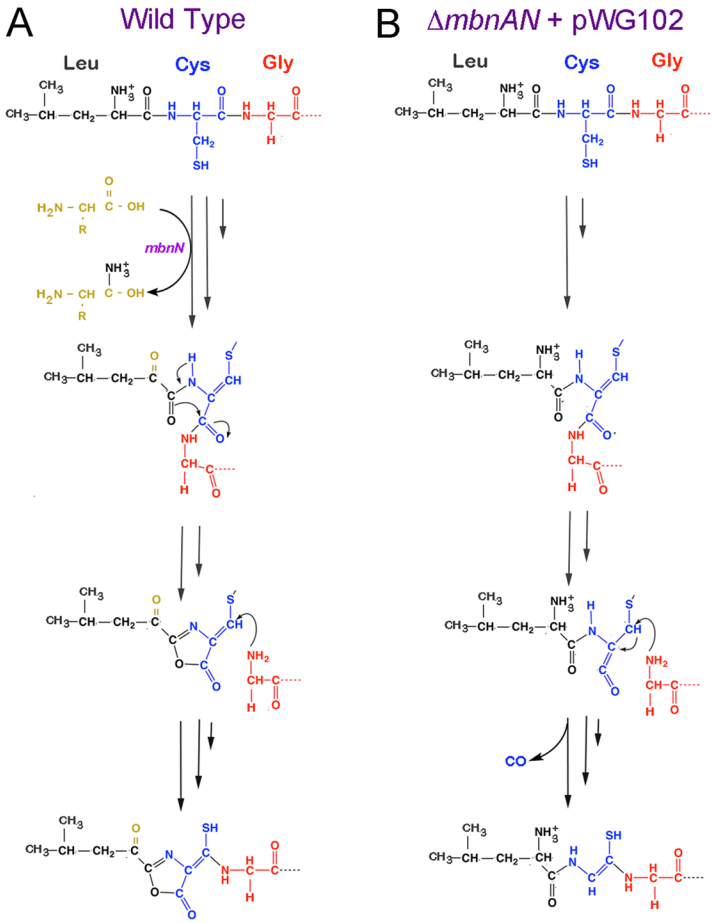

Figure 6. Proposed pathway of formation of (A) the N-terminal oxazolone group with associated thioamide group in wild type methanobactin from *M. trichosporium* OB3b and (B) the resulting altered pathway in Δ*mbnAN* + pWG102.

Supplementary Information

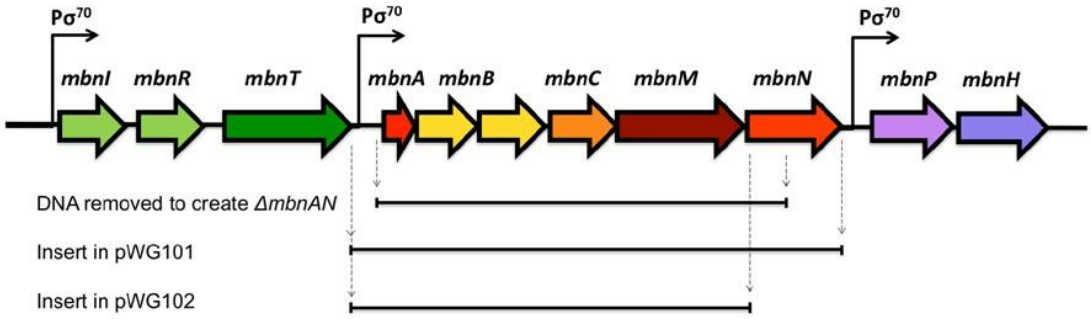

Figure S1. DNA removed to construct *M. trichosporium* OB3b Δ*mbnAN* mutant and inserts used to construct pWG101 and pWG102.

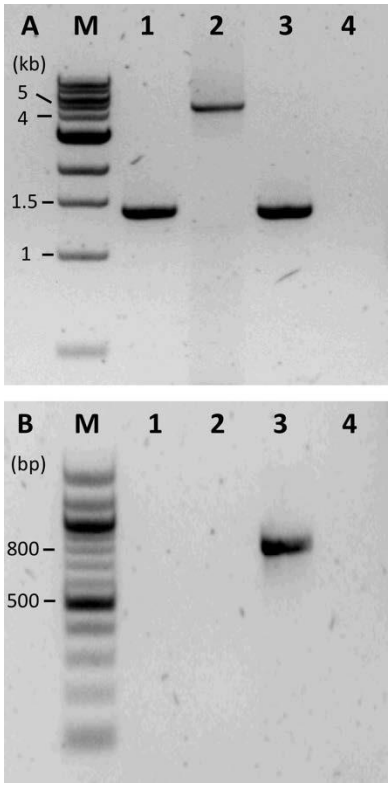

Figure S2. Confirmation of construction of *M. trichosporium* O_B_3_b_ _Δ*mbnAN* mutant. Figure S1A - PCR of *mbnABCMN* using primers mbn21/22. M - molecular weight markers. Lanes 1 – 4 are PCR of *mbnABCMN* from: 1 - *M. trichosporium* OB3b *mbnAN* mutant (expected product of 1.4 kb); 2 - *M. trichosporium* OB3b wildtype (expected product of 4.8

kb); 3 – pWG012 plasmid (positive control; expected product of 1.4 kb); 4 - distilled deionized water (negative control). Figure S1B - PCR of 14 pK18mob*sacB* plasmid backbone using primers pK18-bb-F/R. M - molecular weight markers; Lanes 1 – 4 are PCR of pK18mob*sacB* plasmid backbone from: 1 - *M. trichosporium* OB3b *mbnAN* mutant; 2 - *M. trichosporium* OB3b wildtype; 3 - pWG012 plasmid (positive control; expected product of 800 bp); 4 -distilled deionized water (negative control).

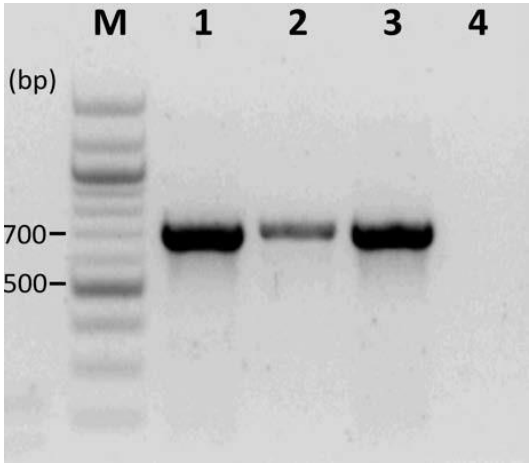

Figure S3. Confirmation of expression of *mbnPH* i_n_ _Δ*mbnAN* mutant using primers mbnPH-F/R (expected product size of 700 bp) M: molecular weight markers. Lanes 1 – 4 are RT-PCR of *mbnPH* from: 1 - *M. trichosporium* OB3b Δ*mbnAN* grown in the absence of copper; 2 - *M. trichosporium* OB3b Δ*mbnAN* mutant grown in the presence of 1 µM copper; 3 - *M. trichosporium* OB3b wild type grown in the absence of copper (positive control); (4) distilled deionized water (negative control).

Figure S4. Fermenters of (A) wild-type *M. trichosporium* OB3b, (B) Δ*mbnAN*, and (C) Δ*mbnAN* + 34 pWG101 cultured in NMS media amended with 0.2 μM $CuCl_2$.

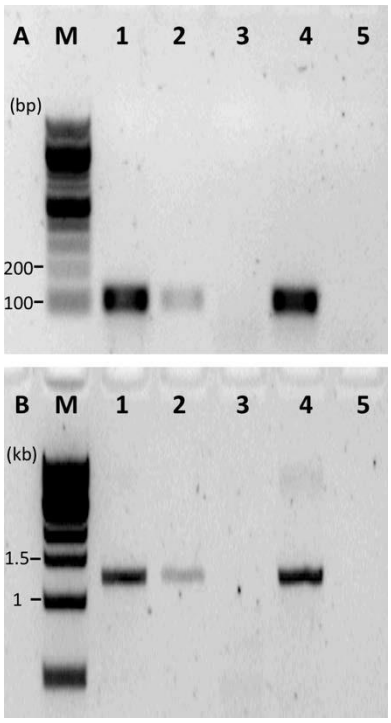

Figure S5. Expression of *mbnA* and *mbnN* in Δ*mbnAN* + pWG101. Figure S3A - RT-PCR of *mbnA* using primers qmbnA_FO/RO (expected product of 100 bp). M - molecular weight markers. Lanes 1 -5 are RT-PCR of *mbnA* from: 1 - *M. trichosporium* OB3b Δ*mbnAN* + pWG101 grown in the absence of copper; 2 -*M. trichosporium* OB3b Δ*mbnAN* + pWG101 grown with 1 μM copper; 3 - *M. trichosporium* OB3b Δ*mbnAN* grown in the absence of copper (negative control); (4) *M. trichosporium* OB3b wild type grown in the absence of copper (positive control); (5) distilled deionized water (negative control). Figure S3B-RT-PCR of *mbnN* using primers mbnN-F/R (expected product size of 1.2 kb). M molecular weight markers . Lanes 1 – 5 are RT-PCR of *mbnN* from: 1 - *M. trichosporium* OB3b Δ*mbnAN* + pWG101 grown in the absence of copper; 2 - *M. trichosporium* OB3b Δ*mbnAN* + pWG101 grown in the presence of 1 μM copper; 3 - *M. trichosporium* OB3b Δ*mbnAN* grown in the absence of copper (negative control); 4 - *M. trichosporium* OB3b wild type grown in the absence of copper (positive control); 5 - distilled deionized water (negative control).

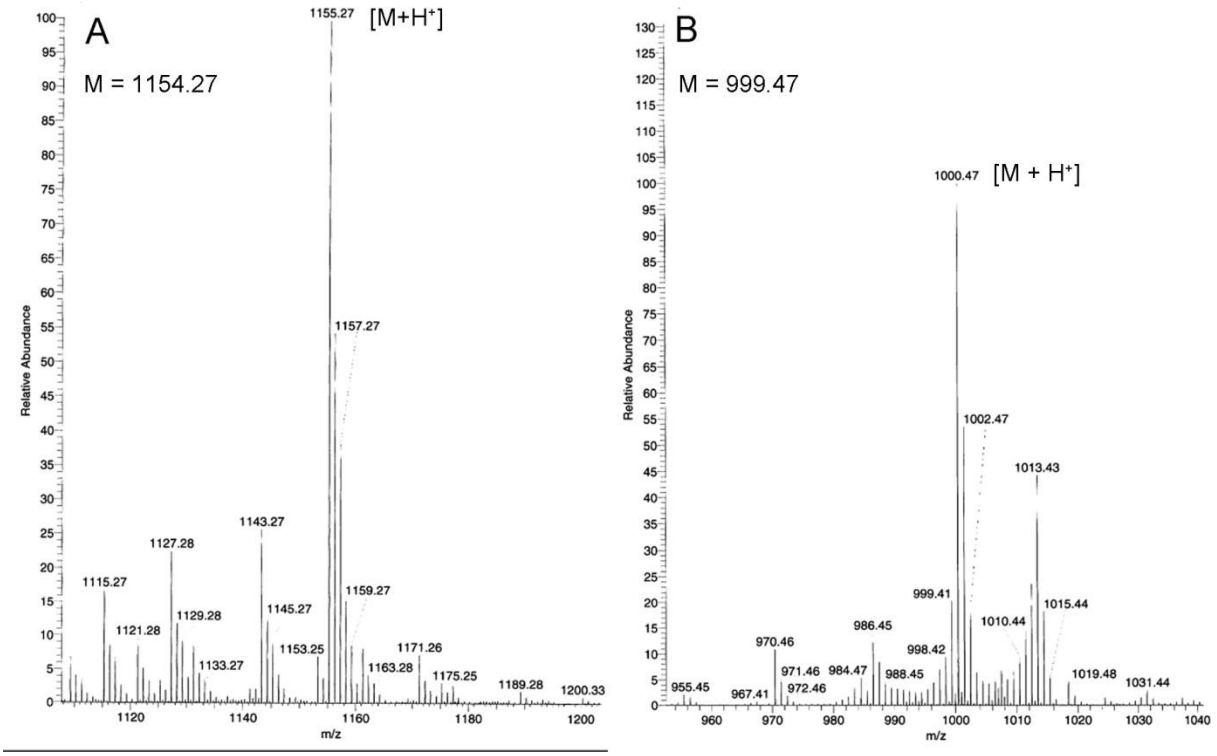

Figure S6. LC-MS/MS mass spectra of methanobactin from (A) Δ*mbnAN* + pWG101 (B)Δ*mbnAN* + pWG102 (B).

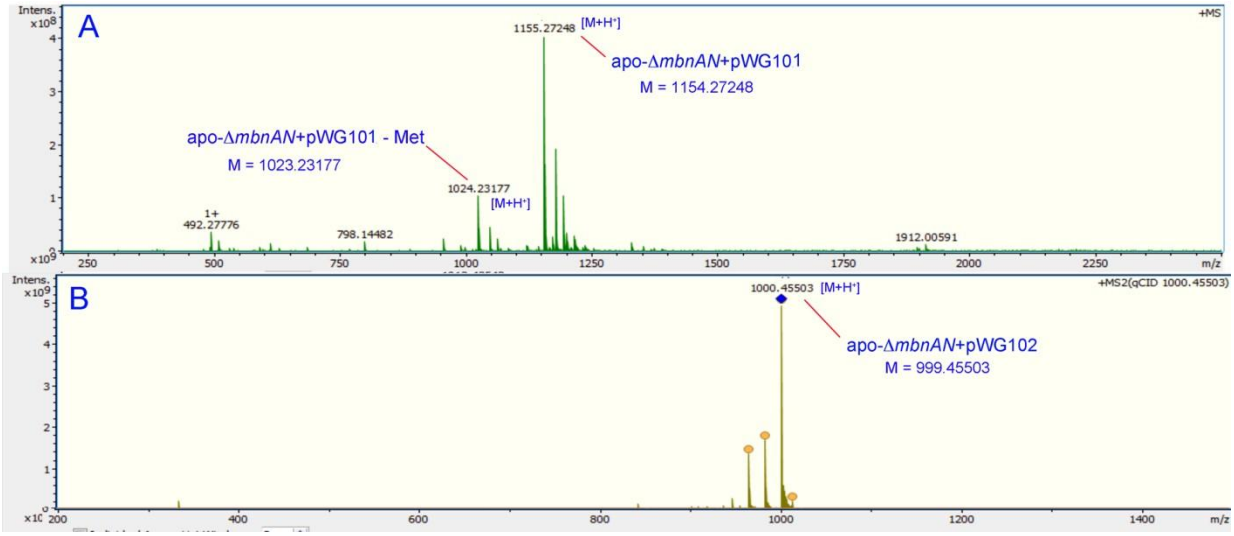

Figure S7. FT-ICR mass spectra of methanobactin from (A) Δ*mbnAN* + pWG101 and (B) Δ*mbnAN* + pWG102. Samples were collected from a Dianion HP-20 column.

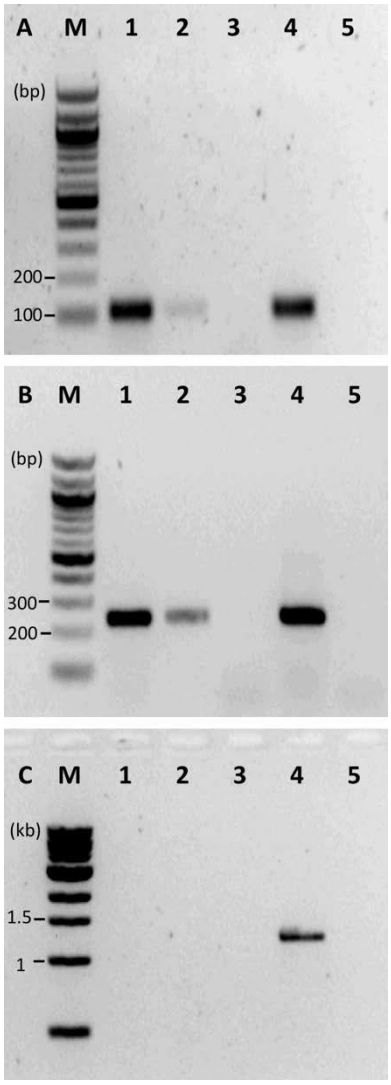

Figure S8. Expression of *mbnA*, *mbnM* and *mbnN* in Δ*mbnAN* + pWG102. Figure S4A – RT-PCR of *mbnA* using primers qmbnA_FO/RO (expected product size of 100 bp). M - molecular weight markers. Lanes 1-5 are RT-PCR of *mbnA* from: 1 - *M. trichosporium* OB3b Δ*mbnAN* + pWG102 grown in the absence of copper; 2 - *M. trichosporium* OB3b Δ*mbnAN* + pWG102 grown with 1 μM copper; 3 - *M. trichosporium* OB3b Δ*mbnAN* grown in the absence of copper (negative control); (4) *M. trichosporium* OB3b wild type grown in the absence of copper (positive control); (5) distilled deionized water (negative control). Figure S4B – RT-PCR of *mbnM* using primers mbnM-F/R (expected product size of 220 bp). M – molecular weight markers. Lanes 1 -5 are RT-PCR of *mbnM* from: 1 - *M. trichosporium* OB3b Δ*mbnAN* + pWG102 72 grown in the absence of copper; 2 - *M. trichosporium* OB3b Δ*mbnAN* + pWG102 grown with 1 μM copper; 3 - *M. trichosporium* OB3b Δ*mbnAN* grown in the absence of copper (negative control); (4) *M. trichosporium* OB3b wild type grown in the absence of copper (positive control); (5) distilled deionized water (negative control). Figure S4C – RT-PCR of *mbnN* using primers mbnN-F/R (expected product size of 1.2 kb). M - molecular weight markers. Lanes 1 -5 are RT-PCR of *mbnN* from: 1 - *M. trichosporium* OB3b Δ*mbnAN* + pWG102 grown in the absence of copper; 2 - *M. trichosporium* OB3b Δ*mbnAN* + 78 pWG102 grown with 1 μM copper; 3 - *M. trichosporium* OB3b Δ*mbnAN*

grown in the absence of copper (negative control); (4) *M. trichosporium* OB3b wild type grown in the absence of copper (positive control); (5) distilled deionized water (negative control).

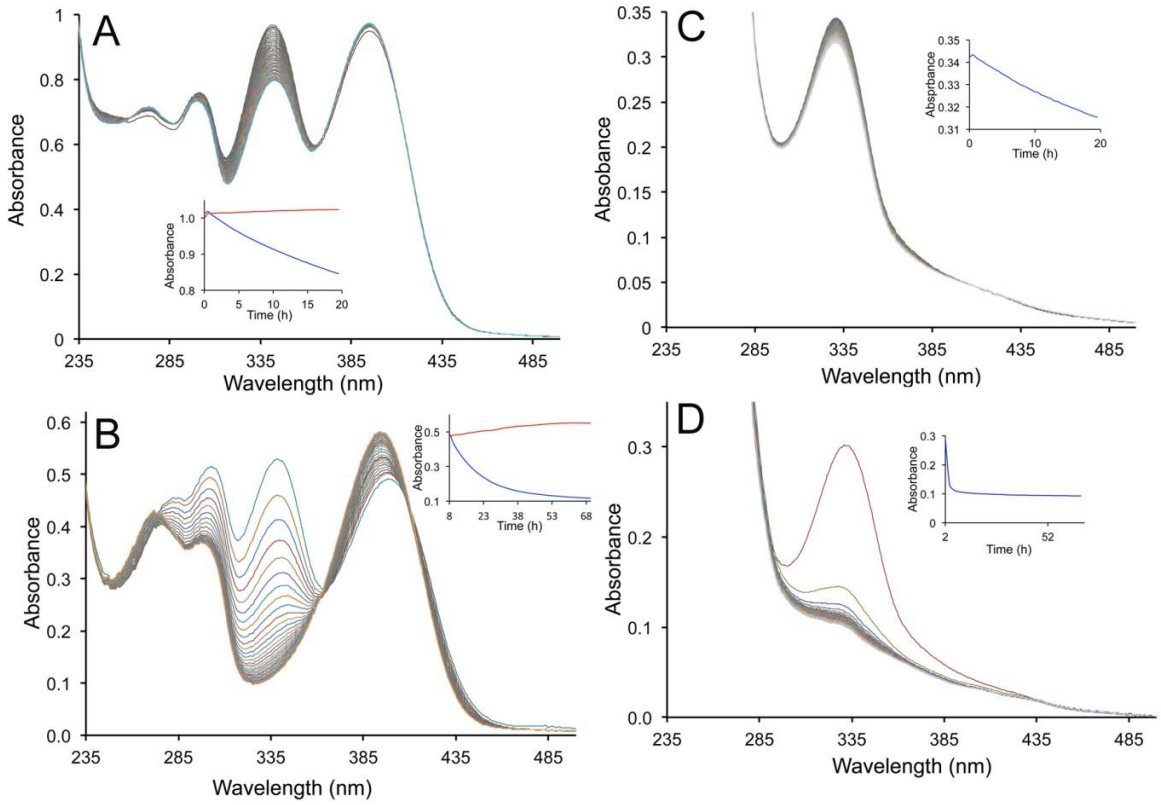

Figure S9. UV/visible absorption spectra of methanobactin from Δ*mbnAN* + pWG101 (A and B) and Δ*mbnAN* + pWG102 (C and D) of samples incubated in either 10 mM HCl (A and C) or 100 mM HCl (B and D). Spectra were taken either at 20 min (A and C) or at 120 min (B and C) intervals. Insets A and B, absorbance changes at 340 nm (blue trace) and 394 nm (red trace). Inserts C and D, absorbance changes at 337 nm (blue trace).

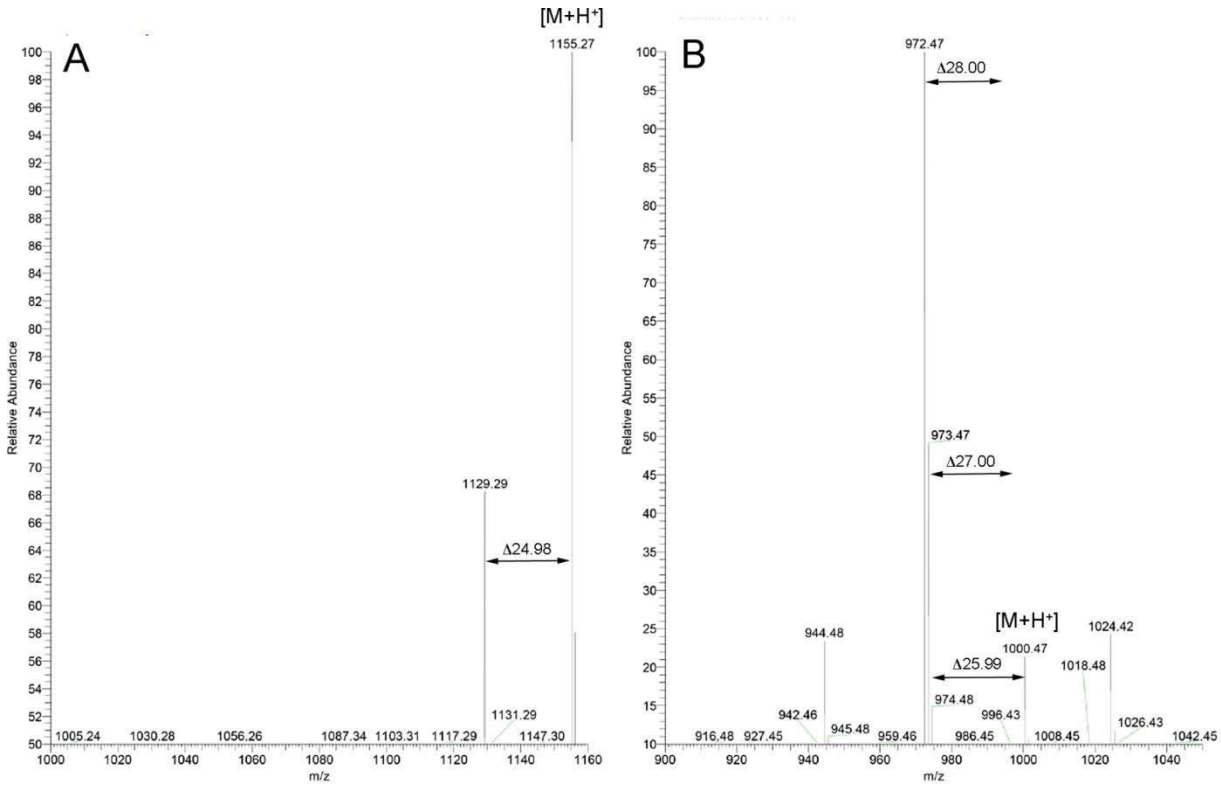

Figure S10. LC-MS of methanobactin from (A) Δ*mbnAN* + pWG101 and (B) Δ*mbnAN* + pWG102 following a 12 h incubation in 100 mM HCl.

CHAPTER 7

CONCLUSIONS

Methanobactin is a member of growing class of ribosomally produced posttranslationally modified proteins (RIPPs) (1). It is primarily produced by methanotrophs in copper limiting conditions and function as chalkophore (analogous to siderophores for binding iron) for acquiring copper important for methanotrophs' physiology (1,2). There has also been evidence of a secondary role of methanobactin in the "copper switch" of methane monooxygenases (3). Based on the six determined structures of methanobactins, the key structural characteristic of all methanobactins are two heterocyclic rings and associated thioamide groups that come together to form the metal binding site (1,4). This site has a very high affinity for copper and other metals (1). Based on the role of methanobactin in copper acquisition in methanotrophs, tight binding affinity for copper is consistent but the binding of other metals at first seemed only serendipity. But as I have shown in this dissertation, the binding of various non-cuprous metals by methanobactin can have important role in methanotrophic physiology.

Towards this end, we started with determining the mechanism of mercury binding by methanobactin from *Methylocystis* strain SB2 and compare it with mercury binding by methanobactin from *Methylosinus* trichosporium OB3b. Both forms of methanobactin were able to bind organic and inorganic forms of mercury found in the environment and were different spectrally and thermodynamically. $HgCl_2$ and $Hg(CN)_2$ were bound by both rings of mb-SB2 while CH_3HgCl was only bound by oxazolone ring and thioamide group. Similar to mb-OB3b, copper could not displace Hg bound to methanobactin, but in contrast to mb-

OB3b, Hg displaced copper bound to mb-SB2. These results tell us that differences in rings and peptide backbone amino acids between mb-SB2 and mb-OB3b can result in difference in mechanisms of binding mercury.

Binding of mercury by methanobactins can have environmental and physiological implications. In situ, methanobactin may be involved in metal mobilization and immobilization. Methanobactin binding to mercury was shown to reduce the bioavailability of toxic metals like mercury and protect the methanotrophs. Mercury incorporated in methanotroph biomass and remained bound to the methanobactin. Mb-OB3b was able to protect other methanotrophs besides *Methylosinus trichosporium* OB3b, like *Methylomicrobium album* BG8 and *Methylocystis* strain SB2 as well from mercury toxicity. These data suggest infidelity in part of methanobactin uptake mechanism amongst methanotrophs. Recent evidence by others also show that methanotrophs that produce the classic two ring methanobactin, can oxidize CH_3Hg^- via the methanol dehydrogenase-methanobactin complex to CO_2 and Hg-bound to methanobactin (5).

Binding of various non-cuprous metals by methanobactin can have physiological relevance for methanotrophs such as altering of the copper-switch. It is well known that increasing copper increases the expression of pMMO versus sMMO in switch over methanotrophs (1, 3). But *Methylosinus trichosporium* OB3b grown in the presence of copper together with gold was able to express sMMO. This is most likely due to gold binding by methanobactin hence decreasing the copper uptake. Just like mercury, gold displaces copper bound to methanobactin and has comparable affinity to methanobactin. These results suggest that preferential expression of a form of methane monoxygenase can be attained and this can be particularly useful in use of methanotrophs in environmental remediation.

Discovery of structural gene of methanobactin and its operon (1, 2, 3, 6) have opened the field to elucidate the mechanism of biosynthesis of methanobactin and its mechanism of uptake by methanotrophs. Work on *Methylosinus trichosporium mbnT::Gm*^{R} (deletion mutant of TonB-dependent transporter gene in the operon), showed that methanobactin is internalized by methanotrophs using this transporter. On the other hand, growth of this mutant in the presence of copper and exogenous methanobactin showed decrease in copper uptake and change in the expression of *mmoX* and *pmoA*. Additionally, the phenotype of mutant without the addition of methanobactin under various copper conditions was not distinguishable from the wild type. Exogenous methanobactin most likely ties up most of the copper available and other uptake mechanisms are not able to internalize the copper.

We also examined the role of the aminotransferase in methanobactin biosysnthesis in *M. trichosporium* OB3b. The N-terminal leucine of methanobactin produced by a aminotransferase (*Δ mbnN*) mutant was not deaminated confirming its involvement in mb-OB3b biosynthesis. The results also showed that this posttranslational modification was necessary for the formation of the N-terminal oxazolone ring.

Future work in elucidating the biosynthesis of methanobactin, would involve determining the role of rest of the genes of this operon in posttranslational modifications. One of the strategies will be to characterize the product (form of methanobactin) produced by each gene deletion mutant. Figure 1 represents the comparison of products formed by wildtype *Methylosinus trichosporium* OB3b and the mutant missing *delC* gene. Based on the UV-visible spectra, the products from mutant might represent the intermediate products with incomplete posttranslational modifications to form the mature product. One of the intermediate products from the mutant is characteristic of a molecule with thioamide groups

while the other one seems to be missing oxazolone ring B. Further, as a proof of concept, purification of each biosynthetic proteins of the operon will be achieved and determined if the proteins can transform the precursor methanobactin peptide to the mature one, *in vitro.*

References

1. **DiSpirito AA, Semrau JD, Murrell JC, Gallagher WH, Dennison C, Vuilleumier S**. 2016. Methanobactin and the link between copper and bacterial methane oxidation. Microbiol Mol Bio Rev **80(2)**: 387-409.

2. **Kenney GE and Rosenzweig AC**. 2013. Genome mining for methanobactins. BMC Biology **11**:17.

3. **Semrau JD, Jagadevan S, DiSpirito AA, Khalifa A, Scanlan J, Bergman BH, Freemeier BC, Baral BS, Bandow NL, Vorobev A, Haft DH, Vuilleumier S, Murrell JC**. 2013. Methanobactin and MmoD work in concert to act as the 'copper-switch' in methanotrophs. Environ Microbiol. **15(11)**:3077-3086.

4. **Kenney GE, Goering AW, Ross MO, DeHart CJ, Thomas PM, Hoffman BM, Kelleher NL, Rosenzweig AC**. 2016. Characterization of methanobactin from *Methylosinus sp*. LW4. J Am Chem Soc. **138(35):**11124-7.

5. **Lu X, Gu W, Zhao L, Farhan UHM, DiSpirito AA, Semrau JD**. Gu B. 2017. Methylmercury uptake and degradation by methanotrophs. Science Adv **in press**.

6. **Krentz BD, Mulheron HJ, Semrau JD, DiSpirito AA, Bandow NL, Haft DH, Vuilleumier S, Murrell JC, McEllistrem MT, Harstel SC and Gallagher WH**. 2010. A comparison of methanobactins from *Methylosinus trichosporium* OB3b and *Methylocystis strain* SB2 predicts methanobactin are synthesized from diverse peptide precursors modified to create a common core for binding and reducing copper ions. Biochemistry **49**:10117-10130.

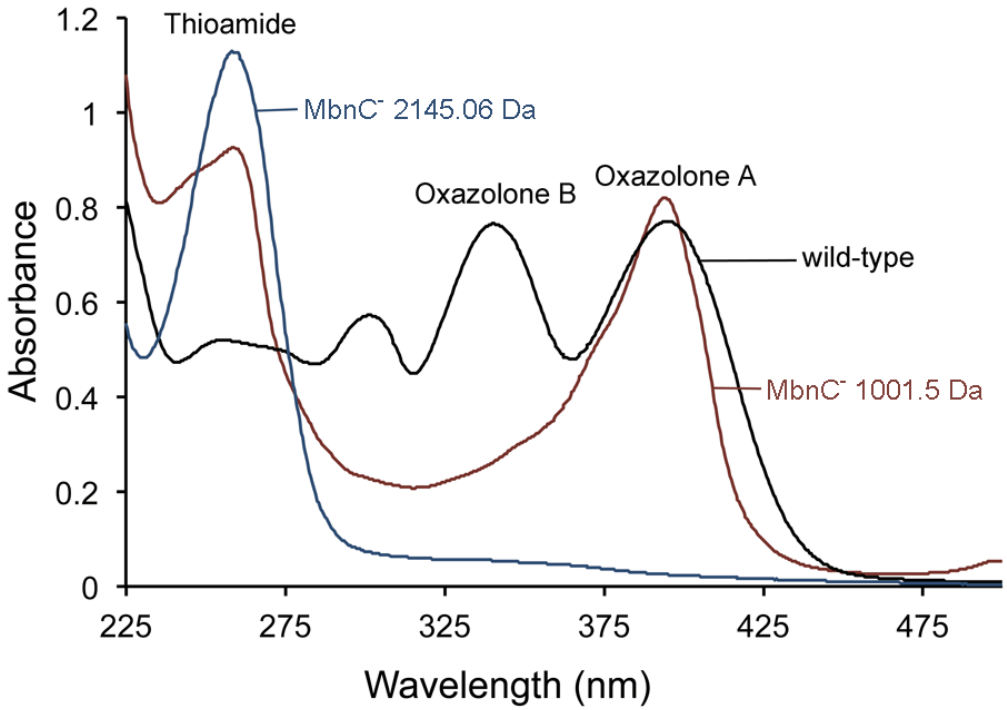

Figure 1: UV-visible spectra of methanobactins: (—) represents methanobactin purified from wild type *Methylosinus trichosporium* OB3b, (—) and (—) represent products purified from *Methylosinus trichosporium* OB3b mutant lacking *delC* gene.